DEVELOPING METHODS FOR INCORPORATING ANTIMICROBIAL BIOCIDAL NANOPARTICLES IN THERMOPLASTICS

By

Saleh Alkarri

A DISSERTATION

Submitted to
Michigan State University
in partial fulfillment of the requirements
for the degree of

Packaging – Doctor of Philosophy

2023

ABSTRACT

Infectious diseases can disseminate through various means, with one prevalent mode being transmission via contaminated surfaces. This is a widespread issue, particularly in hospitals, contributing to the increase in nosocomial infections and associated fatalities. Anti-microbial surfaces can play a pivotal role in reducing the spread of diseases and can find applications in hospital beds/chairs, the public transportation sector, and others. COVID-19 further heightened the need for such anti-microbial surfaces. Plastics, widely used in every aspect of life, have no inherent biocidal properties. Therefore, plastic articles/surfaces lack any defense against accumulating infectious diseases on the surfaces. Efforts are undertaken in this direction to create anti-microbial polymers. Even though these approaches have been demonstrated to be effective anti-microbial agents, they have limited opportunities for commercialization at an industrial scale. For large-scale commercial applications, a simple process to render plastics anti-microbial will be to incorporate various inorganic crystal biocides via compounding. Traditional leachable biocides are utilized by this approach in making plastics anti-microbial. Nevertheless, the use of leachable biocides raises safety concerns. Conversely, non-leachable anti-microbial agents, which are safe, exhibit reduced effectiveness when incorporated into plastics through blending methods.

This Ph.D. dissertation aims to develop novel methods for incorporating anti-microbial biocidal nanoparticles into thermoplastics. In this regard, the anti-microbial activity of leachable and non-leachable biocidal nanoparticles was tested after being incorporated into thermoplastic material via both melt-compounding and surface embossing. Properties of the thermoplastic composite, such as thermal, rheological, mechanical, flowability, permeability, and leachability,

are studied before and after the addition of anti-microbial. A novel methodology of incorporating the nanoparticles into the surface of thermoplastics through thermal embossing is developed and compared with the traditional melt-blending approach. The study demonstrates the effectiveness of surface embossing as compared to melt-blending for the non-leachable anti-microbial agents. The study also confirms the ROS mechanism for the non-leachable magnesium hydroxide and copper infused magnesium hydroxide nanoparticles.

Dedicated to my scholarship sponsor (SABIC).
Thank you for always believing in me.

ACKNOWLEDGMENTS

First and foremost, I am very thankful to SABIC for honoring me with the scholarship opportunity to pursue my Ph.D degree, and for being very supportive in every aspect during my Ph.D studies and research. I am also appreciative to the Ph.D advisory committee from Michigan State University; Dr. Muhammad Rabnawaz, Dr. Rafael Auras, Dr. Teresa Bergholz, and Dr. Maria Rubino for their guidance and advcises. I am extremely grateful to my colleagues from SABIC Technology and Innovation (T&I) Team, Dr. Maria Soliman, Dr. Jérôme Vachon, Dr. Zahir Bashir, Mr. Tariq Syed, Mr. Abdulrahman Alawwad, Mr. Saad Alhussain, and Mrs. Estelle Poulet for their valuble guidance, unwavering encouragement, and understanding throughout my academic pursuits and everyday endeavors. I would also like to thank the collaborators from Aqua Resources Corp, Mr. Lee Maddan and Dr. John Cairney for their technical support on my studies, and the generous donation of the chemicals. I am very appreciative to all the mentioned above for their generous assistance and encouragement that have enriched my experience and life in the United States.

TABLE OF CONTENTS

LIST OF TABLES

LIST OF FIGURES

LIST OF ABBREVIATIONS

NPs	Nanoparticles
UV	Ultraviolet
ZnO	Zinc oxide
GO	Graphene Oxide
CNT	Carbon nanotube
SEM	Scanning electronic microscopy
EDX	Energy dispersive X-ray
DSC	Differential scanning calorimetry
TGA	Thermogravimetric analysis
MFI	Melt flow index
WVTR	Water vapor transition rate
OTR	Oxygen transition rate
QA	Quaternary ammonium
MIC	Minimum inhibitory concentration
ROS	Reactive oxygen species
DNA	Deoxyribonucleic acid
FDA	Food and Drug Administration
PVC	Polyvinylchloride
PC	Polycarbonate
PBA	Bisphenol A
PEG	Polyethylene glycol
PEO	Polyethylene oxide

PDMS	Polydimethylsiloxane
PMMA	Polymethylmethacrylate
PS	Polystyrene
PP	Polypropylene
PE	Polyethylene
HDPE	High density polyethylene
LDPE	Low density polyethylene
LLDPE	Linear low density polyethylene
PET	Polyethylene terephthalate
PMPC	Poly(2- methacryloyloxyethyl phosphorylcholine)
PCBMA	Poly(carboxybetaine methacrylate)
PSBMA	Poly(sulfobetaine methacrylate)
PB	Polybetaines
PMHS	Polymethylhydrosiloxane
PU	Polyurethane
PEI	Polyethyleneimine
PPO	Polypropylene oxide
SMA	Styrene-maleic anhydride
PAN	Polyacrylonitrile
P(AN-*co*-MTA)	Thermally stable polyacrylonitrile (PAN) with anti-microbial methacrylic copolymers bearing cationic moieties with 1,3-thiazolium and 1,2,3-thiazolium side-chain groups.
PTTBM	Poly(4-(1-(2-(4-methylthiazol-5-yl)ethyl)-1H-1,2,3-triazol-4-yl)butyl methacrylate).
PAA	Polyacrylic acid

PLA	Polylactide
T_m	Melting temperature
T_c	Crystallinity temperature
T_g	Glass transition temperature

CHAPTER 1: INTRODUCTION AND LITERATURE REVIEW

1.1 Objective

The aim of this chapter is to understand how the anti-microbial polymeric materials are developed, and what could be their mode of action. The toxicity of such anti-microbial additives when used in healthcare and food packaging application will be discussed. In addition, the goals of this Ph.D dissertation will be outlined and a roadmap for the ensuing work will be given.

1.2 Introduction

Scientists have estimated that there is a total of ~1,400 known species of pathogens affecting humans, such as viruses, bacteria, fungi, protozoa, and helminths. This represents less than 1% of the number of microbes on Earth, yet, this small number is related to an average of 16 million deaths per year, many of them being preventable.[1] Therefore, since the pioneering discoveries of Louis Pasteur and Robert Koch, researchers, and in general healthcare systems, developed cures towards diseases arising from these infectious microbes. The unchecked advances of infectious microbes can not only bring premature deaths but also can bring societies and economies to a standstill as seen in 2019 by the outbreak of COVID-19. Antibiotics are the medicines used to treat people and animals from bacterial infections by either killing bacteria or inhibiting growth.

Antibiotics are effective at killing many strains of harmful bacteria, but some disadvantages must be considered. Firstly, antibiotics, while being effective solutions against bacteria, are not so effective against viruses. Secondly, certain bacteria have become resistant to a minimum of one out of three different anti-microbial drug categories, and this often arises due to patients terminating the antibiotic treatment as soon as external symptoms subsidize or due to the over-prescription of antibiotics.[2-5] The three categories of anti-microbial drugs are dependent on the

activity spectrum in which it can be classified as narrow, broad or extended-spectrum agents. Antibiotics falling within the narrow-spectrum, such as penicillin G, would be more effective on Gram-positive bacteria. Whereas antibiotics classified within the broad-spectrum, such as tetracyclines and chloramphenicol would be effective on both Gram-positive and Gram-negative bacteria. An extended-spectrum classified antibiotics are usually chemically modified to affect a wider range of bacteria, mainly those classified as Gram-negative. An extended-spectrum antibiotic is one that because of chemical modification affects additional types of bacteria, usually those that are classified as Gram-negative.[6] The development of new types of antibiotics cannot keep pace with the new drug-resistant varieties due to the high costs of research and development of new drugs and the time needed to obtain regulatory clearance.[7] Further, the rapid evolution of antibiotic resistance severely limits the usefulness of new antibiotics and the economic return for years of research and millions of dollars of investment.[8] As a result, many people are infected with multidrug-resistant bacteria every year [9], leading to premature deaths.

Infectious diseases can be spread via contaminated surfaces through the transfer of existing microorganisms to mucous membranes in the body.[10] This is a key issue in hospitals with the rising number of nosocomial infections and associated deaths.[11] Plastics with anti-microbial properties are one of the solutions to reduce the spread of infections and this interest was further strengthened by the recent COVID-19 pandemic where humanity experienced a fear of virus transmission through fomites.[12] Most common plastics have no inherent biocidal properties, and thus may be surfaces upon which microbes may persist and become a source of infection.[13]

One class of anti-microbial polymeric systems is focused on antibiotic or drug release. The aim is the controlled and targeted release of the antibiotic or drug, and the polymer serves as an inert matrix for holding the biocide. In contrast to the antibiotic cure to counter infectious

microbes, researchers have explored anti-microbial polymer's unique properties in roles other than as media for "controlled drug release". Anti-microbial polymers contain substance(s) to kill microorganisms or stop their multiplication and growth. The anti-microbial polymer articles can be engineered to (i) prevent the adhesion of microbes and/or (ii) have functional groups that kill microbes or (iii) contain nano additives that destroy microbes.

These engineered methods have peculiar advantages. Firstly, it is a preventive solution method that is applied to stop the infection from arising in the first place. Secondly, it has the possibility to use polymer containing moieties with multiple anti-microbial mechanisms that cannot be outwitted by pathogens.[14] Unlike antibiotics, there is a low potential for the microbes to develop resistance. Thirdly, the polymer could be incorporated with additives that are effective against bacteria as well as viruses. Anti-microbial polymers can be easily adapted to wider applications. They can be applied either as a coating to protect working surfaces and medical instruments from microbial growth, or they can be melt-compounded and molded into shapes that are exposed to manual handling which are accumulation points for microbes such as in doorknobs, keypads, shopping cart handles, etc. Plastics with anti-microbial activity could be a replacement for consumable disinfectants or could be an additional defense in the armor against infectious microbes.

In contrast to biocide-releasing polymers, "polymeric biocides" are macromolecules with microbe killing "functional groups" in the side chain or in the main chain backbone (**Figure 1**). That is, the polymer itself is the microbe killer. Such anti-microbial polymers are designed to imitate the anti-microbial defensive structures created by the immune systems of diverse organisms to eliminate microorganisms.

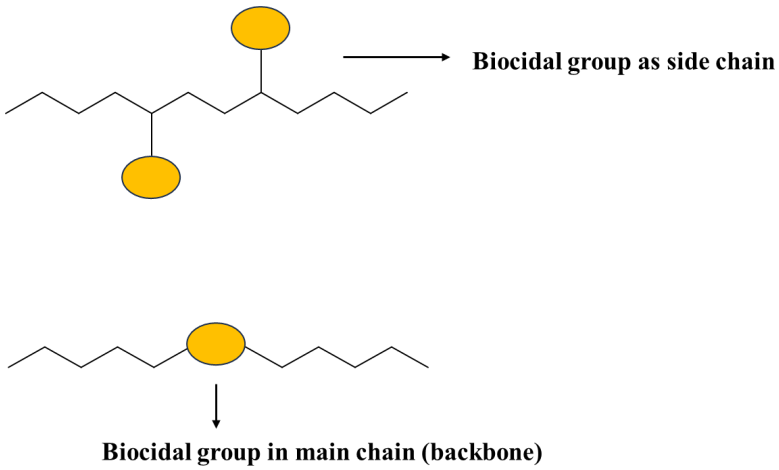

Figure 1. Illustration of biocidal group incorporated in the polymer backbone or as a sidechain.

Another category that could be defined as, "biocidal polymers", inhibits the adhesion of microbes, or has additives (not antibiotics) that kill microbes. In this case, the polymer itself may be inert. Biocidal polymers include nanocomposites and blends of an inert polymer + polymeric biocide.

1.3 Polymer

A natural or synthetic material made of macromolecules is a polymer. Examples of natural polymers are wool and silk, while synthetic polymers include vulcanized rubber, polystyrene, and polyethylene.[15] Polymers have unique chemical and physical properties, making them useful in everyday life. For example, the improved qualities of rubber and resistance to deformation allow vulcanized rubber to be used in car tires. They are synthesized using polymerization, whereby constituent monomers react together to form polymer chains. The two general types of polymerizations include either condensation or addition reactions. Condensation polymerization involves many condensation reactions between monomers with two or three functions which release small molecules such as water as a side product.[16] Advantages include strength, durability, low density, and being chemically unreactive, while disadvantages include pollution and unrecyclablity (Division of Polymeric Materials American Chemical Society, 2002). Examples are

silicones and nylon.[17] Addition polymerization involves the recurrent addition of monomers with two or three bonds to form a polymer chains.[18] Advantages include high melting points and rigidity, while drawbacks are depletion of oil and pollution.[18] Examples include polyvinylchloride (PVC) and Teflon.[19]

1.3.1 Biocidal-releasing polymers

The "biocidal releasing polymers" are either antibiotic or drug-loaded polymers which are mainly used when the patient is already infected. The aim is "controlled drug release" and "targeted delivery" to the infected site. There are five categories of biocide-releasing polymers used for drug release, as follows: (i) nanoparticles (NPs) of special polymers, (ii) polymer micelles, (iii) polymer vesicles, (iv) dendrimers, and (v) polymeric hydrogels.[20]

1.3.2 Nanoparticles (NPs) of special polymers

Nanoparticles (NPs) are unique substances manufactured on a nanoscale, where a minimum of 50% of the particles within the size distribution have one or more external dimensions ranging from 1 nm to 100 nm. Polymeric NPs have been used for targeted drug release against cancer cells, and the polymer itself is anti-microbial in the form of NPs. This category contrasts with what is described later on by anti-microbial polymer nanocomposites consisting of polymers with metal oxide or metal NPs.[21, 22] The polymeric NPs are made of self-assembled (hierarchical) structures, and the targeted delivery to infected sites is achieved by controlling the surface chemistry attributes of the resultant formations. The delivery of the drug from the biocide-releasing polymer NPs can be over days and even weeks. There are some advantages of using biocide releasing polymeric NPs: (i) their ability to protect the drugs to resist enzymatic breakdown, whereas the amount of drug needed is lower, hence the toxicity to the recipient is also lower and (ii) they have the possibility of overcoming bacterial resistance mechanisms.[23] In fact, some

polymeric self-assembled NPs use a multi-modal mechanism of action to destroy microbes such as (i) outer bacterial membrane destabilization, (ii) disturbing the inner membrane, and (iii) upsetting ionic flows across microbe cell walls.[24, 25]

1.3.3 Polymer micelles

The "polymer micelles" from the core-shell polymeric NPs are created via the self-organization of block copolymers with both hydrophilic and hydrophobic parts (a combination of hydrophobic and hydrophilic components). The core houses hydrophobic drugs, while the shell is designed to form water-soluble micelles for delivering poor-solubility drugs. In some cases, they have the ability to function as anti-microbial polymers independently, without the need for additional biocidal agents.[26] Biodegradable anti-microbial polymeric micelles made from self-assembled amphiphilic polycarbonate (PC), showed disruption of the bacterial cell wall and membrane resulting in bacterial breakdown.[27] The Gram stain differentiates organisms from the domain bacteria, based on the cell wall structure. Gram-positive cells possess thick peptidoglycan layers, external to the cell membrane and Gram-negative cells have thin peptidoglycan layers situated between two membrane layers.[28] The Gram-positive bacteria are more sensitive towards anti-bacterial substances than Gram-negative bacteria because of their cell wall structure which is protected by an outer membrane.[29] While effective against Gram-positive bacteria, these micelles showed limited effectiveness against Gram-negative bacteria. To address this challenge, a random copolymer configuration was employed in place of a block copolymer, enhancing accessibility to the hydrophobic drugs, with an increased capacity for membrane insertion and disruption.[30] Rod-shaped micelles are effective against *C. albicans*, a type of fungus that presents challenges in eradication due to its multi-layered, thicker, and relatively less negatively charged cell walls.[31, 32] There is some debate about whether the suitable polymer chains could exhibit increased activity

when existing as free molecules in a solution, rather than supramolecular structures with reduced polymer chain mobility.[33] In systems relying on supramolecular structures, the reduced mobility may impede the cationic groups within the polymer, limiting their interaction via electrostatic forces with bacterial cell walls [24], or shield the hydrophobic drug components within the core from the required disruptive interaction with bacterial membranes.[34]

1.3.4 Polymer vesicles

The "polymer vesicles", also called "polymersomes", is a system for biocide-releasing anti-microbial polymer. It is a class of artificial vesicles consisting of hollow spheres (~50 nm to 5 μm in diameter) with a bilayer membrane that can be used for targeted and controlled drug delivery. The hollow cavity can be filled with both hydrophobic and hydrophilic drugs, and the bilayer membrane is made of amphiphilic synthetic linear diblock or triblock copolymers. One block is hydrophobic, and the other block or blocks are hydrophilic. Amphiphilic materials have both a water-loving polar moiety and a fat loving non-polar moiety. Polymers used for the hydrophilic blocks include polyethylene glycol (PEG) and polyethylene oxide (PEO), while the lyophilic or hydrophobic blocks can be made of polydimethylsiloxane (PDMS), poly(lactic acid), or poly(methyl methacrylate) (PMMA). Stronger interaction between polymer and bacteria occurs when the polymers are self-assembled into vesicles which are structured as hollow spheres, rather than where polymer chains are unassembled. The polymersomes have three different regions available for functionalization: (i) the inner hydrophobic cavity, (ii) the polymer membrane, and (iii) the periphery.[35] The effectiveness could be due to the increased local concentration of positive charges [36], and such polymer vesicles have been used for example for simultaneous anti-bacterial and anti-cancer medication.[37]

1.3.5 Dendrimers

The "dendrimers" are unusual polymers that are multi-branched with a spherical disposition, and this forms another class of materials used as biocide releasing polymers. They can be designed with a core–shell architecture made of a hydrophobic core surrounded by repeating-unit branches with functionalized terminal groups.[38, 39] Such structure of polymers allows for stronger adsorption and binding to cell membranes compared to linear polymers.[40] Biocidal agents can be mobilized withing the dendritic assembly by non-covalent encapsulation or by covalently binding to the terminal functional groups[40, 41] followed by a targeted release.[42-44] The dendrimer loaded with the drug leads to the distruption and fragmentation of the bacterial membrane, subsequently resulting in the discharge of electrolytes and nucleic materials from the cell, ultimately leading to its death.[41]

1.3.6 Polymeric hydrogels

The "polymeric hydrogels" are 3D cross-linked polymers with hydrophilic groups that can be swollen by water. They can absorb more than 20% of their weight of water. Gelation (that is cross-linking in the presence of water) can be induced by a change in temperature, pH, or UV irradiation. They can have mechanical features and morphologies similar to natural tissues. They can be biocompatible; hence hydrogels are also used for drug-delivery systems to the infected site directly. Their hydrophilic nature is advantageous for the solubility of antibiotics like ciprofloxacin, amoxicillin, or gentamicin.[25] Anti-microbial systems based on hydrogelling polymers also overlap in their functionality with other categories of anti-microbial polymers which rely on using inorganic NPs like zinc oxide (ZnO) and metal NPs like silver (Ag) which kill microbes by multiple mechanisms.[45, 46] Due to their water content, the hydrogels whether loaded

with antibiotics or NPs that kill microbes, cannot be used for shaping hard articles like a door handle.

1.3.7 Thermoplastics

Thermoplastics are polymers that can be melted and reshaped many times. When heated, they melt and harden when cooled. They can be either amorphous (the polymer chain structures are random and irregularly shaped) or semi-crystalline (the polymer chain structures have a pattern and a definite shape that forms crystals.[47] Homopolymers (chains that have one monomer type) and copolymers (chains with two or more bonded monomer types) are important when discussing polymers.[48] Other important terms are crystallization point T_c (change from liquid state to crystalline state), melting point T_m (change of physical state from solid to liquid), and glass transition point T_g (change from glassy to soft rubbery state).[49] Common semi-crystalline thermoplastics in food packaging and healthcare include polypropylene (PP), polyethylene (PE), and polyethylene terephthalate (PET), while polycarbonate (PC) is an amorphous type of thermoplastic.

Polypropylene (PP) is a semi-crystalline product of propylene polymerization. It is created by repeating propylene monomer (C_3H_6) to create a long-chain $(C_3H_6)_n$ polymer unit. It is translucent, semi-rigid, and resists heat and fatigue.[50] It also has a good chemical resistance against bases and acids. It can be a homopolymer or copolymer (with ethylene), with the former having a higher strength-to-weight ratio, stiffness, and strength.[50] The melting point (T_m) is 163.8 °C, it crystalizes at (T_c) 123-129 °C and has a glass transition temperature (T_g) of -25 °C.[51] This polymer is used for packaging and textiles.[52] Catalysts commonly used are metallocene or Ziegler-Natta. By 2022, the PP market stood at 126.75 billion USD.[53]

Polyethylene (PE) is a product of ethylene polymerization and different types are industrially sold depending on the technology used. The chain structure is repeating ethylene $(C_2H_4)_n$ molecules, which react in the presence of a catalyst, breaking the double bond and creating a chain.[50] There are three types of PE: HDPE (with organometallic catalyst), LLDPE (typically made with the use of an alpha-olefin comonomer which also results in a low crystallinity), and LDPE (made with organic peroxide initiator). HDPE is linear PE. LLDPE has short-chain branches from the incorporation of low amounts of butene or hexene comonomers.[54] LDPE has long chain branches and is produced by high-pressure polymerization of ethylene.[50] Mechanical features of LDPE include flexibility, transparency, and high-impact strength. LLDPE has a higher puncture and impact resistance and tensile strength than LDPE. HDPE is hard to semi-flexible, resists moisture, and maintains high tensile properties. PE is generally inert and resists bases, acids, and oils.[50] They melt (T_m) at 120 - 130 °C, crystallize (T_c) at 110 -120 °C, and have a glass transition point (T_g) of -100 °C.[51] The polymer is used in carrying and fabricating materials due to its high chemical resistance, electrical insulation, transparency, and flexibility.[55] HDPE and LLDPE are made using the Phillips or Ziegler catalysts. By 2021, the polyethylene market stood at 102.49 billion USD.[56]

Polyethylene terephthalate (PET) is a condensation polymerization product of terephthalic acid and ethylene glycol (EG).[57] PET is processed using typical manufacturing methods such as extrusion, injection molding, and blow molding.[58] It can be semi-crystalline or amorphous.[50] The structure consists of repeating $C_{10}H_8O_4$ units. It has high Shore hardness, good tensile elongation, as well as excellent tensile strength and elasticity moduli.[59] Chemical features include resistance to low pHs.[50] It can be a homopolymer or copolymer. The glass transition point (T_g) is between 69 °C and 85 °C, crystallization (T_c) is 170 °C, and the melting point (T_m) is 260 °C.[60]

It is used in textiles and packaging due to its high mechanical strength and durability. A commonly used catalyst is antimony trioxide.[61] By 2022, the PET market stood at 30.12 billion USD.[56]

Polycarbonate (PC) is an amorphous polymer typically made from the condensation reaction of Phosgene (or carbonate) and Bisphenol A (PBA) polymerization. Phosgene and BPA are reacted in a methyl chloride solvent. The reaction is followed by centrifugation, filtering, concentrating, and drying the solution.[62] Catalysts, commonly tertiary amines, are used in the process. Chemical properties of PC include resistance to alkalis, acids, and water.[50] Mechanical features are high impact strength and stiffness. In practical use, PC is amorphous after extrusion with a glass transition temperature (T_g) of 147°C.[63] PC is used primarily in bulletproof windows due to its remarkable toughness, lightness, and almost unbreakable nature.[64] As of 2021, the PC market stood at 21.8 billion USD.[65]

1.4 Anti-microbial surface modification

1.4.1 Design of surfaces to prevent adhesion of microbes

A strategy to prevent microbes from depositing and proliferating on a surface is through the use of microbial-repellent (anti-fouling) surfaces. They can be induced by coatings that aim at preventing the attachment of microbes and proteins on surfaces. Casein contrast with the use of biocides, these surfaces do not actively kill microbes, but only prevent their attachment and growth over the surface where they could develop a biofilm. (**Figure 2, mechanism (A), (B), and (C), top, inset**) illustrates the main principles used to prevent microbes from adhering to a surface, via alteration of the surface charge and chemistry, hydrophobicity, surface roughness, topography, or stiffness (**Figure 2, bottom, inset**). (**Figure 2, (A), top, inset**). Steric repulsion can be, for instance, created by having Nano protrusions or cilia on the surfaces. Hydrophilic polymers such as PEG oligomers use steric repulsion to repel microorganisms.[66-68] While a smooth surface

favors adhesion, a surface with topography from the presence of Nano protrusions prevents the clinging of microbes. Similarly, a soft surface favors attachment compared with a stiff surface. (**Figure 2, bottom, inset**) shows an anti-fouling mechanism induced by electrostatic repulsion. Zwitterionic polymers, which have both positive and negative charges, can be used for this purpose. Poly (2- methacryloyloxyethyl phosphorylcholine) (PMPC)[69], poly (sulfobetaine methacrylate) (PSBMA)[70, 71], poly (carboxybetaine methacrylate) (PCBMA)[70] and polybetaines (PB)[72] are examples using electrostatic repulsion as the anti-adhesion mechanism.

The method in (**Figure 2, (C), top, inset**) deploys surfaces with low energy where wetting is prevented. The structures required to prevent adhesion are however not easy to fabricate. Common thermoplastics such as polystyrene (PS), polycarbonate (PC), and polyethylene (PE), have been used to fabricate textured anti-microbial surfaces.[73] They can be assembled into super hydrophobic micro/nanostructures which have low surface energy so that wetting is reduced (**Figure 2, top, inset**). With such super hydrophobic surfaces, about 2% of the bacteria in a droplet adhered, and less than 0.1% persisted on the surface following rinsing.[73] Bacterial cells can colonize a super hydrophobic surface from a nanostructured topography only when the air is entrapped between the water droplets, and the Nano surface protrusions are excluded.[74]

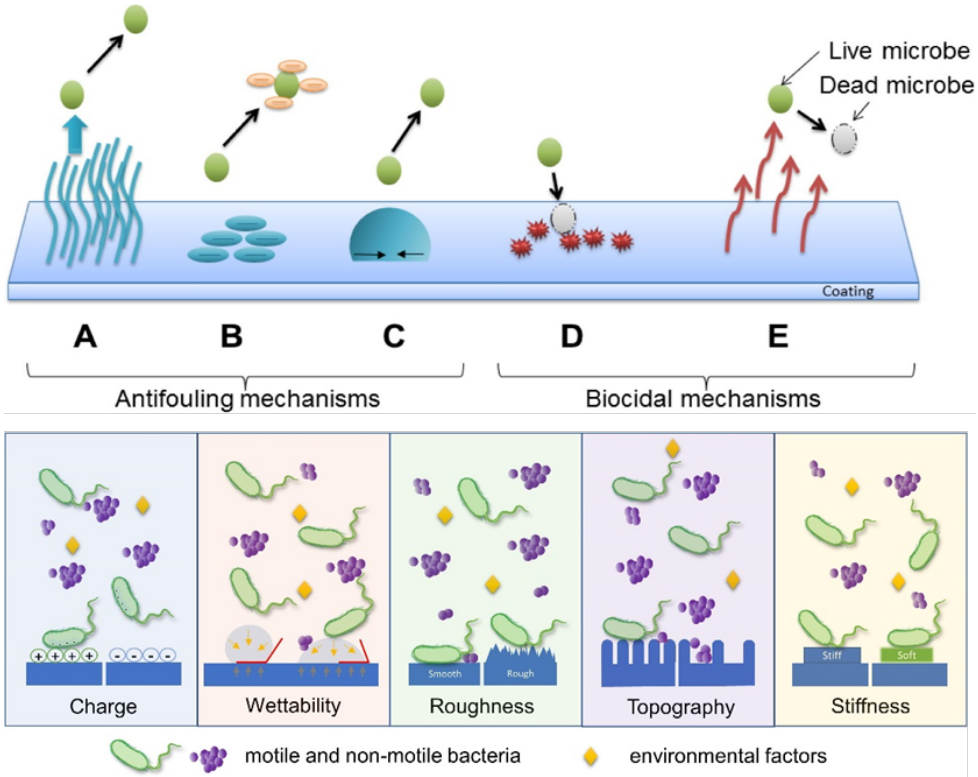

Figure 2. Instances of polymer-based anti-microbial mechanisms include: (A) steric repulsion, (B) electrostatic repulsion, (C) surfaces with low surface energy (demonstrating high contact angle), (D) release of biocides, and (E) direct contact-based microbial eradication (top) , reprinted with permission from ref. [75], Elsevier license No: 5573800071354. Copyright (2016) Acta Materialia Inc. Diagram showing different surface characteristics that have a substantial impact on bacterial adhesion (bottom), reproduced from ref. [76], open access. Copyright (2021) Zheng, Bawazir, Dhall, Kim, He, Heo and Hwang.

1.4.2 Killing microbes by making biocidal active surfaces

While prevention of the adhesion and deposition of microbes on the surface is one design for anti-microbial polymers, the other method is to have surfaces that are biocidally active (**Figure 2, (D) and (E), top, inset**). Polymeric biocides and biocidal polymers are anti-microbial because of their intrinsic nature and/or due to biocidal groups and segments incorporated in the chain backbone and/or as sidechains.[77-79] A commonly employed biocidal component capable of being linked to different polymer chains is the quaternary ammonium (QA) salt. QA salts are used as a disinfectant that kills bacteria, yeasts, and molds.[80] The QA moiety has been attached to copolymers made of polymethylhydrosiloxane (PMHS) and polydimethylsiloxane (PDMS), and

from these anti-microbial films can be made. The QA salt moiety has also been attached to polyurethane (PU), and such PU can be used as an anti-microbial coating.[79]

Alternatively, cationic polymers like polyethyleneimine (PEI) can be used to generate anti-microbial structures on surfaces. PEI polymers can be produced as a linear or branched polymer, or even as a dendrimer (**Figure 3**). The linear polymer is soluble in hot water, and melts at 73 °C. The anti-microbial activity of PEIs derives from their cationic character which can bind to the negatively charged membrane of the microbes that are attracted to it, leading to its puncture and cell lysis. Moreover, PEIs can undergo N-alkylation to incorporate quaternary amino functional groups, which, as previously noted, also possess anti-microbial properties.

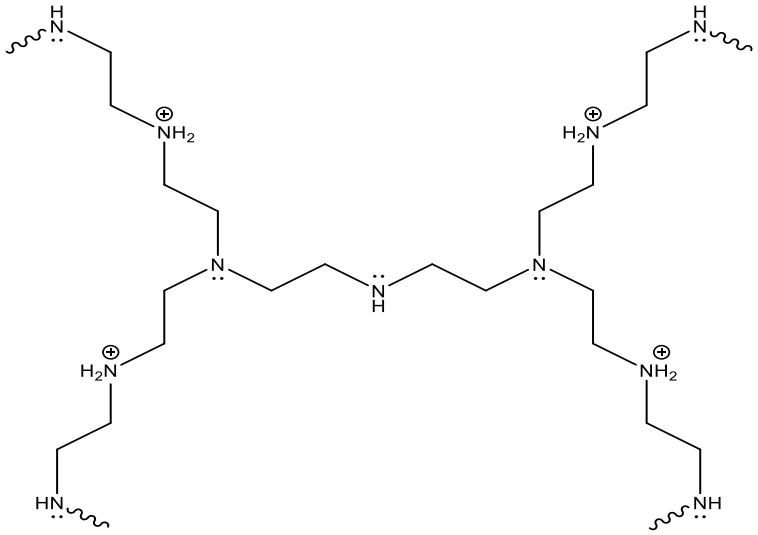

Figure 3. Chemical structure of polyethyleneimine (PEI) containing cationic moieties that is responsible for anti-microbial activity.

N-halamine is another biocidal moiety capable of almost instant destruction of a broad spectrum of microbes.[81, 82] N-halamine-containing polymers do not generate harmful substances or release halogens unless they are exposed bacteria.[83] The synthesis of N-halamine-based polymers and graft copolymers can be easily achieved economically way. While N-halamine

polymeric surfaces are highly biocidal, their drawback is the loss of chlorine upon UV irradiation.[84]

1.4.3 Polymeric surface structures combining anti-adhesive and biocidal properties towards microbes

It was mentioned that one strategy of anti-microbial polymers is to prevent deposition and adhesion of microbes on the surface, and another strategy is to have an active disintegration of microbes through biocidal groups and additives (or a combination of both). The first strategy is classified as (biopassive), and the second is classified as (bioactive). Some groups have worked towards combining the best of both worlds by combining such approaches, which can drastically improve the overall anti-microbial property of a material.

The chemistry of bio-passive surfaces includes minimizing protein adsorption and maintaining a surface charge to stop microbial proteins.[85] Creating these surfaces involves applying a coating and grafting.[85] Additives that can be used include anti-fouling agents such as polyethylene glycol (PEG), which forms dense layers over treated surfaces.[86] Important considerations include the type of surface, adhesion degree, and longevity required.[85]

Bioactive surfaces have immobilized bioactive molecules targeted at advancing or promoting specific interactions.[87] Their chemistry involves creating an apatite layer on a material in the "living body bond to the living bone".[88] Additives that can be added include calcium phosphate and sodium titanates.[88] Important considerations include the material type and cell reaction.

Indeed, the strategy of repelling and killing microbes has been done by conjugating anti-adhesive polymers with biocidal moieties or polymers. Muszanska et al. demonstrated this approach with a triblock copolymer consisting of a core block of polypropylene oxide (PPG) and

two side blocks of PEG (anti-adhesive).[89] In the PEG chain portion, Muszanska et al. The anti-microbial enzyme (lysozyme) was added as a conjugate through covalent bonding. This particular triblock copolymer resulted in brush-like configurations consisting of one or two lysozyme molecules per chain of the triblock polymer. Surfaces treated with these brushes exhibited properties that prevented adhesion and inhibited microbial growth.

There are other combinations described for the simultaneous prevention of deposition and biocidal activity. Anti-adhesive PEG along with a cationic PC exhibited strong anti-bacterial and anti-adhesive properties.[90] The anti-adhesive property was achieved through chain blocks leading to the assembly of particular structures while the biocidal property came from using specific mechanisms like cationic groups that are known to destroy cell walls.

Such anti-adhesive + biocidal polymers are often used as coatings. A conventional but modified plastic coupon was compression molded from PP/PP-graft-maleic anhydride (g-MA). A coating of branched polyethylene imine (PEI) and styrene-maleic anhydride (SMA) copolymer was made into a block polymer with a PEI/SMA/PEI configuration, and this was spin-cast on the coupon from PP/PP-graft-maleic anhydride.[91] The coating had 100 nm pores which were formed from hydrophobic styrene subunits that acted for anti-adhesion. The cationic primary amine groups had intrinsic biocidal properties and chlorinated N-halamine-based groups were attached. (**Figure 4**) shows the bacterial count for PP/PP-g-MA, chlorinated PP/PP-g-MA, PP-PEI-SMA-PEI, chlorinated PP-PEI-SMA-PEI. In the bar chart, bleach is shown as the benchmark for *E. coli* bacterial destruction. It can be seen that PP-PEI-SMA-PEI has activity against bacteria, but the chlorinated PP-PEI-SMA-PEI is second best after the bleach. The authors showed there was no *E. coli* adhesion on the PEI/SMA/PEI-coated PP surface.[91]

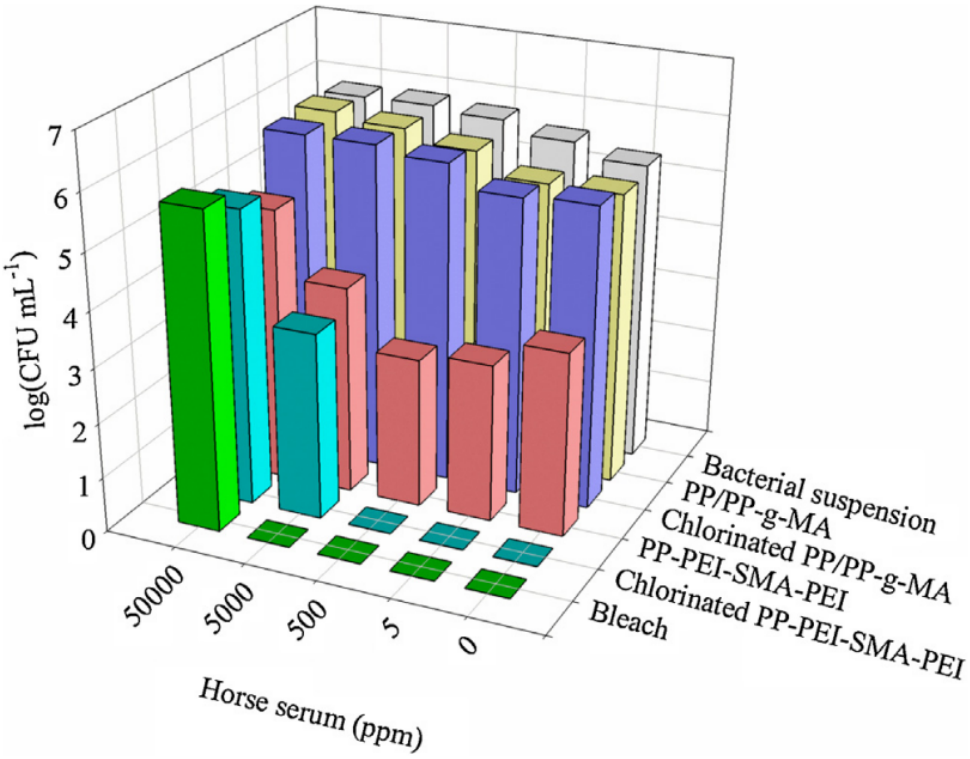

Figure 4. The anti-microbial characteristics of PEI/SMA/PEI systems, both chlorinated and non-chlorinated, compared to their counterparts. Reprinted with permission from ref. [91], Elsevier License No: 5573800439614. Copyright (2016) Elsevier B.V.

1.4.4 Coating

Since only the surface of a material is in contact with microbes, a coating can be applied to confer anti-microbial properties aiming at killing or restricting the development of microorganisms such as fungi.[92] Some coatings were developed to kill disease-causing microbes and pathogens through cellular membrane perturbation.[93-95] Anti-microbial polymer coatings are broadly utilized in dental implants. Anti-microbial surfaces have an anti-biofouling effect that resists the attachment of microbes to a surface. According to Chidanand et al. (2022), the global anti-microbial coating market was 3.7 billion in 2020 and is estimated to be $11 billion by 2030.[96]

1.5 Anti-microbial polymers

1.5.1 Anti-microbial polymer blends

Blending polymers possessing anti-adhesive or anti-microbial properties can create peculiar nanostructures and chain conformations that amplify these two effects to prevent microbial growth. An example is to blend an inert polymer with a copolymer derived from it and decorate the latter with anti-microbial moieties. A specific case was a blend of polyacrylonitrile (PAN) and anti-microbial methacrylic copolymers with attached cationic moieties (1,3-thiazolium and 1,2,3-thiazolium side-chain groups) P(AN-co-MTA) (**Figure 5, (A)**).

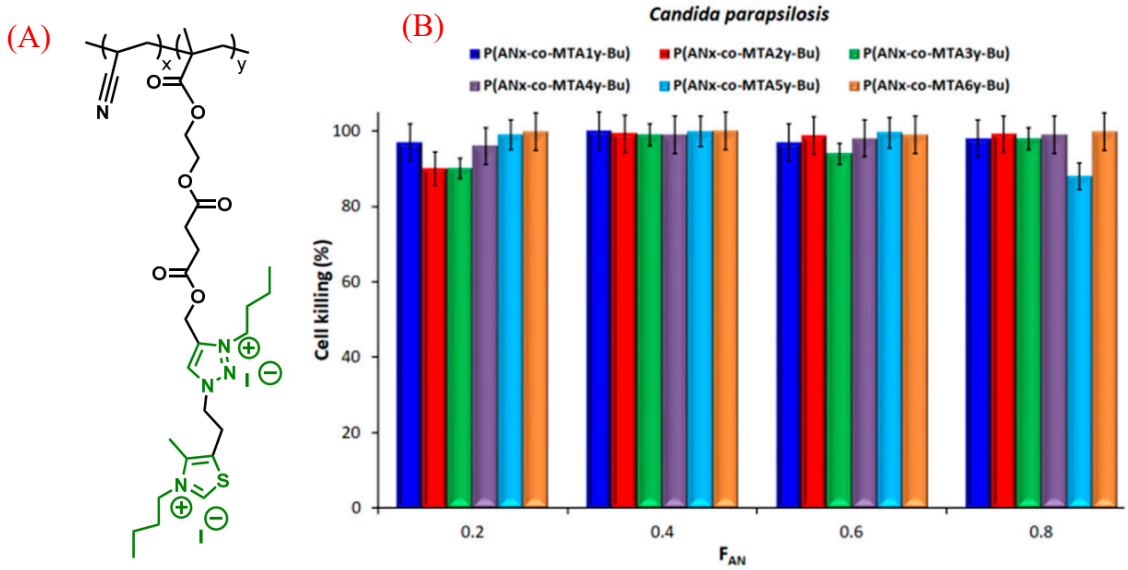

Figure 5. The chemical configuration of quaternized P(AN-co-MTA) copolymers originating from acrylonitrile (A). The degree of cell elimination against the C. paraplosis microorganism upon exposure to anti-microbial films (B). Reproduced from ref. [97], open access.

The biocidal cell-killing efficiency was significantly improved, to almost 100%, through the increase of the positive charge density (**Figure 5, (B)).** An additional example of a surface possessing biocidal properties involved a polymer combination containing polystyrene (normally inactive) and block copolymers consisting of polystyrene combined with an anti-microbial block called poly(4-(1-(2-(4-methylthiazol-5-yl)ethyl)-1H-1,2,3-triazol-4-yl)butyl methacrylate), which

was decorated with methyl or butyl groups (PS-b-PTTBM). This blend yielded a highly positive charge material.

Likewise, one way to influence the adhesive properties of the polymer system is to blend a protein-repellent polymer, such as PEG, with other inert polymers, such as polyacrylic acid (PAA). This was achieved by developing brush-like films made with optimized ratios and molar masses of PEG and PPA.[98]

Blending polymers that repel microbes (biopassive) with those possessing biocidal properties allows for the creation of polymeric structures that demonstrate both resistance to biological elements and active microbe-killing capabilities (bioactive).[99] Additionally, combining one biocidal polymer with another enhances synergistic biocidal properties, significantly intensifying microbe eradication.

In all the methods above, some of the polymers with biocidal moieties are either not scalable to commercial production due to the cost, or the anti-microbial system can only be applied as a coating. Another limitation is that many of the inherently biocidal polymers would not be extrudable or injection moldable, as they contain moieties that make the polymer dissolve or swell in water. The mechanical resilience and wear of these coatings and moisture-induced tackiness of these are not studied or reported. These might create issues for practical use.

1.5.2 Leachable and non-leachable anti-microbial agents

Leachable anti-microbial agents are substances embedded into plastic articles that release anti-microbial features by diffusing or leaching, thereby stopping microbial growth in the surrounding environment.[100] The primary feature is being physically embedded in a matrix. An example that has been extensively studied is silver nanoparticles (Ag NPs). For centuries, silver has served as a biostatic agent. Upon exposure to moisture, an electrochemical process occurs,

releasing silver ions. These ions penetrate microbes, incapacitating their ability to function, proliferate, or reproduce. Advantages include continued protection and functioning against various microorganisms.[101, 102] A drawback is the loss of anti-microbial properties over time since the leaching will cause the depletion of the agent, especially in applications in contact with water. In addition, there have been quite some controversies about the use of Nano-sliver. For instance, some point to the risk of having a prolonged exposure to silver ions causing adverse effects on human health. Also, waste management is a concern when looking at these tons of silver disposed which may be spilled over to the surroundings.[103, 104] **Figure 6** shows a schematic diagram depicting the modes of action for "leaching" and "non-leaching" biocides.

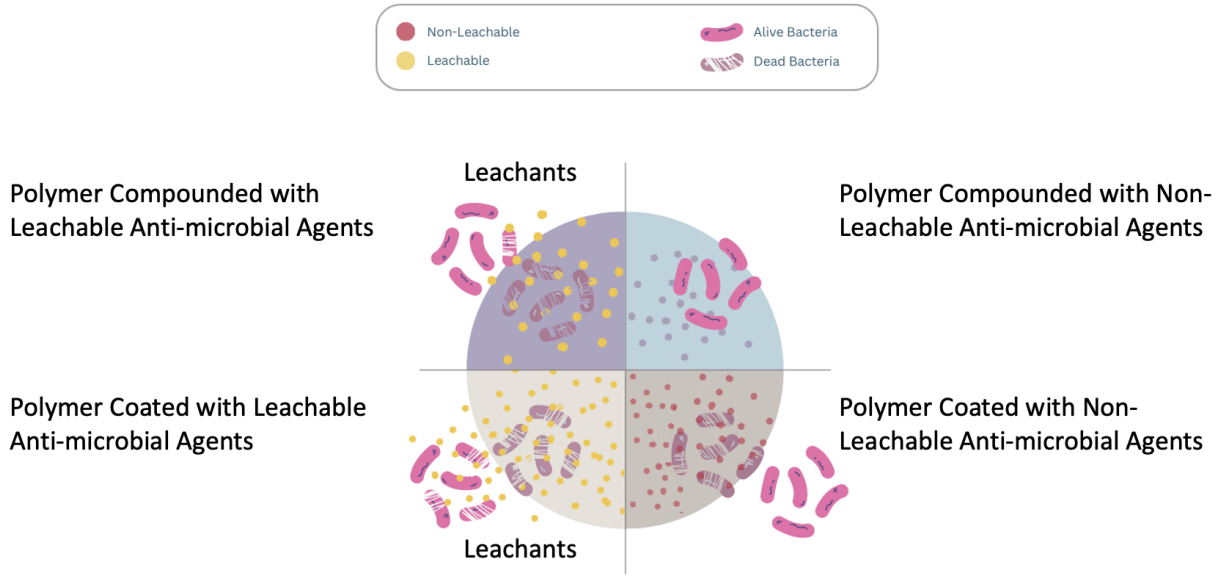

Figure 6. The mode of action for leaching and non-leaching anti-microbial agents when used in plastics through melt-compounding (left) and via thermal embossing (right).

To overcome these issues, non-leachable anti-microbial agents were sought. These agents, that cannot "spread" to the surrounding environment, they may function as coatings that remain on the surface of the article treated. Microbial killing therefore occurs by direct interaction with these substances on the surface of treated articles. The anti-microbial activity is thus confined to the surface of treated articles and does not leach or diffuse into the surrounding environment.[105]

This effect can be achieved through chemical embedding, and coatings are the primary implementations. Examples include Organo-silanes.[106] Advantages include long-lasting protection and a low risk of leaking to the environment and coating can be applied post-manufacture of the article. They are inexpensive and could be applied as a coating for plastics. Drawbacks are a limited range of anti-microbial protection when used in melt-compounding.[100]

Inorganic anti-microbial agents

Ag NPs

They are made up of nanoscale Ag. Applications include sterilization of medical and consuming products such as textiles and refrigerator surfaces.[107] Features include oligodynamic, high surface area to volume ratio, and possibly synthesizing into multiple shapes and sizes.[108] The toxicity of the material is reliant on the availability of biological or chemical coatings as well as their surface charges. They are mostly insoluble in water.[109] The ionic radius of Ag ions is 126 pm.[110] Toxicity is dependent on particle size. Most Ag NPs are toxic to humans since their small particles easily enter the human skin.[111] They work by disrupting cell walls and cytoplasmic membranes, denaturing ribosomes, stopping the production of adenosine triphosphate, eliciting the production of reactive oxygen species (ROS), membrane disruption, DNA replication interference, denaturing and perforating membranes.[112] The FDA has approved some Ag-based NPs for wound dressing and anti-microbial products.[113]

Cu NPs

They are made of nanoscale copper particles. They are used for anti-microbial purposes and porosity enhancement. Features include robust anti-microbial activity and a high surface area-to-volume ratio. They are not soluble in water. Cu has an ionic radius of 57 pm.[114] Cu NPs can be rated class 3, which is moderately toxic.[115] They work by generating reactive oxygen species

(ROS), which interferes with cellular function and leads to DNA damage.[116] The FDA approves several Cu-based compounds for particular purposes.

CuO NPs

They comprise nanoscale copper oxide. They are used as anti-microbial agents in industrial, biomedical, and agricultural fields.[117] They have a brownish-black color, effective anti-microbial activity for a broad range of pathogens and bacteria, are relatively inexpensive, have a longer shelf life, and have a significant surface area-to-volume ratio.[118] They are slightly soluble in water but up to 37.1-100.1 $mg \cdot kg^{-1}$.[119] Cu^{++} ions have an ionic radius of 73 pm.[120] They can be toxic to living organisms, causing ROS generation, cytotoxicity, oxidative stress, immunotoxicity, and genotoxicity.[121] They work by creating ROS that damages biomolecules and cell membranes.[122] Information on FDA approval is not available.

CaO NPs

They are made up of nanoscale calcium oxide. They are used in water purification, catalysis, anti-bacterial agents, adsorption, and purifying vehicle exhaust.[123] Properties include white powder, spherical shape, and high adsorption efficiency.[124] They are slightly soluble in water.[125] Calcium ions (Ca^{++}) have an ionic radius of 99 pm.[126] They are generally safe for humans in low concentrations but can cause respiratory issues when inhaled. The primary methods of action are ROS on its surface and the alkaline effect.[127] The NPs are not approved by the FDA, but calcium oxide is recognized as a safe substance that can be used in plants and animal products.[128]

MgO NPs

They have shown anti-microbial activity against different fungi, bacteria, and antibiotic-resistant strains. Uses include water treatment systems, food packaging, and healthcare

products.[129] They have enhanced stability, a high surface area, and potent anti-microbial activity. They do not fully dissolve in water but are slightly soluble at high pH levels (1.71 = mg L^{-1} at pH = 6.69).[130] The ionic radius of Mg^{++} is 0.72 pm.[131] They are generally considered safe (they are used as antacids), although long-term exposure may lead to lung irritation or injury.[132] They can disrupt cellular activity and release ROS. They have been approved by the FDA as a safe and functional anti-bacterial agent.[133]

$Mg(OH)_2$ NPs

These are NPs of inorganic compounds used as anti-acids. They can act against bacteria, fungi, and viruses including Covid-19. They are applied in medical devices, wound healing, and drug delivery systems. They have a large surface area, are biocompatible, and have good stability.[134] They are sparingly soluble in water and able to form colloidal suspensions. The ionic radius of Mg^{++} is 72 pm.[131] They are generally considered safe, although high concentrations can cause gastrointestinal complications. The mode of action involves activating ROS.[135] They are FDA-approved.

Cu-Infused $Mg(OH)_2$ NPs

They contain magnesium hydroxide incorporated with copper ions in their structure. They have enhanced anti-microbial activity due to Cu ions that possess inherent anti-microbial properties. Biomedical applications include wound dressings and implants. They are stable and biocompatible with $Mg(OH)_2$. $Mg(OH)_2$-based NPs are sparingly soluble in water at 0.00122 g/100 mL.[136] The ionic radius of the Cu ion is 73 pm, while that of Mg^{+} is 72 pm.[137] Cu^{+} is toxic at higher concentrations.[138] The mechanism is by releasing Cu ions, which can cause oxidative damage to microbial cells.[139] They are not currently approved as safe by the FDA.[140]

$CuCl_2$ NPs

These are an anti-microbial agents consisting of copper and chlorine ions. They are primarily utilized in water treatment, surface coatings, and medical devices. Unique features include a high surface area-to-volume ratio, increased reactivity, and enhanced stability. They are water-soluble and can be applied in aqueous environments.[141] The ionic radius for Cu ions is around 73 pm, while that for chlorine ions is 181 pm.[142] They are toxic to human cells.[143] Toxicity is dependent on concentration. The mode of action comprises cell membrane disruption, causing intracellular components to leak.[144] They can also cause ROS, causing damage to various cellular components. They are not FDA-approved.

TiO_2 NPs

They are made up of nanoscale titanium dioxide. Applications include toothpaste, paper, plastics, drugs, textiles, and cosmetics.[145] They restrict bacterial growth, have a high refractive index of 2.4, are transparent, and carry strong absorption of ultraviolet energy.[146] They are generally insoluble and resist dissolution.[147] They are potentially toxic due to their potential to induce liver and brain lesions in humans and lung tumors in rats.[148] Mode of action includes ROS, lipid peroxidation, cell wall damage, and attachment to biological macromolecules and intracellular organelles.[149] TiO_2 is approved by the FDA for use in food and drug-related products.[148]

ZnO NPs

The nanoscale particles are made of zinc oxide. They are primarily used to coat, paint, and in cosmetics. However, they can induce oxidative stress and trigger apoptosis.[150] Its properties include white-powdered, tetrahedral shape, thermochromism, and insolubility in water (between 0.3– 3.6 mg/L can dissolve).[151, 152] The material is insoluble in water. The ionic radius of Zn^{++} is

79.6 pm.[153] Toxicity of ZnO NPs is unlikely in humans because they rarely or minimally penetrate the stratum corneum and other skin layers.[154] According to Mendes et al. (2022), ZnO NPs are multi-target compounds that impact numerous microbe structures.[155] However, their primary site of action is by damaging the cytoplasmic membranes. It produces ROS, increasing membrane lipid peroxidation.[156] The FDA approved these NPs due to safety and non-toxicity in low concentrations.[157]

GO NPs

They are made of graphene oxide. GO agents are primarily used in cellular imaging, drug delivery, and cancer treatment.[158] Despite having a nanoscale size, the oxide induces oxidative stress and interacts with the cell membrane, making it toxic.[159] It is hydrophilic due to ketones, hydroxyl groups, and carboxylic acids on the graphene. It has a high specific surface area of about 890 m^2g^{-1}. It is also a semiconductor.[159] Since it is hydrophilic, the NPs usually dissolve in water, with the highest solubility of 6.6 μg/mL in deionized water.[160, 161] At particular concentrations, GO can be toxic to species such as earthworms and zebrafish.[159, 162] The mode of action of the material remains unclear despite extensive research. Suggested modes include oxidative stress generation.[163] The FDA has not approved the material as an anti-microbial agent, but there are approvals for cancer drug delivery systems such as PEGylated liposomal doxorubicin.[164]

Shape and size of NPs

The shape and size of NPs play a substantial role in the anti-microbial activity. Smaller NPs have a higher surface area relative to their volume.[165] This improves the interaction with microbes, providing better anti-microbial protection since microbes are more likely to be inhibited.[165] They are also more capable of penetrating microbes especially if the NPs have sharper edges. Smaller NPs which can create reactive oxygen species (ROS) allow higher

generation of ROS, improving the ability to kill microbes.[166] The shape also has an impact.[166] Shapes such as nanotubes cause physical damage to microbes by piercing membranes leading to deterioration and death.[167]

Soluble and non-soluble anti-microbial agents

Soluble anti-microbial agents, such as antiseptics, anti-parasitic, and antibiotics, dissolve in water.[168] Costs differ based on type, concentration, and quantity but are generally affordable. For example, Walmart sells a 32 oz. bottle of Equate 91% isopropyl alcohol antiseptic for $3.98 and Equate 32 oz. 70% isopropyl antiseptic for $2.96.[169] Advantages include proven effectiveness, availability in numerous formulations, and work for bacteria, viruses, and fungi. Cons include side effects and resistance, especially for bacteria.

Non-soluble agents do not need to dissolve in a liquid to be applied to a surface or object. They include metal surfaces, polymers, and metallic NPs.[170] Advantages include lasting longer and killing more types of microbes.[170] Cons include environmental risks and costs. Because they do not diffuse from the point of application there is no problem with creating a 'kill zone' in the proximity of the treated object, and, as noted earlier, the concentration of NP on a treated article does not diminish due to diffusion away from its point of application.

1.6 Polymer nanocomposites with biocidal metals and inorganic nanocrystals

In this concept, an extrinsic biocidal additive is blended with an inert polymer or with a biocidal polymer. Certain metals and inorganic crystals (often metal oxides and hydroxides) show biocidal properties. As mentioned above well-known examples of the former are Nano Ag and Nano Cu as well as carbon-based materials like carbon nanotubes and graphene. We also previously mentioned examples of inorganic crystals that show biocidal properties with copper oxide (CuO), titanium dioxide (TiO_2), magnesium oxide (MgO), magnesium hydroxide

($Mg(OH)_2$) and zinc oxide (ZnO). One approach to nanocomposites with these materials is to combine them with polymeric biocides. For example, biocidal Ag NPs[163], Cu NPs[164], or carbon-nanostructures[165] can be added to polymeric biocides such as PEG[166], PEI[167], zwitterionic PCBMA[168] or cationic poly(2-(tert-butylaminoethyl) methacrylate) (PTBAM)[169], to develop highly biocidal nanocomposites (**Table 1**).

Table 1. Studies involving polymer-based nanocomposites that demonstrate effective use against a range of microorganisms on different surfaces. In most studies, the polymer matrix chosen is not a common, inert thermoplastic but polymers that have biocidal properties, such as PEG, PEI, etc. Reproduced from [171], open access. Copyright (2021) Iulia Babutan, Alexandra-Delia Lucaci, and Ioan Botiz.

Blend/Composite	Configuration/ Nanostructure	Dimension	Anti-microbial Mechanism	Efficacy	Microbe of Interest	Ref.
PMMA/Ag, PTBAM/Ag	Nanofibers	40 nm diameter, 10 µm long	Bioactive reinforced	-	*E. coli, S. aureus*	[172]
PEI/Ag	NPs grafted on SAM	10-14 nm thick (total)	Bioactive reinforced	~6 log 0.86 log	*E. coli* *S. aureus*	[173]
PVDF-g-PCBMA/Ag	Pores/brushes	-	Bioactive reinforced	-	*E. coli, S. aureus*	[174]
PLA/PEG, PLA/PEG/Ag	Films; NPs	~40 µm thick 25 nm thick	Biopassive + bioactive	-	*E. coli, S. aureus*	[175]
P2VP-b-PEG	Smart micelles	60 nm (unloaded)	Bioactive		-	[176]
PEI/Cu	Positively charged NPs	34 nm radius	Bioactive reinforced	87% 96% 80%	*E. coli* *P.aeruginosa* *S. aureus*	[177]
Pectin-PEI-Cu	Films with Cu NPs	100 µm thick	Bioactive reinforced	-	*S.aureus, E.coli*	[178]
PDMEMA-MWCNTs	Nanotubes	26 nm diameter	Bioactive reinforced	42% -	*E.colli* *S. aureus* *E. coli*	[179]
MWCNTs-APPI/MWCNTs-APPI-Ag Nps	Nanotubes Ag NPs	15 nm diameter	Bioactive reinforced	96%/99% 96/99% 87%/83%	*B. subtilis* *S.aureus* *E. coli*	[180]
PE/PEG/GO-NH_2	Films	-	Bioactive reinforced	90%	*E.coli*	[181]

An example is anti-bacterial coatings for implantable devices.[182] Biocidal metals like Nano Ag (1-100 nm diameter) overcome the ability of bacteria to develop resistance because they operate with multiple and simultaneous anti-bacterial mechanisms. This reduces the chance of a bacterium developing mutations on multiple genes.[182]

1.7 Attraction between NPs and microorganisms due to electrostatic charges

Charge attraction between NPs and microorganisms serves a substantial role in anti-microbial activity.[183] NPs typically are positively charged[184], while the microorganisms have a negatively charged phospholipid membrane. When they interact, microorganisms are inhibited and die from different nodes of actions, such as the creation of ROS, electrostatic interaction, membranes intercut, and microbe resistance reduction, depending on the NPs nature.[185]

1.8 Mode of mechanisms of anti-microbial NPs

Nine different modes of action have been established to describe how anti-microbial NPs can kill microbes, as illustrated in (**Figure 7**). These modes of action will be described below. A particular emphasis on inorganic NPs mode of action is also described.

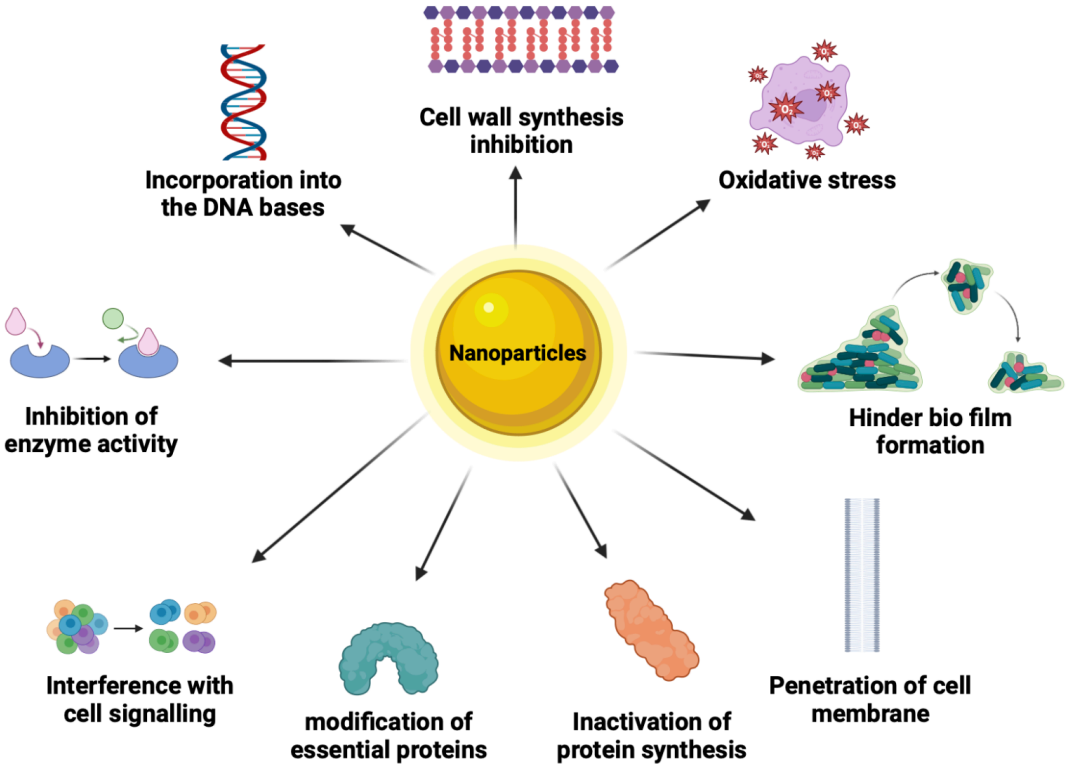

Figure 7. Summaries of the multiple mechanisms by which biocidal Nanoparticles can wreck bacterial cells. One or more mechanisms may operate with a given NPs. Modified from ref. [186]. Copyright (2014) American Scientific Publishers.

1.8.1 Cell wall synthesis inhibition

The cell wall of a bacterial cell includes the membrane and the peptidoglycan layer which is composed of long sugar polymers. The role of this peptidoglycan on the cell is to protect it from stress and maintain its integrity. The peptides within peptidoglycan are interconnected through cross-linking facilitated by trans glycosidase, aiding in its development. Further linking of glycine residues contributes to the durability of the bacterial cell wall.[187] Nevertheless, when NPs or beta glycopeptides are present, they specifically inhibit cell wall synthesis by impeding the cross-linking or assembly of peptidoglycan.

1.8.2 Oxidative stress

Aerobic bacteria rely on oxygen for the oxidation of nutrients to generate energy. Nonetheless, Reactive Oxygen Species (ROS) induce bacterial death by directly damaging lipids and proteins through oxidation. ROS can trigger non-oxidative mechanisms like autophagy leading to bacterial demise. Moreover, an imbalance in ROS levels creates oxidative stress, causing an accumulation of uncontrolled hydroxyl radicals.[188] These radicals, in turn, degrade nucleic acids, proteins, and carbohydrates, culminating in cell death.

1.8.3 Protein synthesis inhibition

Proteins are organic molecules in bacterial cells that have both structural and enzymatic roles.[187] NPs can disrupt the structure of protein molecules and thus their function in cell architecture and metabolism.

1.8.4 Inhibition of enzyme activity

Enzymes play crucial roles in numerous cellular functions. For instance, transpeptidase catalyzes the final stage of cell wall biosynthesis.[189] When anti-microbial NPs attach to the active sites of these enzymes, they diminish the compatibility between the enzyme and its substrate. Consequently, this inhibition prevents the enzymes from functioning, impeding essential cellular processes within the cell.

1.8.5 Hinder biofilm formation

Biofilms refer to intricate layers of matrices surrounding bacteria, serving the purpose of aiding bacteria in their survival within challenging or adverse environments.[190] Microbial cells that attach to a surface in a moist environment can survive and proliferate. When the microbial cell number increases, it leads to a biofilm formation, a polysaccharide matrix with embedded cells. Biofilms allow microbial cells to survive under harsh conditions and are 1000 times less

susceptible to most biocides. Therefore, a biofilm protects the bacteria from any form of stress. Toxins excreted from biofilms spread pathogenic and resilient infections and can lead to multi-resistant bacterial strains. NPs target any of the three stages of biofilm formation which are adhesion, maturation, and dispersal of the biofilm. For example, a NP can target adhesion. In such cases, the bacteria will not have the capacity to attach to a surface.

1.8.6 Interference with cell signaling

Cell-to-cell communication is important in coordinating the behavior of a group of bacterial cells. These behaviors within a set of bacterial cells are important in tasks such as antibiotic tolerance. Anti-microbial agents can target cell-to-cell communication, hindering the group's behavior towards tolerance to antibiotics.[191]

1.8.7 Modification of essential proteins

Cells rely on some essential proteins to carry out metabolism and other processes. By modifying essential proteins such as amino acids, a bacterial cell will lose the capacity to carry out processes such as biofilm dispersal.[192] Therefore, NPs can alter the configuration of the proteins resulting in the inactivation of the bacterial cells' functions.

1.8.8 Penetration of cell membrane

NPs affect the cell membrane by binding to it through electrostatic forms.[193] The results are changes in the potential of the cell membrane, loss of membrane polarity, and disintegration of the cell membrane. For example, Ag NPs cause pits on the cell membrane, causing increased permeability.[193] Consequently, increased permeability causes an imbalanced transport of ions in and out of the cell, causing cell death.

1.8.9 Incorporation into the nucleic bases

NPs can be incorporated into the nucleic bases, changing their configuration.[194] Nucleic acids are responsible for the coding of genetic information. Therefore, when NPs is incorporated into the bacterial cell, DNA cannot be transcribed which then inhibits protein synthesis, and hence the cells lose functionality.

1.8.10 Mode of action for inorganic NPs

As mentioned above, Ag exhibits biocidal properties against various bacteria, fungi, and viruses because of its diverse mechanisms of action. This includes the release of Ag^+ ions when in contact with water. The liberation of Ag^+ ions is influenced by various factors, including the dimensions and configuration of the NPs. Smaller NPs would have a large surface area to volume ratio and hence release more ions. Ag ions interact with -SH groups on bacterial cell surface because there is a large number of Sulphur-containing proteins in the bacterial cell membrane.[195] The released Ag^+ ions from Ag NPs can engage with phosphorus components in DNA, resulting in the deactivation of DNA replication.[195] Thus, silver ions (Ag^+) engage in detrimental interactions with proteins found in the microbial cell wall and membrane, resulting in disruptions to cellular transport systems, imbalances in electrolytes, membrane puncturing, loss of cytoplasmic organelles, modification of bacterial cell division, ultimately resulting in cell demise.[196] It is active against both Gram-positive and Gram-negative bacteria.[45, 46]

Another anti-bacterial mechanism caused by Ag^+ is due to the Reactive Oxygen Species (ROS) that it generates. ROS are highly reactive molecules and radicals formed from O_2 such as **peroxides, superoxide, hydroxyl radical, singlet oxygen, and alpha oxygen**. (**Table 2**) shows some of the ROS. While ROS is used as cell signaling molecules for normal biological processes,

the generation of too much ROS can damage multiple cellular organelles and processes. The ROS created by Ag^+ induces oxidative stress in bacterial cells.[195]

Table 2. List of various radical forms of reactive oxygen species (ROS) formed by NPs.

The Radicals (not stable)	The Non radicals (stable)
Superoxide (O_2•-)	Hydrogen peroxide (H_2O_2)
Hydroxyl (OH•)	Hypochlorous acid
Peroxyl, alkoxyl (RO_2•,RO•)	Ozone (O_3)
Oxides of nitrogen (NO•,NO_2•)	Singlet oxygen ($^1O_2$)

It must be remembered that while ROS generation by NPs may be effective against microbes, excessive amounts of ROS can do the same damage to human cells in the same way.

Ag NPs have been thus added to inert as well as biocidal active polymers. For example, it has been added in inert PMMA and in the polymeric biocide PTBAM (cationic poly(2-(tert-butylaminoethyl) methacrylate) to form nanofiber composites.[172] Both these Ag/nanofiber-based composites exhibited great anti-microbial performance against *Escherichia coli* (*E. coli*) and *Staphylococcus aureus* (*S. aureus*), but the PTBAM/Ag nanocomposite was naturally better as the matrix itself was a polymeric biocide. Ag has been added in zwitterionic PCBMA and has also been used to make polylactide (PLA)/PEG/Ag nanocomposites. Thus, the Ag reinforced the anti-microbial properties of the polymeric biocide PCBMA[174], and acted cooperatively with the anti-adhesive properties of PEG[175] polymers to form an effective anti-microbial nanocomposite. Like Nano Ag, Nano Cu also has strong anti-microbial properties, and thus, has been used with polymeric biocides and inert polymers.[197] Cu also kills bacteria by multi-mechanisms, including the release of toxic Cu ions[198] as well as inhibiting biofilm formation.[199] Details on these mechanisms can be found in the review of Tamayo et al.[197] Examples of the reinforcement of anti-microbial properties of polymers containing biocidal Cu include PEI/Cu and nanocomposites of pectin with Cu^{++} incorporated into PEI.

Among the inorganic crystals, TiO_2 disrupts bacterial cell membranes. It eliminates bacteria by creating reactive oxygen species (ROS) upon exposure to light. ZnO demonstrates anti-bacterial effects with minimal toxicity to mammalian cells. Its mode of action involves causing damage to the lipids and proteins found in the bacterial cell membrane and triggering ROS production. ZnO NPs exhibit efficacy against bacterial spores resistant to high temperatures and high pressures.[45, 46]

Motoike et al.[200] compared the activity of dolomite powder, CaO, MgO, and $Mg(OH)_2$ against the avian influenza virus strain A/whistling swan/Shimane/ 499/83 (H5N3). They studied the effect of heating the powder and found a relation between the crystal sizes of the minerals and the anti-viral activity. Dolomite is a natural mineral composed of calcium and magnesium carbonates ($CaMg(CO_3)_2$) and it can be decomposed to MgO and CaO.

$$CaMg(CO_3)_2 \rightarrow MgO+CaCO_3+CO_2 \text{ at } 750\text{-}800\ ^\circ C \quad (1)$$

$$CaCO_3 \rightarrow CaO + CO_2 \text{ at } 900\text{-}1000\ ^\circ C \quad (2)$$

Both MgO and CaO have strong activity against viruses. CaO and MgO, obtained by the thermal decomposition of dolomite above 800 °C had strong anti-viral activity, but the effect was weakened when the temperature reached beyond 1400 °C, the effectiveness of CaO surpassed that of MgO but quickly hydrated in the presence of water which reduced its anti-viral activity. Conversely, the hydration process of MgO occurred more slowly under identical conditions. When comparing MgO and $Mg(OH)_2$ separately, it was observed that MgO exhibited a greater antiviral effect than $Mg(OH)_2$.

MgO NPs create ROS, but they also release some Mg^{++} cations; however, Mg^{++} does not have similar destructiveness as Zn^{++}[201]. Leung et al. investigated the destruction of *E. coli* bacterium by MgO NPs and found that there were non-ROS mechanisms also. (**Figure 8**) below

displays Leung et al.'s TEM images of *E. coli* bacteria showing cell membrane damage, after treatment with three different MgO NPs. There was no evidence of MgO NPs penetration into the cells. As these authors did not find evidence of lipid peroxidation (oxidative stress), they concluded that non-ROS based mechanisms exist for this combination (MgO and *E. coli*). They hypothesized that the damage was due to a combination of the attachment of the NPs to the membrane and the effects of pH change, and Mg^{++} release.

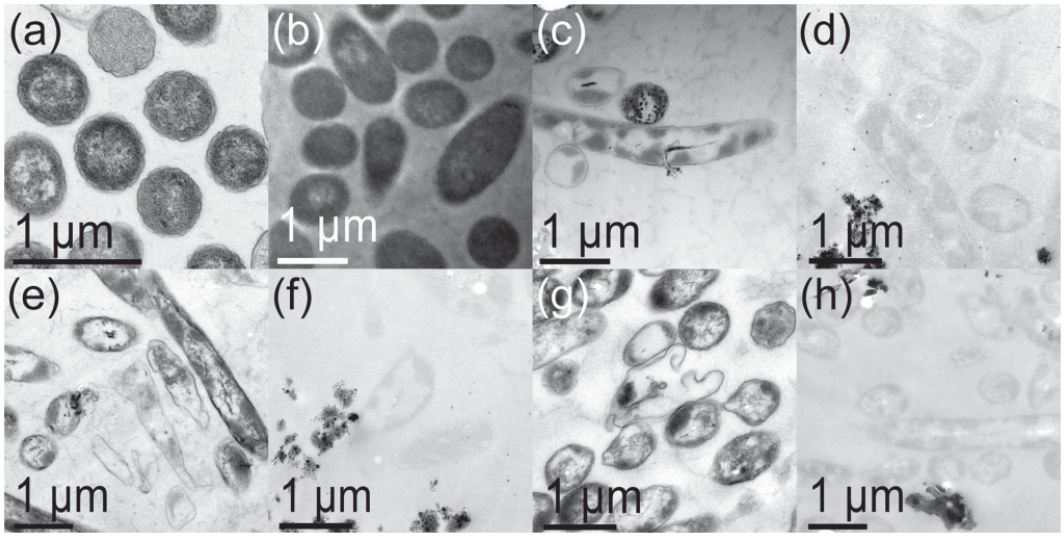

Figure 8. Transmission electron microscopy (TEM) images depict E. coli bacteria post UV and/or MgO nanoparticle exposure: a), b) Control images with and without staining; c), d) Images of 1-MgO with and without staining; e), f) Images of 1A-MgO with and without staining; g), h) Images of 2-MgO with and without staining. Reprinted with permission from ref. [201], John Wiley and Sons License No. 5570460962564. Copyright (2013) Wiley-VCH Verlag GmbH & Co. KGaA, Weinheim.

The anti-microbial activity of MgO NPs (**Figure 9**) was studied against a variety of microorganisms such as (*C. jejuni, E.coli, and S.*Enteritidis) at 6 different time intervals (0, 2, 4, 6, 8, and 10 h).

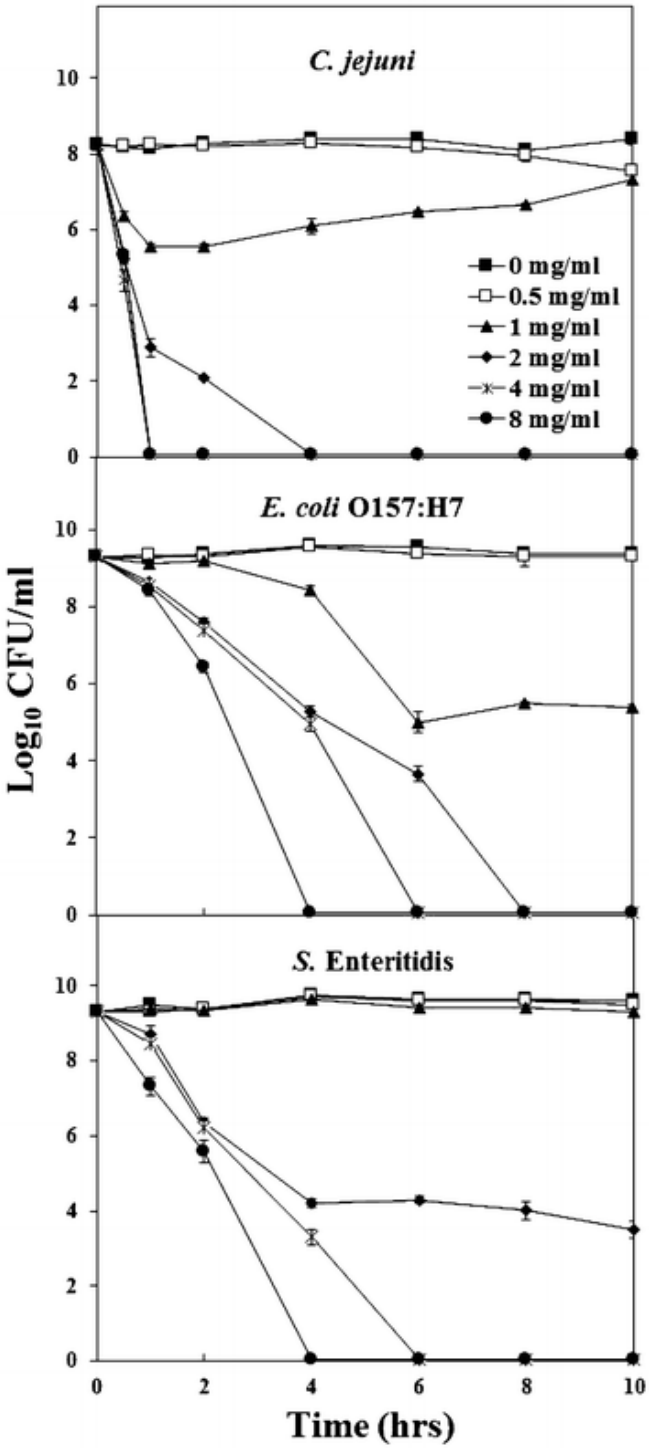

Figure 9. The anti-microbial impact of MgO nanoparticles against C. jejuni, E. coli O157:H7, and S. Enteritidis was evaluated. Different concentrations of nanoparticles were administered to approximately 10^8 CFU/ml of C. jejuni and 10^9 CFU/ml of either E. coli O157:H7 or S. Enteritidis. Subsequently, at various intervals following treatment, viable cell counts were determined by culturing bacterial colonies on MH agar plates. Each CFU/mL value represents the average from six separate replicates. Reproduced from ref. [202], open access. Copyright (2016) Yiping He, Shakuntala Ingudam, Sue Reed, Andrew Gehring, Terence P. Strobaugh Jr, and Peter Irwin.

He et al.[202] reported the effect of ZnO on the three most common foodborne pathogens *Campylobacter jejuni (C.jejuni)*, *E.coli* O157:H7, and *Salmonella*. These bacteria reside in the intestinal tracts of birds (e.g., chicken) and cattle.[4, 5, 203] These pathogens can be transferred to food throughout the stages of harvesting, processing, distribution, and food preparation. Contamination with these has been found in meat, dairy products, and other foods. In this work, a suspension of ZnO nanocrystals was added to bacterial broths of these three pathogens with a redox dye that changed color. Metabolically active cells reduced the non-fluorescent blue resazurin dye to fluorescent red resorufin. Inactive cells do not undergo resazurin reduction, indicating the occurrence of cell death (no color change from blue indicates the microbes are dead).

He et al.'s[202] SEM images (**Figure 10**) showed the untreated cells of all three bacteria had intact and smooth surfaces. The cells treated with sub lethal doses of MgO displayed deep craters on their membrane surface. The shortening of the cells suggested there could be some leakage of the cellular contents caused by the treatment. These authors showed that oxidative stress was a mechanism for the destruction of bacteria. They showed and measured hydrogen peroxide released in MgO suspensions, and the incapacitation of the cells was linked to this. They identified several mechanisms underlying the action of MgO NPs on bacteria: (1) MgO NPs generate a consistent level of hydrogen peroxide (H_2O_2) when in suspension, causing oxidative stress in cells; (2) physical contact between the NPs and the bacterial surface disrupts the bacterial membrane, resulting in membrane leakage; (3) elevated concentrations of NPs cause substantial membrane damage, release of cellular contents, irreversible oxidation of biomolecules such as DNA, proteins, and lipids, ultimately leading to cell death.

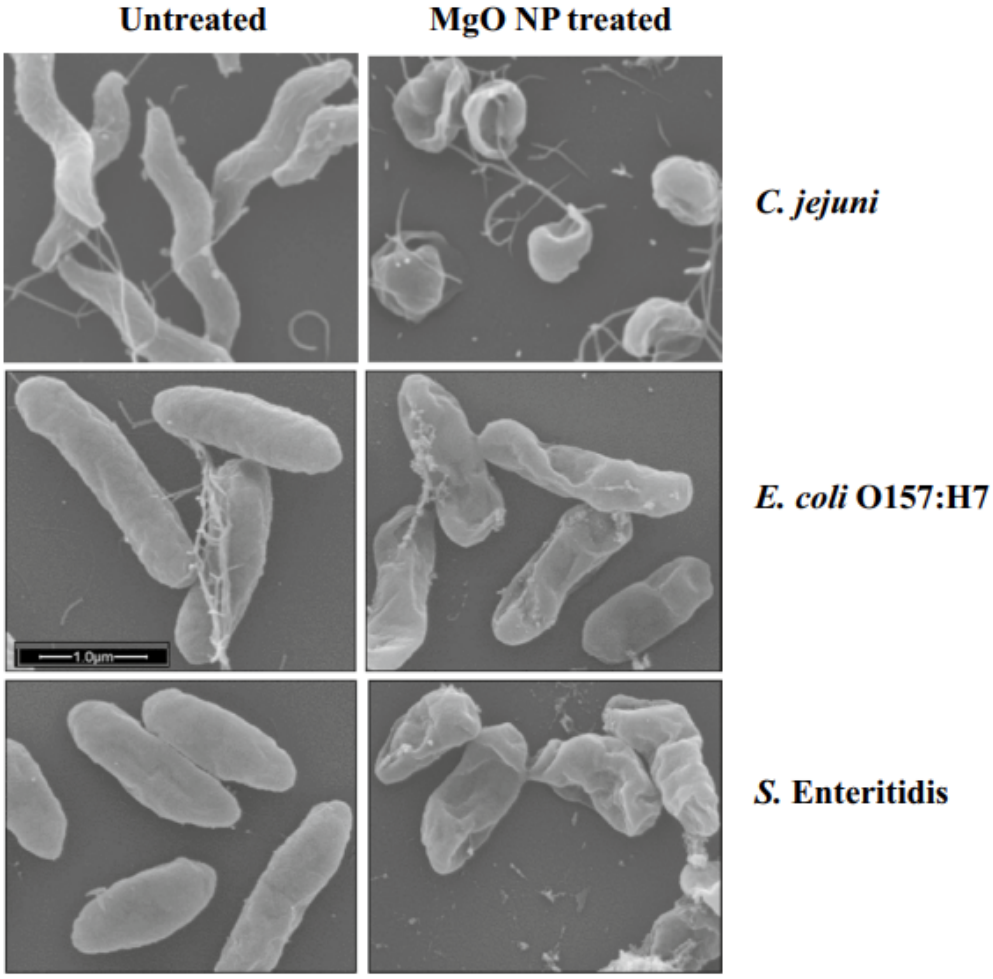

Figure 10. Scanning electron micrographs depict the bacterial cells of C. jejuni, E. coli O157:H7, and S. Enteritidis. SEM images were captured from treated bacterial cells of C. jejuni, E. coli O157:H7, and S. Enteritidis (right panel) subjected to 2 mg/mL MgO nanoparticles for 8 h. The control cells (left panel) were incubated under identical conditions without the addition of nanoparticles. Reproduced from ref. [202], open access. Copyright (2016) Yiping He, Shakuntala Ingudam, Sue Reed, Andrew Gehring, Terence P. Strobaugh Jr, and Peter Irwin.

Aqua Resource Corp. has developed $Mg(OH)_2$ Nano platelets which they claim have strong activity against bacteria, fungi, and viruses. They have also developed NPs of copper-infused magnesium hydroxide (Cu-infused $Mg(OH)_2$) which is even more potent, and they have shown over 90% kill against the COVID-19 virus in 4 h. The information on Aqua's biocidal $Mg(OH)_2$ and Cu-infused $Mg(OH)_2$ NPs is not available in the open literature, but some information is disclosed here with their permission.

Aqua reports that $Mg(OH)_2$ NPs do not work by leaching ions or penetrating the cell. They kill by contact of the platelets with the cell (**Figure 11**). These results are consistent with those of other groups (see **Figure 8** and **Figure 10**).

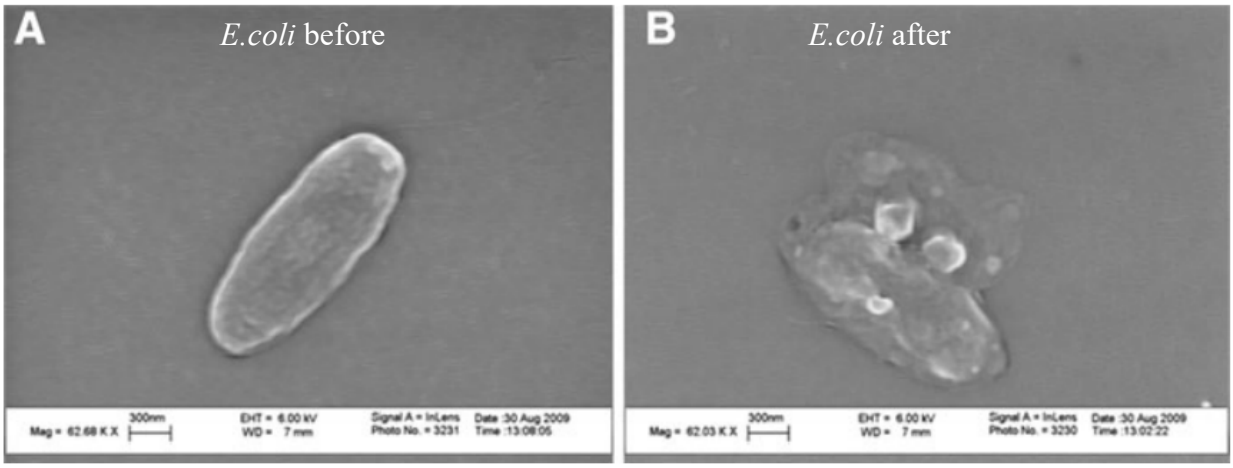

Figure 11. SEM images of E. coli cells before (A) and after (B) exposure to a 2 mg/mL solution of $Mg(OH)_2$ nanoparticles for 5 h. Reprinted with permission from ref. [204], Springer Nature License No. 5570470387084. Copyright (2023) Springer Nature.

For oxides of Cu, Ti, Zn, and Ag, and Ag elements, metal, metal ions are generated, and these diffuse to the microbes and interfere with and kill them through some of the mechanisms mentioned earlier. (**Figure 12**) shows an illustration of the ionic leaching mechanisms for some types of NPs.

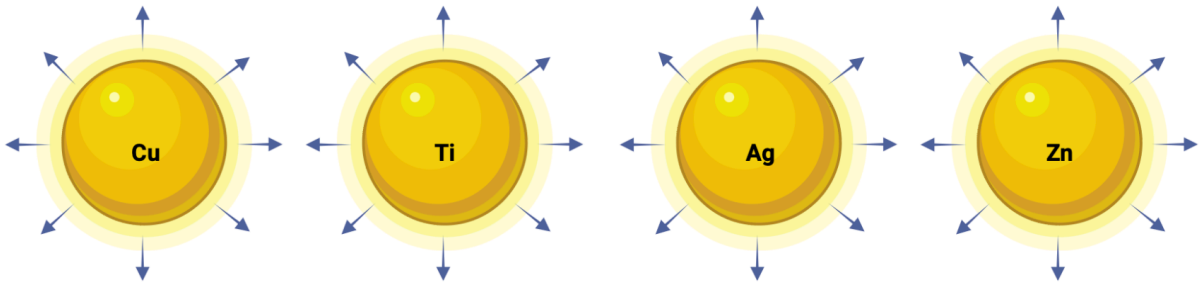

Figure 12. Particles with ionic charge diffusion to kill the microbes.

For $Mg(OH)_2$, according to Aqua[204], the dominant killing mechanism is by contact of the microbes with the crystals (**Figure 13**), and there is no outward diffusion of ions. Some semiconductor NPs generate ROS, and this damages the bacterial cells.

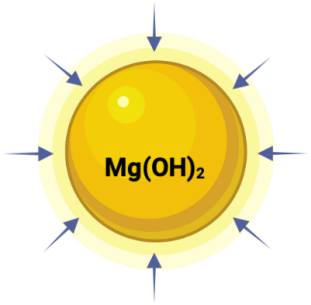

Figure 13. Shows the killing mechanisms of $Mg(OH)_2$ which requires direct contact with the microbes.

In the case of the copper-infused $Mg(OH)_2$, Aqua anticipated the extra potency because both methods could operate together: leaching of Cu ions and ROS from $Mg(OH)_2$ (**Figure 14**).

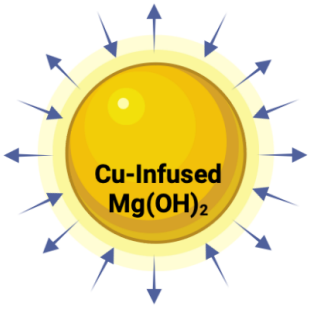

Figure 14. Shows the anticipated killing mechanisms of Cu-infused $Mg(OH)_2$ which kill microbe by at least two different modes of mechanism.

Besides the inorganic metal oxides and metals, organic nanomaterials like carbon nanotubes (CNTs)[179], graphene (Gr)[205], graphene oxide (GO)[206], and reduced graphene oxide (RGO)[207] kill microbes[208]. Three mechanisms (**Figure 15**), wrapping and choking of the microbe by the ultra-thin graphene layers, insertion due to a "Nano-knife effect", and oxidative stress due to ROS, have been proposed by different authors to explain the anti-microbial action observed with graphene materials.[209] Zou et al.[210] reviewed the mechanisms of the anti-microbial activities

of graphene and point out that while the effect is undeniable, the mechanisms proposed are controversial because of inconsistent experimental designs.

Different authors have proposed identical mechanisms to explain opposite experimental results and multiple theories of mechanisms have been suggested to elucidate a particular phenomenon. Wang et al.[23] showed theoretically that a three-layer graphene sheet would be less effective than a monolayer sheet of the same lateral size to pierce through the lipid bilayer of the microbe (Nano knife). On the other hand, Mangadlao et al.[211] showed increasing the number of layers in GO films resulted in stronger anti-microbial activity against *E.coli*. According to their findings, anti-microbial activity is also caused by surface characteristics influenced by the quantity of layers. Thus, from these different works, the picture that emerges is that both the surface and the sharp Nano edges of graphene influence anti-microbial activity.

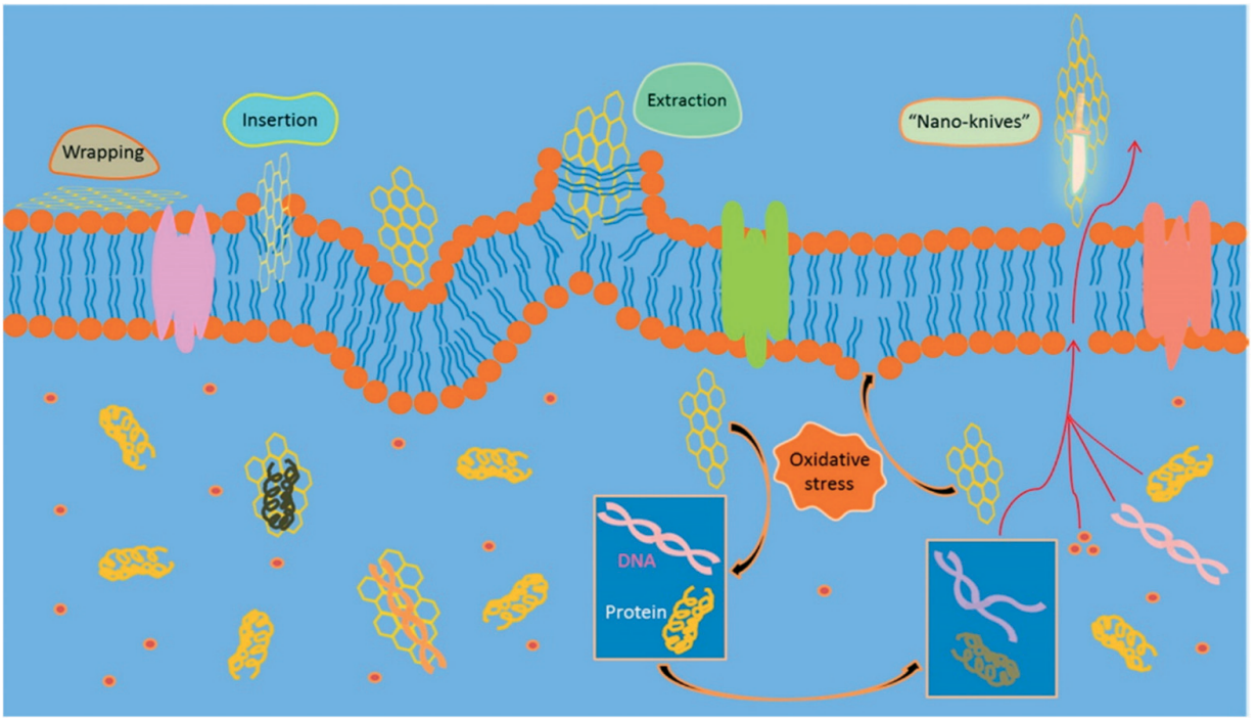

Figure 15. Mechanisms of the anti-microbial activities of graphene materials (GMs). Reprinted with permission from ref. [212], Copyright (2016) American Chemical Society.

1.9 Broad-spectrum or narrow-spectrum anti-microbials, and shape of micro-organisms

Zou et al. note that besides the intrinsic anti-microbial properties of graphene materials, the experimental surroundings (i.e., liquid, or solid state, aerobic or anoxic conditions, on a plastic or a metal, and in vitro or in vivo environment) and selected micro-organism genera (i.e., Gram-positive, or Gram-negative, round, or rod-shaped) should be considered in assessing the anti-microbial potency.

1.9.1 Bacteria

Single-cell, microscopic organisms usually measure between 1-2 um.[213]. Their types depend on shape: spirilla (spiral), cocci (spherical), bacilli (rod), vibrio (comma-shaped), and spirochetes (corkscrew).[214] The severity of bacterial infections ranges from non-harmful (many live in healthy human bodies, for example, *lactobacillus* and *bifidobacterial*) to potentially fatal (such as *H. pylori* and *S. pneumonia*).[215]

NPs may not be as useful as chemical bleach which destroys all microbes, but, when specific organisms are the problem, a nanocomposite solution has value. The same considerations also apply when assessing other anti-microbial nanomaterials like metal oxide NPs and metal NPs.

According to cell shape, bacteria are classified as coccus (spherical), bacillus (rodlike), spiral, or filamentous depending. The anti-microbial potency may depend on cell shape as well. An anti-microbial that kills many types of microorganisms would be the most desirable. The inhibition of various bacterial elements (such as the cell wall, cytoplasmic membrane, and chromosome) is greatly influenced by the shape or structure of specific microorganisms. Among most pathogenic microbes, while the cell wall/membrane, cytoplasm, and nucleus share similarities, their components and configurations remain distinctive. For instance, Gram-negative bacteria like *E. coli* and *P. aeruginosa* possess a thin peptidoglycan layer (approximately 2−3 nm)

situated between their inner and outer cell membranes. In contrast, Gram-positive bacteria such as *S. aureus* and *Staphylococcus epidermidis* (*S. epidermidis*) exhibit a thicker peptidoglycan layer (ranging from 20 to 80 nm) within their cell wall, and not all anti-microbials are equally effective with such bacteria.

1.9.2 Fungi

Fungi are another type of microbe that affects polymers. They are a type of eukaryotic microorganism between 4 -100 micrometers that get nutrients from organic matter.[216] Types include yeast, molds, and smuts.[217] Even though most fungi are harmless, there are some dangerous fungi, such as *Aspergillus* and *Cryptococcus*, which can affect breathing in humans and animals and cause severe sickness. The size and shape of fungi differ depending on the type. For example, yeasts are spherical and have a diameter of 3 - 5 μm.[218]

1.9.3 Viruses

Whereas bacteria are living microorganisms, viruses are technically inert chemical Nanoparticles (i.e. non-living) that acquire replication capability when inserted inside a living organism. These are microscopic pieces of genetic information enclosed in a capsid that assumes a helical or icosahedral shape and is mostly between 20-100 nm, but some can reach 1000 nm in length.[219] They are usually more dangerous than bacteria. Famous types include influenzas, retroviruses, herpesviruses, and coronaviruses.[214] Some viruses, such as *Ebola* and *Zika*, can be fatal to humans. Antibiotics are not effective for viral infections.

1.10 Anti-microbial testing protocols

The test methods to measure the survival of micro-organisms are set up under specific physio-chemical conditions, and their relevance or non-relevance to actual practical conditions needs to be borne in mind. The anti-microbial testing protocols for testing anti-microbial properties

on polymer include several procedures, which depend on the type of microorganism being viral, bacterial, or fungal materials that are being tested. ISO standards explore the assessment of anti-bacterial activity on non-porous surfaces such as plastics. One method is direct inoculation, explained in ISO 22196: 2011.[220] Parameters that must be observed include determining test microorganisms, growing them in a liquid culture medium, and allowing contact between bacteria and products. Additional steps include inoculation through swab, immersion, or touch transfer (swab), removing the bacteria, incubating the material to facilitate bacterial growth, sampling, and colony counting, and data reporting and statistical analysis.[221] Another method is the agar diffusion method, explored in ISO/TS 16782: 2016. It involves transferring anti-microbial agents via diffusion from a chromatogram to an agar plate. After diffusing for a few minutes, the chromatogram is removed, and the plate is incubated.[222]

ISO 21702 is a protocol designed to test the anti-viral properties of plastics and non-porous materials. It comprises loading a pre-determined virus concentration on treated and reference surfaces.[223] The next step is leaving the surfaces in a humidified chamber at room temperature for about 24 h. Surviving viruses are obtained and washed with liquid media.[223] The recovered amount of infectious virus is then measured, and its infectivity assessed, allowing a researcher to compare the anti-viral properties of the treated surface compared to the reference surface.[223]

ISO 16256: 2021 provides an international standard for testing the activity of anti-microbial agents against disease-causing yeast fungi. The first step is the preparation of yeast cultures, broth medium, and anti-microbial agents. Then, one inoculates the yeast into the medium. The cultures should be incubated for a particular timeframe. The step suggests determining the agent's minimum inhibitory concentration (MIC). The last step is analyzing MIC results, which

can be done using EUCAST or CLSI. EUCAST involves spectrophotometrically calculating yeast growth after incubation, while CLSI involves visual assessment of the growth.[224]

1.10.1 In vivo testing method

In vivo testing comprises performing tests, procedures, and experiments on or in living organisms.[225] Concerning microbial polymers, the testing is used to evaluate the effectiveness of the protection offered by anti-microbial polymers. Features include complex interactions and practical settings.[225] The advantages are specificity and detail and mirroring real-life situations, while disadvantages include higher costs, increased complexity, and taking longer time.[225]

1.10.2 In vitro testing method

In vitro testing comprises performing experiments in controlled lab settings, usually involving isolated microbes, to assess the protection offered by anti-microbial polymers or coatings.[225] The setting allows researchers to explore how anti-microbial materials interact with test organisms.[225] Features of in vitro testing include isolation and simple interactions.[225] Advantages include cost-effectiveness, speed, reliability, and simplicity.[226] Disadvantages include the inability to capture the innate complexity of organ systems, limited evaluation of impacts, and challenges in simulating the impacts of long-term exposures.[227]

The real understanding of the test method used enables control of the growth of micro-organisms in real situations such as a plastic surface (packaging film, medical tool, etc.). Whether the Nanocomposite will work in an actual device requires correlating the test with the design of the article. Further for practical use, plastic nanocomposites should not be harmful to human cells if the application is used for healthcare or food packaging.

The survey of the literature shows there is likely to be uncertainty about the mechanism (especially when there is more than one). The knowledge across disciplines that are needed to

interpret the results is a factor in the field of anti-microbial Nanocomposites, which can lead to contradictory explanations for the mechanism.

1.10.3 Anti-microbial plastic results variation

There is notable variation in anti-microbial results for polymeric and microbial surfaces, and they can be attributed to reasons such as testing methodologies, type of anti-microbial agents, environmental settings, solubility, hydrophilic, and exposure time.[228-230] For example, results of how much anti-microbial protection is offered by anti-microbial coating on a polymer such as chitosan may differ due to the environment exposed.[230] Chitosan from a dumpster is likely to contain a different microbe concentration than from another dumpster, leading to varying results of anti-microbial protection offered by coating.[230] Hydrophilic properties can also contribute to the variation. Hydrophilic surfaces attract water, while hydrophobic ones repel water. Since water is vital for microbe growth and development, hydrophilic surfaces are more likely to contain more microbial growth.[231] The type of agent is also relevant. Leachable agents release anti-microbial compounds from the polymer matrix, while non-leachable ones do not since they are embedded within the polymer where no direct interaction would happen between the NPs and the microbes. They offer varying degrees of protection over time. As a result, testing for microbial activity may have vastly different outcomes.[232] The solubility of an agent also contributes to the variation. Soluble agents may be more effective when applied to a surface since they kill all existing microbes they interact with.[233] However, they dry away shortly afterward, lessening anti-microbial protection. Non-soluble ones kill existing microbes, and those come into contact with a surface later. Therefore, the results may differ. Exposure time also matters. The longer the exposure times, the higher the likelihood of microbes being killed even when using fewer concentrations.[234] Thus, the testing method has to be intelligently matched to the anti-microbial/plastic system being

investigated and care has to be taken that the test method does not create the conditions for a desirable anti-microbial result.

1.11 Toxicity

Testing for NPs is critical for protecting human safety and the environment. Given the health risks of NPs, popular methods of testing their impact include lactate dehydrogenase and endotoxin signaling to ROS detection and apoptosis, with no specific approach in the numerous protocols.[235] As a complementary test, experts conduct a spectroscopic exam to assess the permeation of the epithelial barrier and determine the extent to which NPs deposit themselves in living cells.[235] The procedure comprises preparation, selecting the test surface, exposure, evaluating the impact of the particles on the surface, assessing the effect on particles, and data analysis.

1.12 Anti-microbial market size

The anti-microbial polymer market has experienced significant growth in recent years. According to Fortune Business Insights (2023), the worldwide anti-microbial polymer market size was $ 41.2 billion in 2022, $ 43.9 billion in 2023, and estimated to reach 73.7 billion by 2030.[236] The increasing demand for anti-microbial polymers can be attributed to numerous advantages compared to untreated plastics, which are attacked by algae, fungi, and bacteria. The increasing demand can also be attributed to better performance, durability, and diverse applications. The use of polymers will increase as adoption in automotive manufacturing and packaging grows. The recent Covid pandemic which was of global reach has also spurred interest in methods to prevent the spread of microorganisms.

1.13 Conclusion

This review has covered various uses of polymers for anti-microbial control. In one aspect, polymers were hosts for storing biocide/antibiotics, for controlled and targeted drug release. This method is useful when the person is already infected. Another type is "polymeric biocides" which have moieties in the polymer chain capable of killing microbes. Further, the adhesion of microbes to object surfaces is prevented by engineering the surfaces which prevents the growth of microbes in areas handled by people. Biocidal polymers are nanocomposites with inorganic crystals capable of microbe destruction by multiple methods. They could be a viable alternative to antibiotics and disinfectants. With biocides that show multiple mechanisms of killing like Ag^{+}, the pathogens cannot develop resistance as they can with antibiotics.

Medical devices, implants, wound dressings, and contact lenses require microbe-free surfaces, and coating them with polymers possessing anti-adhesive and/or anti-microbial properties is one of the approaches to rendering the required microbe-free properties. Design choices include the synthesis of polymers with only anti-adhesive (bio-passive) or anti-microbial (bioactive) properties. Further, combining both methods is possible. However, in most of these approaches, the polymers are not standard commodity plastics used for fabricating engineered articles. The biocide-releasing and biocidal polymers (like PEG, PEI, etc.) described in the literature can often be applied only as coatings to both polymer and non-polymer surfaces.

1.14 Research goals

As a result of the comprehensive review of anti-microbial agents, several types of anti-microbial agents were reported such as natural, organic, and inorganic. Some natural anti-microbial substances may affect an individual's health and, in some cases, act as a poison since they are endocrine disruptors that are normally associated with developmental and reproductive

harm.[237] Organic anti-microbials, such as lactic acid, play a vital role in the production of food for animals and the protection of public health, while the irresponsible use of these products may cause anti-microbial resistance.[238] This is one of the disadvantages of using organic anti-microbial.[237] Inorganic anti-microbials, such as Longbei inorganic antibiotic powder, also play an essential role in our society. They can be used on farm and home equipment to prevent the spread of viruses and bacteria since they damage the physical features of the bacteria and viruses.[239] However, these agents typically contain some chemicals that might harm human health if they are toxic.[237]

Inorganic anti-microbial materials have been classified as "leachable" and "non-leachable".[239] Leachable anti-microbial agents, such as silver and copper are incorporated into plastics via melt-blending. Such leachable anti-microbial agents exhibit their anti-microbial properties by the release of the agents from polymers via leaching to the surroundings. Unfortunately, leachable anti-microbial agents are often considered to be toxic to human cells and cannot be used at high concentrations, especially in food contact applications.[240]

The direction of this work is to use standard plastics (like PP, PE, PC, PET, etc.) which are extruded into sheets to make packaging materials, and injection molded to make engineering articles, in such a way that they have anti-microbial surfaces. For this, the aim is to use the nanocomposite route, starting with $Mg(OH)_2$ nanoplatelets. In return, reduces the microbe accumulation potential of key items that are used by the general public. For example, door handles, fridge handles, handlebars of supermarket shopping carts, hand straps in metro railway carriages, surfaces in hospitals, and surfaces in bathrooms, which are moist and warm, and are prone to grow molds. Food packaging materials like films and sheets are exposed to manual handling and therefore are potential sources for ingestion of microbes into humans. Also included is the

possibility of using microbe-killing woven and non-woven fabrics in producing medical masks. This need has been highlighted as a result of the pandemic caused by the COVID-19 virus. The presence and accumulation of the COVID-19 virus on surfaces and its role in spreading disease is topical and needs preventive measures besides vaccinations.

In this work, we are interested in polymer articles that give anti-microbial inhibition by (i) preventing the attachment of microbes to surfaces (anti-adhesive mechanisms), (ii) having active biocides on the polymer surface for killing microbes, and (iii) possibly a combination of (i) and (ii). The method of incorporating biocidal inorganic NPs like $Mg(OH)_2$ and Cu-infused $Mg(OH)_2$ in commodity plastics during the device fabrication stage is a challenge, due to the killing mechanism of these biocides needing direct contact of the NPs with the microbes. Device fabrication methods include sheet extrusion, production of filament and fabrics, and shaped articles by injection molding and 3D printing. It will be shown that not all these fabrication methods work with such biocides as they require direct contact with the microbes. For such biocidal NPs to work, they have to be dispersed and secured at the surface of the plastic articles during their fabrication. Hence, it is a fabrication challenge. As part of the scope of work, a test method to check any decrease in the anti-microbial activity of the plastic article with the anti-microbial crystals was developed. This was critical. Although there are some standards available, there are a number of issues with them. Finally, the mechanism of destruction of microbes by inorganic crystals like $Mg(OH)_2$ and Cu-infused $Mg(OH)_2$ was explored.

In chapter 2, a complete design of the experiment was conducted to study the water contact angle on different polymeric sheets (PP, PE, PET, and PC), and to investigate the effect of surface preparation (plasma treated, non-plasma treated, and coated sheets with anti-microbial $Mg(OH)_2$ nanoparticles from an aqueous suspension). Whether the suspension spreads on the plastic surface

or collects as droplets on it determines the uniformity of deposition of the nano crystals after drying. The higher the water contact angle, the more hydrophobic the surface will be. The hydrophobic surface will cause a non-uniform coating due to the intrinsic wetting issue. Additionally, the hydrophobic surface will add a layer of difficulties when the surface is tested for anti-microbial activity because the bacterial cultures are usually prepared in aqueous solution, and this might cause weak repeatability and reproducibility.

In chapter 3, a new approach for fabricating anti-microbial polypropylene (PP) surfaces with (i) leachable copper (II) chloride dihydrate ($CuCl_2.2H_2O$), and (ii) non-leachable magnesium hydroxide ($Mg(OH)_2$) biocides, is reported. The fabrications were conducted via two methodologies: (i) melt-blending and subsequent injection molding of compounded biocide additives with PP and (ii) thermal embossing of anti-microbial agents on the surface of a PP substrate. The overall properties of the various PP samples will be characterized as follows: (1) the morphology of PP samples are characterized using the SEM and EDX analysis to study the dispersity between the NPs and PP for both melt-compounded and thermal embossed samples, (2) the thermal properties are characterized using the DSC and TGA methods to investigate the thermal stability of the developed samples, (3) the anti-microbial properties were evaluated against *E. coli* K-12 MG1655 for 0, 4, and 24 h, (4) the rheological properties for the melt-compounded samples were studied using the melt flow index (MFI) techniques, (5) the density of various PP sample was studied using the density gradient column, (6) the mechanical properties were assessed via the tensile and impact tests, (7) the barrier properties were studied using the OTR and WVTR methods, and (8) the leachability of the anti-microbial agents was studied using the UV light transmission technique.

In chapter 4, a study of the anti-bacterial and anti-viral activities of $Mg(OH)_2$ and Cu-infused $Mg(OH)_2$ when incorporated with PP via two methodologies (i) melt-blending and subsequent injection molding of compounded biocide additives with PP, and (ii) thermal embossing of anti-microbial agents on the surface of a PP substrate, will be discussed. The morphology of the anti-microbial nanoparticles and the dispersion of the nanoparticles within various PP samples is characterized via SEM and EDX. The thermal properties were studied via DSC and TGA techniques. The anti-microbial properties were evaluated against *E. coli* K-12 MG1655 for 0, 4, and 24 h. The anti-viral activity of the NPs was studied in aqueous liquid suspensions against SARS-CoV-2, and the mode of action was investigated on neat NPs and PP samples that were thermally embossed with NPs.

In chapter 5 give a comprehensive conclusion and a future recommendation on how to handle safely the anti-microbial NPs, and how to apply commercially the thermal embossing methods on polymeric articles.

CHAPTER 2: STATISTICAL ANALYSIS OF WATER CONTACT ANGLES OF SEVERAL TYPES OF POLYMERIC SHEETS

2.1 Objective

The objective of this chapter is to investigate the effect of the surface preparation methods (plasma-treated, non-plasma-treated, and coated sheet with anti-microbial $Mg(OH)_2$ nanoparticle) of several polymeric sheets (PP, PE, PET, and PC) on the water contact angle. This work was undertaken because of the biocide $Mg(OH)_2$ is obtained from Aqua Inc. as an aqueous suspension of nano platelets. The spreading of the suspension is different on various plastics. After drying, one can get a uniform deposition if the suspension spreads, or a patchy deposition if the liquid collects into globules on the plastic surface.

2.2 Introduction

The goal of this set of experiments was to study the effect of surface preparation of different types of polymeric sheets on the water contact angle. The higher the water contact angle, the more hydrophobic the surface will be. The hydrophobic surface will cause a non-uniform coating due to the intrinsic wetting issue. Additionally, the hydrophobic surface will add a layer of difficulties when the surface is tested for anti-microbial activity because the bacterial cultures are usually prepared in aqueous solution, and this might cause weak repeatability and reproducibility.

2.3 Data Analysis Method

Twenty replicates of each unique combination of material and coating were studied. There are 4 materials (PP, PE, PET, and PC) and 3 preparations for the plastic sheets (plasma-treated, non-plasma treated, and coated disk with anti-microbial $Mg(OH)_2$ nanoparticles). The surface preparation was tested for a total of 240 experiments. The experiments were not conducted in a randomized order, therefore, there is an opportunity to improve the methodology and reduce the

number of experiments required if this experiment is going to be repeated in the future. An optimal design of experiment (DoE) was created in (JMP software) with three categorical factors for preparations, four categorical factors for materials, and two-way interactions for the model with 2 replicate runs. This optimal design would reduce the number of experiments from 240 to 24.

2.4 Statistical Design

The data were analyzed using analysis of variance (ANOVA) followed by a multiple comparisons test. Multiple comparisons, using Dunnett's test to compare each surface treatment (plasma treated surface, and coated surface with anti-microbial particles) to the control (non-plasma treated surface, and non-coated surface with anti-microbial $Mg(OH)_2$ particles) using JMP software (JMP Pro 16.1.0 (539038), SAS Institute Inc., Cary, North Carolina, USA), were conducted.

2.5 Statistical Analysis

The contact angle for each surface preparation was measured. The average contact angle across all samples was 76.6° with a standard deviation of 13.4°. Water contact angle and hysteresis measurements were performed using an A 590-U1 Advanced Automated Goniometer equipped with DROP-image advanced software to assess the water contact angles (WCAs). Each sample received five drops of deionized water (10 μL) on its surface, which were then recorded. The contact angle was determined at various positions on the surface of each sample, and the reported values represent the average of these measurements. Contact angle hysteresis values were derived from the discrepancy between the receding contact angle and the advancing contact angle, as per Eq. 1. Advancing and receding contact angles were measured using the droplet tilt method.

$$\text{Contact Angle Hysteresis} = \text{Cos}\text{Ø}R - \text{Cos}\text{Ø}A \qquad \text{(Eq. 1)}$$

Non-plasma treated and non-coated PP had a contact of 76.6°. Non-plasma treated and non-coated PC had a contact of 74.1°, which showed a reduction of 2.5°. This reduction was statistically significant with a P value of less than 0.0001. Non-plasma treated and non-coated PE had a contact angle of 81.7°, which showed an increase of 5.1°. This increase was statistically significant with a P value of less than 0.0001. Non-plasma treated and non-coated PET had a contact angle of 64.0°, which showed a reduction of 12.6°. This reduction was statistically significant with a P value of less than 0.0001. Further testing was done using Tukey's Honestly Significant Difference (HSD). This pairwise comparison showed that all pairs compared are different (p-value < 0.0001) as listed in (**Table 3**).

Table 3. All Pairwise Differences Using Tukey's HSD.

Material 1	Material 2	Difference	Std Error	Prob>|t|
PC	PE	-7.6467	0.0423004	<.0001*
PC	PET	10.0667	0.0423004	<.0001*
PC	PP	-12.4900	0.0423004	<.0001*
PE	PET	17.7133	0.0423004	<.0001*
PE	PP	-4.8433	0.0423004	<.0001*
PET	PP	-22.5567	0.0423004	<.0001*

The surface preparation across all materials: the contact angle was reduced by 7.2° by coating the surface with anti-microbial $Mg(OH)_2$ particles. This reduction was statistically significant with a P value of less than 0.0001. The surface preparation across all materials: the contact angle was reduced by 2.6° by applying the plasma treatment on the sheet surfaces. This reduction was statistically significant with a P value of less than 0.0001. Both the coated surface with anti-microbial particles and plasma treated surface were further tested using Dunnett's multiple comparison methods, and they exceeded the lower limit of the tests showing further evidence that they were different from the control as shown in (**Table 4**).

Table 4. Comparisons with Control Summary.

Surface Prep	Lower Limit	Estimate	Upper Limit	Limit Exceeded
Coating	86.20346	69.39375	86.36654	Lower
Plasma	86.20346	74.00875	86.36654	Lower

A multiple comparison test of all the surfaces and treatments using Tukey's HSD shows that all the surfaces and all the preparations are different (p-value < 0.0001) except for for non-coated PP and PE.

The formula used to make the comparison is as follows:

$$q_{S=} \frac{Y_A - Y_B}{SE} \qquad \text{(Eq. 2)}$$

Where Y_A represents the greater of the two means under comparison, Y_B signifies the lesser of the two means being compared, while *SE* denotes the standard error of the combined means as shown in (**Figure 16**).

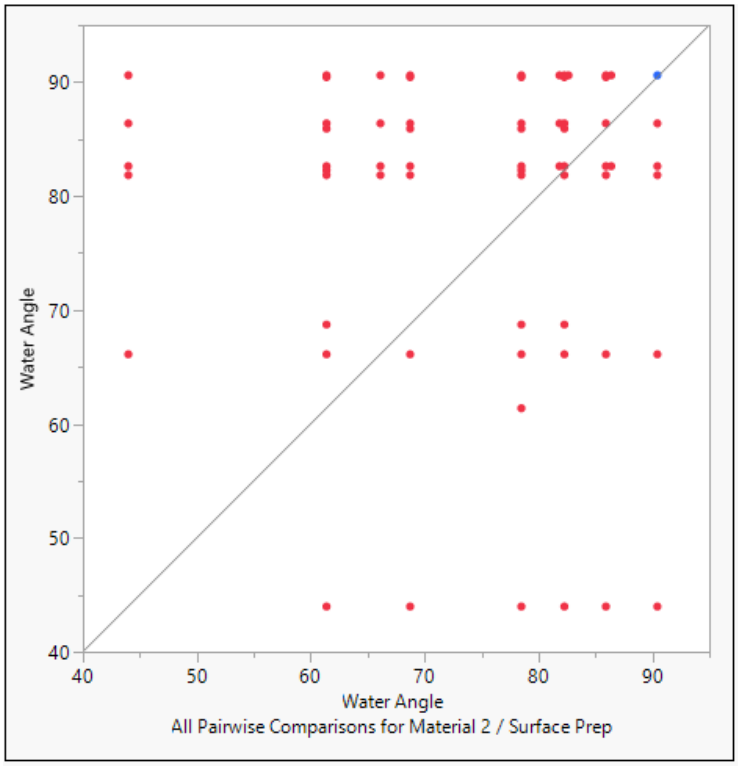

Figure 16. All Pairwise Comparisons Scatterplot.

The mean and standard error for each material and surface preparation are listed in (**Table 5**). It showed that the water contact angle was significantly reduced when the plasma treatment was applied, but in all cases, it never reached 0° which is preferable for better coating quality.

Table 5. The contact angle for each material and surface preparation.

Level	Least Sq Mean	Std Error
PC, Coating	78.490000	0.05180725
PC, Plasma	61.380000	0.05180725
PC, no plasma, no coating	82.265000	0.05180725
PE, Coating	68.725000	0.05180725
PE, Plasma	85.915000	0.05180725
PE, no plasma, no coating	90.435000	0.05180725
PET, Coating	43.980000	0.05180725
PET, Plasma	66.115000	0.05180725
PET, no plasma, no coating	81.840000	0.05180725
PP, Coating	86.380000	0.05180725
PP, Plasma	82.625000	0.05180725
PP, no plasma, no coating	90.600000	0.05180725

2.6 Discussion

A higher contact angle would mean that the material is super hydrophobic. The hydrophobic surface will add a layer of difficulties when the surface is tested for anti-microbial activity because the bacterial cultures are usually prepared in aqueous solution, and this might cause weak repeatability and reproducibility. Meanwhile, the hydrophobic surface will cause a non-uniform coating of the NPs due to the intrinsic wetting issues.

2.7 Conclusion

All contact angles for the studied materials (PP, PE, PET, and PC) were inconsistent across the different surface preparation methods (plasma-treated, non-plasma-treated, and coated sheet with anti-microbial $Mg(OH)_2$ nanoparticle). All combinations are problematic. To avoid the inconsistency of coating due to the intrinsic wetting issues, new methods had to be explored in chapter 3.

CHAPTER 3: FABRICATION METHODOLOGIES FOR ANTI-MICROBIAL POLYPROPYLENE SURFACE WITH LEACHABLE AND NON-LEACHABLE ANTI-MICROBIAL AGENTS

3.1 Objective

The work of this chapter was published in the Journal of Applied Polymer Science 2023, e54757. https://doi.org/10.1002/app.54757

The aim of this chapter is to design a new approach for fabricating anti-microbial polypropylene (PP) surfaces with (i) leachable copper (II) chloride dihydrate, and (ii) non-leachable magnesium hydroxide biocides. The fabrications were conducted via two methodologies: (i) melt-blending and subsequent injection molding of compounded biocide additives with PP and (ii) thermal embossing of anti-microbial agents on the surface of a PP sheet. The obtained biocide-bearing PP surfaces were evaluated against *E. coli* K-12 MG1655 for 0, 4, and 24 h to evaluate their anti-microbial properties. The sub-objectives were investigated as follows:

- Investigate whether the leachable and non-leachable anti-microbial agents would both provide the required activity when used in melt-compounding with the same loading ratio.
- Study the dispersity of the anti-microbial particles in the polymer matrix after compounding and injection molding.
- Develop and validate the 'thermal embossing method' to enable a cost-effective solution for anti-microbial application, and to fully enable the non-leachable anti-microbial agents to be used in polymer application.

- The modified PP surfaces obtained through these approaches were characterized via scanning electron microscopy (SEM), energy dispersive x-ray (EDX) analysis, differential scanning calorimetry (DSC), thermogravimetric analysis (TGA), and their performances were also tested against *E. coli* K-12 MG1655 bacteria.
- The PP samples also underwent further testing to study their overall properties such as (i) melt flow index (MFI), (ii) density, (iii) mechanical properties, (iv) barrier properties, and (v) leachability.

3.2 Experimental

3.2.1 Materials

Polypropylene homopolymer (PP 500P grade) was gifted from SABIC (Riyadh, Saudi Arabia) as a powder having the following characteristics: melting point = 166 °C, density = 905 kg/m^3, and MFI = 3 g/min. $CuCl_2{\cdot}2H_2O$ (purity: 99.99 %) was obtained from Innovative Science (New York, USA) as a dry powder. $Mg(OH)_2$ (purity: 99.99 %) was gifted by Aqua Resources Corp (Florida, USA) both as a dry powder as well as a slurry of $Mg(OH)_2$ dispersed in deionized (DI) water). Isopropyl alcohol was obtained from Macron Fine Chemicals (purity: 99.99 %).

3.2.2 Melt-compounding and injection molding of PP with the anti-microbial additives

The anti-microbial biocides and PP powder were physically mixed and then extrusion compounded using a DSM Xplore 15cc Micro extruder equipped with co-rotating conical twin screws (processing temperature: 210 °C, speed: 10 rpm, time: 3 min). About the PP-to-anti-microbial agent's ratios, $CuCl_2{\cdot}2H_2O$ and $Mg(OH)_2$ were incorporated into PP at loadings of 1 and 5 wt.%. Extrusion compounding led to PP composites containing the biocidal additives at the desired level. The neat PP (without biocide) and PP-bearing biocides were injection molded into a disk shape (disk dimensions: 25 mm in diameter and 1.55 mm in thickness), tensile, and impact

specimens using a 3.5 cc injection mold. The mold temperature was fixed at 60 °C. The disks were used for the testing of anti-bacterial activity.

3.2.3 Melt-compounding and cast film extrusion of PP with the anti-microbial additives

The anti-microbial biocides $CuCl_2{\cdot}2H_2O$ and $Mg(OH)_2$ and PP powder were physically mixed (5 wt.%) and then extrusion compounded using a Leistriz Twin Screw Extruder (Type MIC 27-GL-26D). The screw diameter was 2.7 cm, with an (*L*/*D* ratio of 36/1). All the materials were processed with the same conditions (processing temperature: 210 °C, speed: 10 rpm, residence time: 3 min). The compounded PP pellets were then used to produce the cast film using an RCP-0625 microextruder (Randcastle Extrusion Systems, Inc., Cedar Grove, NJ, USA) equipped with a 20.32 cm flex lip die. The screw diameter was 1.5875 cm with an (*L*/*D* ratio of 24/1) and a volume of 34 cm^3. The temperature profile was set at (150/170/200/215/210/210/210 °C) from feed to die. The screw speed, nip roller, and winding roller were set at 32, 52, and 12 rpm, respectively. PP sheets were prepared with a thickness of 300 μm.

3.2.4 Preparation of $CuCl_2{\cdot}2H_2O$ and $Mg(OH)_2$ suspensions for thermal embossing studies

The $CuCl_2{\cdot}2H_2O$ particles (3330 mg) were combined with isopropyl alcohol (333.3 mL) to prepare a $CuCl_2{\cdot}2H_2O$ particle suspension at a concentration of (10 mg/mL). The suspension was vortexed at a maximum speed for 30 s, and subsequently sonicated in an ultrasonic bath (Branson 2510 Ultrasonic Sonicator, Commack, NY, USA) at 23 °C for 10 min to ensure that the $CuCl_2{\cdot}2H_2O$ particles were uniformly dispersed. After sonication, the suspension was vortexed once more at maximum speed for 30 s.

The $Mg(OH)_2$ particles were obtained commercially as a slurry (7 wt.% $Mg(OH)_2$ and 93 wt.% water). The $Mg(OH)_2$ slurry (14.3 mL) was diluted with isopropyl alcohol (85.7 mL) to prepare a $Mg(OH)_2$ suspension at a concentration of (10 mg/mL). The suspension was vortexed at

a maximum speed for 30 s, and subsequently sonicated in an ultrasonic bath at 23 °C for 10 min to ensure that the $Mg(OH)_2$ particles were uniformly dispersed. After sonication, the suspension was vortexed once more at maximum speed for 30 s.

3.2.5 Deposition of anti-microbial particles over aluminum foil

A metallic rod applicator technique (K303, RK Print Coat Instruments Ltd., UK) was used to deposit the anti-microbial biocidal suspension with a concentration of (10 mg/mL) over aluminum foil (All-Foils, Inc., OH, USA, dimension: 0.00762 x 30.48 x 30.48 cm). The thickness of the wet deposited coating varied between 4-120 microns, and this thickness was controlled by adjusting the diameter of the applicator rod number. The anti-microbial suspension was spread over an aluminum foil using the metallic rod number 5, corresponding to a thickness of 50 microns as a wet film deposition, and left to dry at 23 °C for 10 min.

3.2.6 Thermal embossing of the anti-microbial biocides on PP

The coated aluminum foil with anti-microbial crystals was used to transfer the temporarily deposited particles to the surface of the PP sheet prior to the thermal embossing process. The coated side of the aluminum foil was placed in contact with the PP (**Figure 17**) and pressed above the softening temperature of the PP using a compression molding press (PHI QL438-C, City of Industry, CA, USA). A temperature of 143 °C and 2 bar of pressure for 10 s were used for the PP sheet. Disks were cut (dimensions: 20 mm in diameter, 0.5 mm in thickness) from the PP sheets of thermally embossed particles, and neat PP (without biocides) sheets, and metallic copper (Szone brand, China) using a Kongsberg X24 Edge Cutting Table.

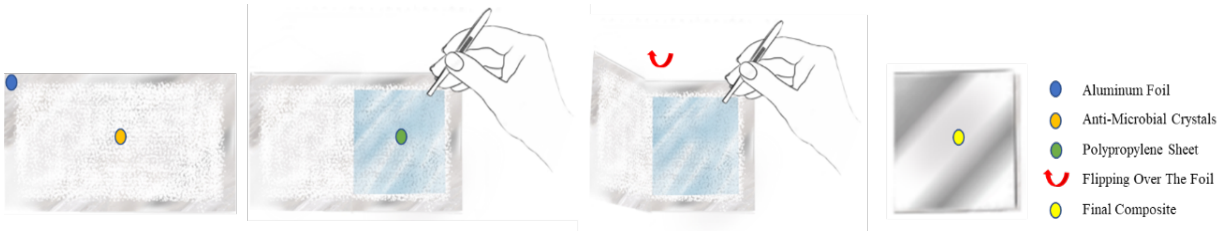

Figure 17. Schematic illustration demonstrating how the Al foil is used before the compression molding process.

3.3 Experimental design

A 2x2 factorial experiment was used to investigate the effect of the anti-microbial agents ($CuCl_2{\cdot}2H_2O$ – leachable, and $Mg(OH)_2$ – non-leachable) based on the method of incorporation (compounding and thermal embossing) against *E. coli* K-12 MG1655.

3.4 Statistical analysis

All experiments were independently replicated, with at least three biological replicates. Differences between means of *E. coli* K-12 MG1655 cell density as affected by the direct exposure to the: (1) metallic copper disk (positive control), (2) neat PP disk (negative control), and (3) incorporated PP disk with anti-microbial agents were compared at 0, 4 and 24 h using Tukey's honest significant difference test and Student's *t*-test's at a 95 % confidence level ($p \leq 0.05$), to judge if any differences in means were significant. Interactions between the type of anti-microbial agents, methods of incorporating the anti-microbial agents with PP (compounding, thermal embossing), and anti-microbial activity were analyzed via four-way analysis of variance (ANOVA) using Origin 2022b software (ver. 9.9.5.167: OriginLab Corporation, Massachusetts, USA).

3.5 Characterization

3.5.1 Scanning Electronic Microscopy (SEM) and Energy Dispersive X-ray (EDX) Sample Preparation Methods

The anti-microbial particles (powders of $CuCl_2{\cdot}2H_2O$ and $Mg(OH)_2$), the compounded and

injection molded PP disks (containing 5 % $CuCl_2{\cdot}2H_2O$ and 5 % $Mg(OH)_2$ by weight), and the thermally embossed disks with ($CuCl_2{\cdot}2H_2O$, and $Mg(OH)_2$ 10 mg/mL suspension) were characterized by SEM using a JEOL 7500F field emission emitter (JEOL Ltd., Tokyo, Japan), and by EDX analysis using an Oxford Instruments Aztec system (Oxford Instruments, High Wycombe, Bucks, England). Samples for this analysis were prepared by mounting on aluminum stubs using the Epoxy glue, System Three Quick Cure 5 (System Three Resins, Inc., Aubur, WA). All the mounted samples were coated with (~ 2.7 nm in thickness) iridium in a Quorum Technologies/Electron Microscopy Sciences Q150T turbo pumped sputter coater (Quorum Technologies, Laughton, East Sussex, England BN8 6BN) and purged with argon gas.

3.5.2 Thermal Analysis

Differential Scanning Calorimetry (DSC)

The melting point (T_m) and the crystallisation temperature (T_c) of PP samples was determined by DSC using a TA Instrument (model Q100 system, USA). The nitrogen flow was set at (70 mL min^{-1}) for all measurements. The samples were thermally analyzed in the temperature range (-20 to 250 °C) at a rate of (10 °C min^{-1}) and held for 1 min to eliminate previous crystallization, mechanical, thermal, processing, and shear history. The samples were additionally cooled to (-20 °C at 10 °C min^{-1}) and re-heated to (250 °C at 10 °C min^{-1}) and the thermal responses were recorded. All samples were replicated at least twice.

The degrees of crystallinity of the PP samples were calculated from the heat of fusion values determined from the **second heating** runs and evaluated according to Equation (3):

$$X_c(\%) = \left[\frac{\Delta H_c}{\Delta H_0 . W}\right] x100 \qquad \text{(Eq. 3)}$$

where X_c is the crystallinity of PP samples, ΔH_c is the heat of fusion, ΔH_0 is the enthalpy of fusion for 100 % crystalline PP [209 J/g][241], and W is the fraction (weight) of PP in the composite.

Thermogravimetric Analysis (TGA)

The thermal stability of the PP samples was tested via TGA using a TA Instrument (model Q50, USA). All the samples (6−10 mg) were heated at (10 °C/min to 600 °C) under a nitrogen flow of (50 mL/min). At least three replicates were analyzed for each sample and the average value of the TGA data was reported.

3.5.3 Anti-microbial Testing Method

E. coli K-12 MG1655 (American Type Culture Collection, Manassas, VA) was used for all experiments to evaluate the anti-microbial activities of the disks. Stock culture was stored at (-80 °C) and streaked to TSA plates (BBL/Difco, Sparks, MD, USA). After incubation at 37 °C for 24 h, a single colony was selected and transferred to 5 mL of TSB (BBL/Difco, Sparks, MD, USA) and incubated at 37 °C for 18 h. After incubation, 1 mL of culture was centrifuged at (13,000 x *g* for 5 min) using a (Fisher Scientific accuSpin micro 17 R) centrifuge and the supernatant was discarded. Cells were suspended in 1 mL of Phosphate Buffered Saline (PBS, Crystalgen, Innovation for Science, Commack, NY, USA) by vortexing. The cell suspension was then transferred to a 15 mL tube and 11.5 mL of PBS was added. Aliquots of this suspension were then exposed to the different types of disks. Each single disk was placed separately in a pod which were contact lens cases from Bosch + Lomb. For each pod containing a single disk, 1 mL of bacterial suspension was added to submerge the disk into the culture broth and the pods were closed. The pods were attached to a mini rotator (Benchmark Scientific, Roto Mini Plus R 2024, Sayreville, NJ, USA) and rotated at 20 rpm around the machine's horizontal axis to continuously agitate the

broth and cause liquid renewal on the surface of the disks (**Figure 18**). At 0, 4, and 24 h intervals, a 100 µL sample of the bacterial suspension was removed for an appropriate number of (1:10 dilutions), plated in TSA, and then incubated at 37 °C overnight. The colony forming unit (CFU) number was counted to determine the cell viability. A neat PP disk was used as a "negative" control sample, while a metal copper disk was used as the "positive" control sample, and any significant change in the PP with anti microbial crystals was assessed against these.

Figure 18. The pods were attached with tape to the mini rotator device for consistent agitation of the bacterial broth and surface renewal of the disks inside the pods. The blue tray holding the pods rotates around the horizontal axis.

3.5.4 Melt Flow Index (MFI)

The MFI analysis for PP samples was performed according to (ASTM D1238-20) by using (Ray-Ran MK 2 advanced microprocessor system) under the following conditions: the barrel temperature was 230 °C and the weight of the piston was 2.16 kg. 5 g sample was preheated for 7 mins, each sample was cut after 1 min, and its relative weight was recorded. Each specimen was repeated seven times. The average and standard deviation were reported.

3.5.5 Density

The density of PP samples was measured by using a density gradient method (Ray Ran, Auto Density Gradient Column, Warwickshire, UK) by (ASTM D 1505, method C in section X 2.3). A solution of Isoporpanol-diethylene glycol was used to create a density-gradient range between 0.79 to 1.11 g/cm^3. Three replicates (disks of 1 cm in diameter) were prepared and submerged in the density gradient column, and the relative densities were recorded.

3.5.6 Mechanical Properties

Tensile and impact bars (test specimens) were kept at room temperature for at least 40 h before testing. The tensile test was performed using an Instron (model 5565, MA, USA) system in accordance with ASTM D638-14 (type V) at a rate of 10 mm/min. A notching cutter (TMI 22-05, USA) was used to notch the impact bars, which were then left at room temperature for 40 h post-notching, under similar conditions to those discussed earlier for the tensile bars. The impact strength was measured in accordance with (ASTM D256) by using Ray-Ran test equipment with a hammer pendulum of 5.417 J. Five replicates were used for each type of mechanical test.

3.5.7 Barrier Properties

Water Vapor Transition Rate (WVTR)

A Permatran-W system (Model 3/34, Mocon Inc., MN, USA) was used to determine the WVTR at (37.8 °C and 90 % RH) in compliance with (ASTM F1249). Water vapor permeation was calculated by multiplying the thickness of film samples (two replicates of each PP sample made by the cast film extruder) by the water vapor transmission values.

Oxygen Transition Rate (OTR)

An Ox-Tran system (model 2/22, Mocon Inc., MN, USA) was used to determine the OTR at (23 °C and 50 % RH) of PP film samples (two replicates of each PP sample made by the cast film extruder) by (ASTM D3985).

3.5.8 Leachability of Agents

A disk of PP sample (dimension 20 mm in diameter) was submerged into a (20 mL in size) glass vial containing 5 mL of DI water and rotated (biaxial in x axis) using a sample mini rotator (Benchmark Scientific, Roto Mini Plus R 2024, Sayreville, NJ, USA) and rotated at 20 rpm for 24 h. A 3 mL of the DI water was then extracted by micropipette and scanned for ultraviolet and visible light transmission by (ASTM E169-16) using a UV-visible spectrophotometer (model UV-1800, Shimadzu Corporation, Kyoto, Japan). Three replicates for each PP sample were scanned over the range of (200 to 800 nm at 480 nm min^{-1}).

3.6 Results

3.6.1 SEM and EDX Characterization

The SEM images of the two selected inorganic biocides are presented in (**Figure 23**). The morphologies of the crystals in the compounded and injection molded disks and the disks cut from the thermal embossed sheets are discussed and correlated with the disposition of the crystals in the PP.

SEM of $CuCl_2 \cdot 2H_2O$ Crystals

The $CuCl_2 \cdot 2H_2O$ crystals have a green color. SEM image of $CuCl_2 \cdot 2H_2O$ in (**Figure 23A**) shows the particles were lath-like in shape, and were in the range of (34-336 μm) in length with a thickness of approximately (19-50 μm). The laths appear to be agglomerated; in some cases, there seem to be crystal overgrowths. An agglomerated bundle of strips had a cross-sectional diameter

of approximately (100 μm).

SEM of $Mg(OH)_2$ Crystals

The $Mg(OH)_2$ crystals have a white color. The SEM image in (**Figure 23B**) shows the particles were platelets in shape, and they were approximately (160-260 nm wide with a 30-50 nm thickness).

SEM and EDX Characterization of PP Compounded with 5 wt.% Anti-microbial Biocides and Injection Molded into a Disk

The SEM characterization did not show any evidence of biocidal crystals on the outer surfaces of PP disks compounded with neither $CuCl_2 \cdot 2H_2O$ nor $Mg(OH)_2$ additives. A few spots on the outer surface of the disks (> 1 μm) in size could be observed at low magnification for PP disks that had been compounded with 5 wt.% $CuCl_2 \cdot 2H_2O$ (**Figure 23C**) and $Mg(OH)_2$ (**Figure 22D**). White spots (highlighted with orange color circles) that can be attributed to the inorganic additives are more visible on the PP sample which had been compounded with 5 wt.% $CuCl_2 \cdot 2H_2O$, than on its counterpart which had been compounded with 5 wt.% $Mg(OH)_2$. This could be because $CuCl_2 \cdot 2H_2O$ has a large particle size and a different shape than $Mg(OH)_2$. The circled white spots in (**Figure 23C** and **Figure 23D**) were examined by EDX. Surprisingly, neither Cu, and Cl, nor Mg and O were detected, but only a carbon peak was identified (**Figure 19** and **Figure 20)**. This finding indicates that the $CuCl_2 \cdot 2H_2O$ and $Mg(OH)_2$ crystals were covered by at least 1 mm of PP. Overall, most particles were embedded in the polymer matrix, and thus no bare crystals for bacterial contact were present on the surfaces of either type of compounded anti-microbial additive.

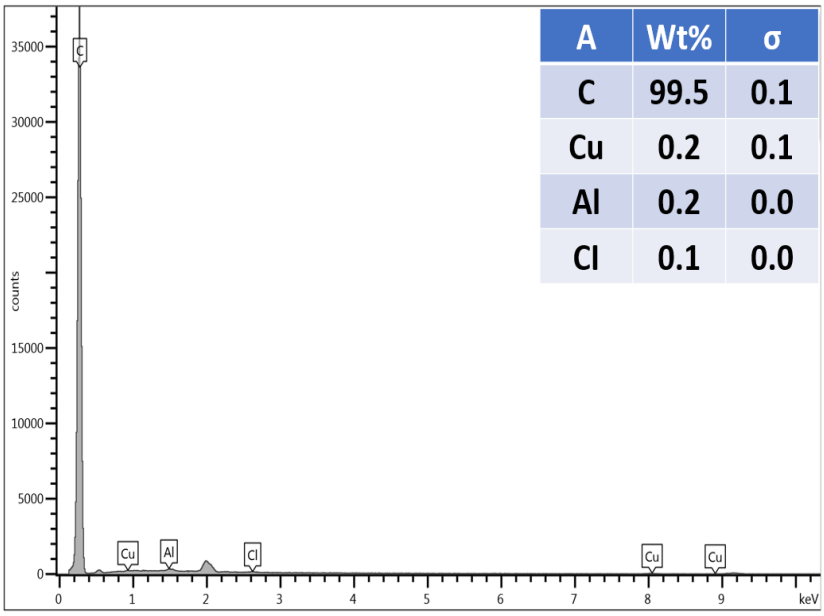

Figure 19. The EDX spectrum of the outer surface of a polypropylene disk compounded with 5 wt.% $CuCl_2.2H_2O$.

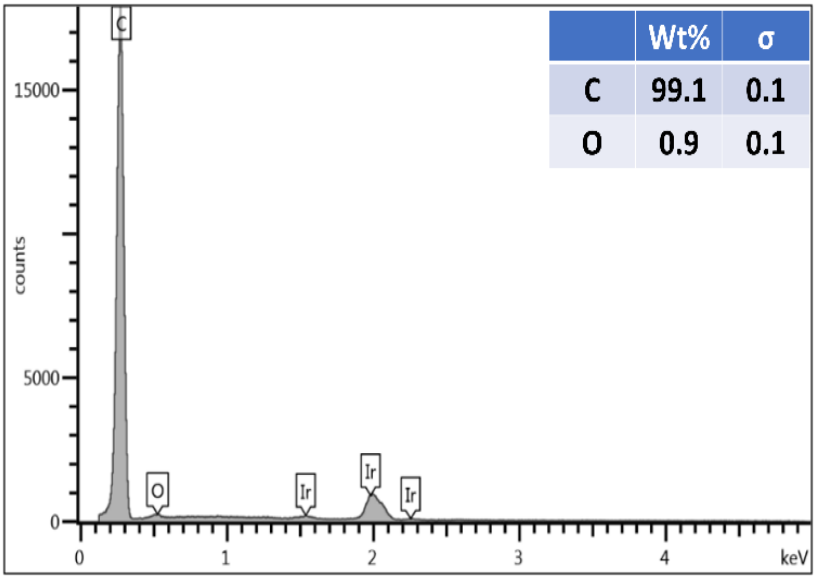

Figure 20. The EDX spectrum of the outer surface of polypropylene disk compounded with 5 wt.% $Mg(OH)_2$.

Cross-sectional SEM and EDX Characterization of PP Compounded with 5 wt.% Anti-microbial Biocides and Injection Molded into a Disk

The cross-sectional SEM images reveal that the biocidal crystals were embedded in both PP disks compounded with $CuCl_2 \cdot 2H_2O$ and $Mg(OH)_2$ additives (**Figure 23**). When PP was compounded with 5 wt.% $CuCl_2 \cdot 2H_2O$ and $Mg(OH)_2$, crystals of these biocidal additives were embedded into the polymer matrix in the form of 5 μm agglomerates (**Figure 23E**), and 3 μm agglomerates (**Figure 23G**), respectively. The shearing treatment that was performed during extrusion had broken down the $CuCl_2.2H_2O$ crystals, causing their morphology to change from lath-like (**Figure 23A**) before extrusion to after extrusion (**Figure 23F**). The shearing did not alter the morphology of the $Mg(OH)_2$ crystals, as demonstrated by the SEM images that were performed before and after the extrusion process (**Figure 23B** and **Figure 23H**), respectively. The particles were not completely dispersed in PP compounded with neither $CuCl_2 \cdot 2H_2O$ nor with $Mg(OH)_2$ additives at 5 wt.%. The agglomerates of $CuCl_2 \cdot 2H_2O$ (**Figure 23F**) and $Mg(OH)_2$ (**Figure 23H**) were examined by EDX, and peaks corresponding to Cu, Cl, C, and Mg, O, C (**Figure 21** and **Figure 22**) were respectively detected. The crystals of $CuCl_2 \cdot 2H_2O$ and $Mg(OH)_2$ adhered strongly to PP.

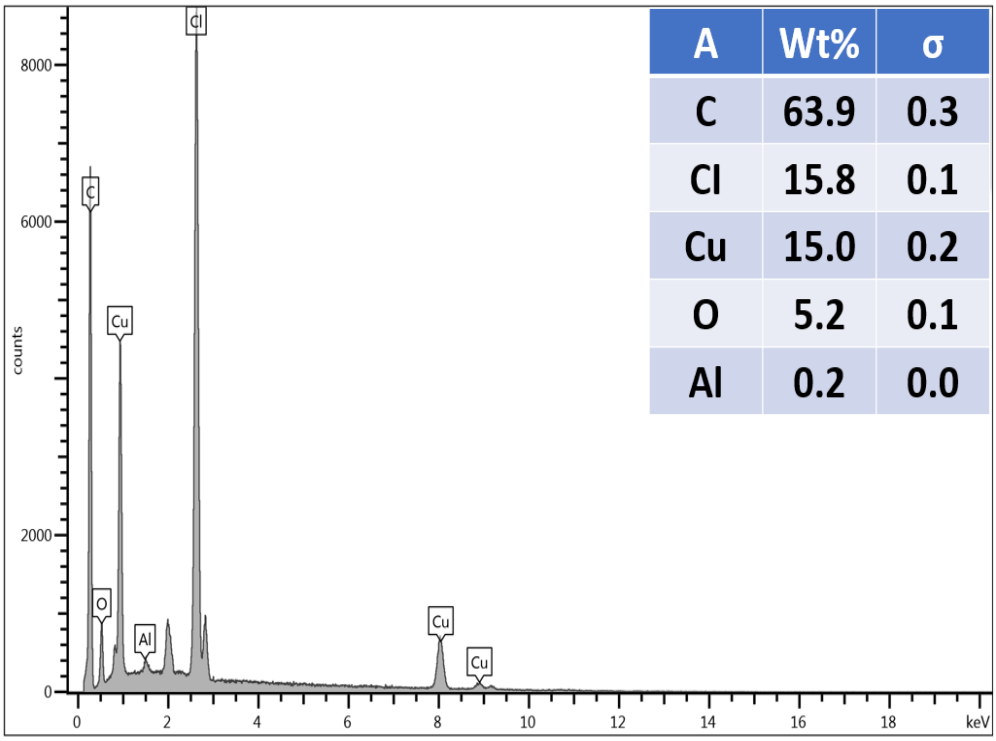

Figure 21. The EDX spectrum of the middle cross-section of the polypropylene disk compounded with 5 wt.% $CuCl_2.2H_2O$.

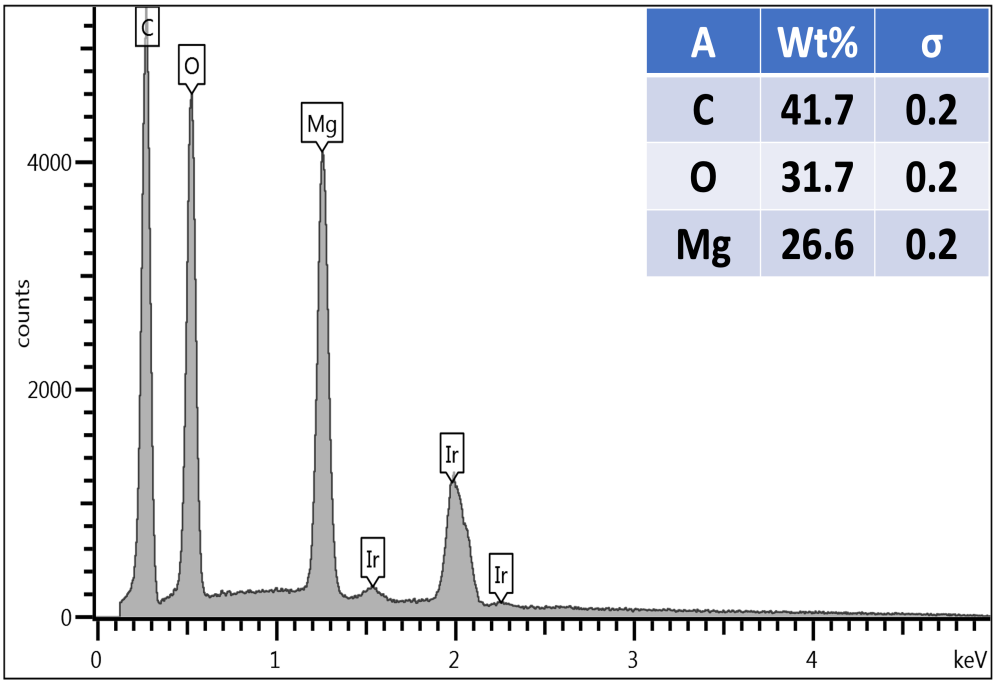

Figure 22. The EDX spectrum of the middle cross-section of the polypropylene disk compounded with 5 wt.% $Mg(OH)_2$.

SEM of PP Outer Surface Disks Thermally Embossed with (10 mg/mL) Anti-microbial Biocides

The SEM images of thermally embossed PP disks (cut from the cast sheet) with $CuCl_2{\cdot}2H_2O$ (**Figure 23I**) and $Mg(OH)_2$ biocides (**Figure 23J**) showed that the crystals are uniformly distributed and fixed across the PP area. In contrast with the disks produced via the compounding approach, the thermally embossed disks showed almost full coverage of the surface of the sheet with the biocidal crystals, with only a few gaps existing between the crystals.

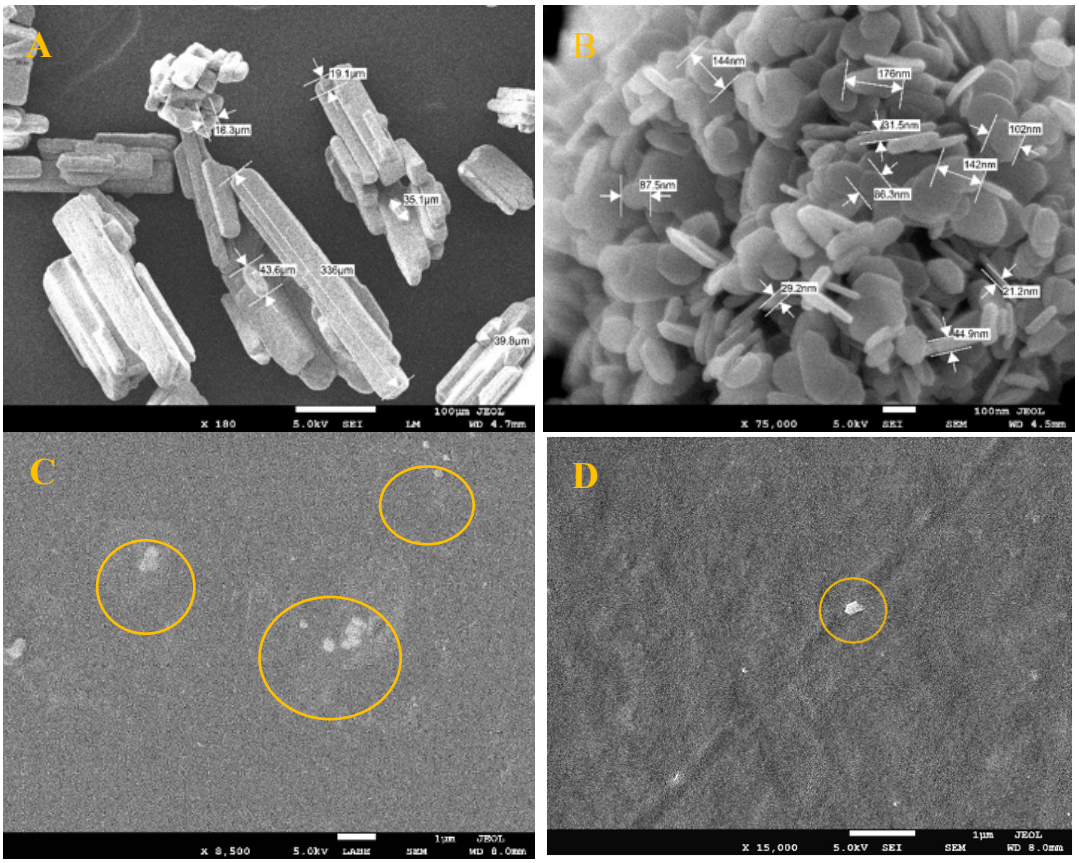

Figure 23. SEM images of $CuCl_2{\cdot}2H_2O$ (A) and $Mg(OH)_2$ particles (B), outer surface view of PP disk blended with 5 wt.% $CuCl_2{\cdot}2H_2O$ (C) and $Mg(OH)_2$ (D), middle cross-sectional view of PP disk blended with 5 wt.% $CuCl_2{\cdot}2H_2O$ (E) and the same at a higher magnification (F), middle cross-sectional view of PP disk blended with 5 wt.% $Mg(OH)_2$ (G) and the same at a closer magnification (H), PP disk thermally embossed with $CuCl_2.2H_2O$ particles (I) and PP disk cut from sheet, thermally embossed with $Mg(OH)_2$ particles (J).

Figure 23. (cont'd)

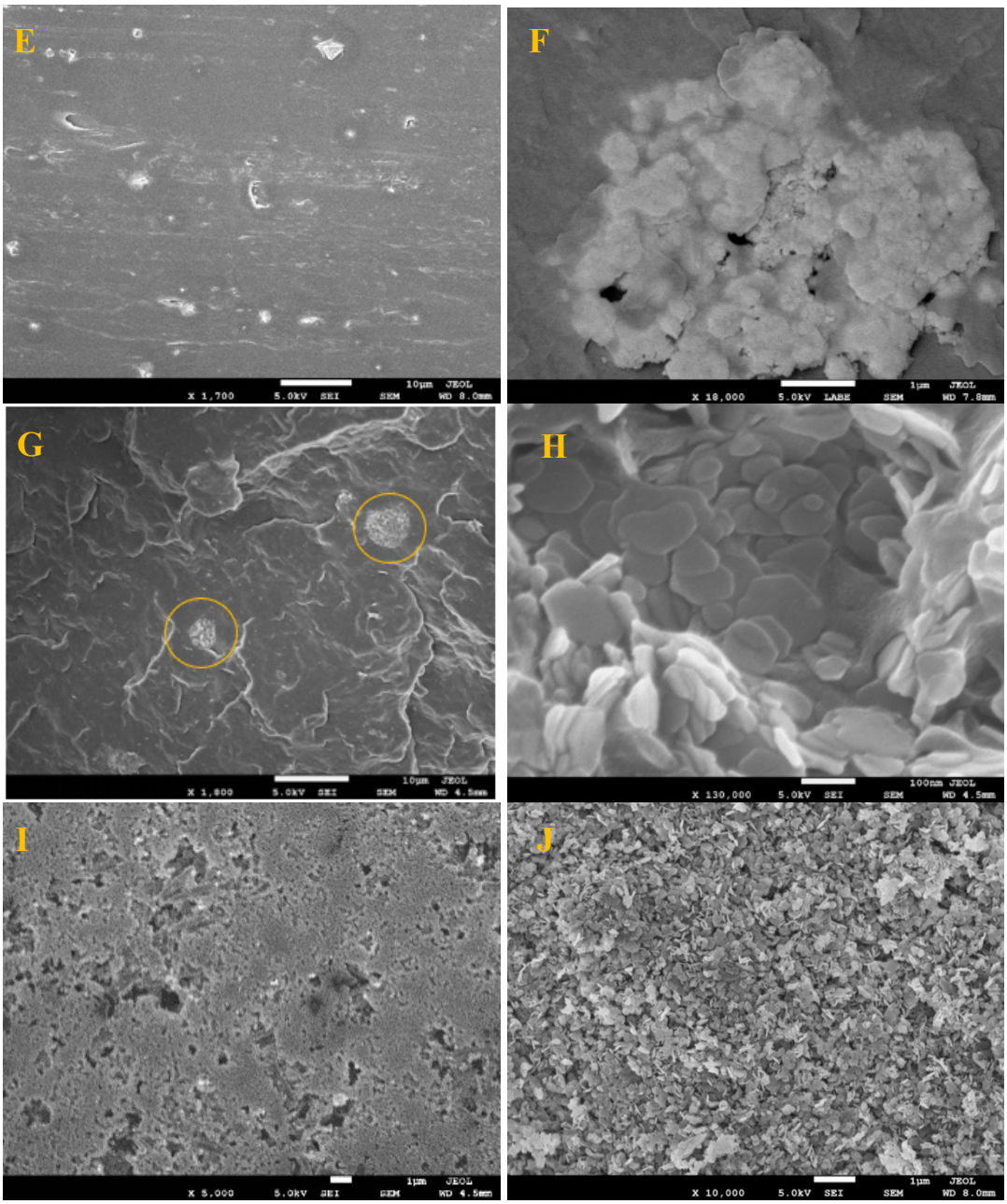

3.6.2 Thermal Analysis

Differential Scanning Calorimetry (DSC)

The DSC data showed minor differences between the neat and modified PP samples. In particular, (**Figure 24**) shows the melting temperature (T_m), and (**Figure 25**) shows the crystallization temperature (T_c) for various PP samples.

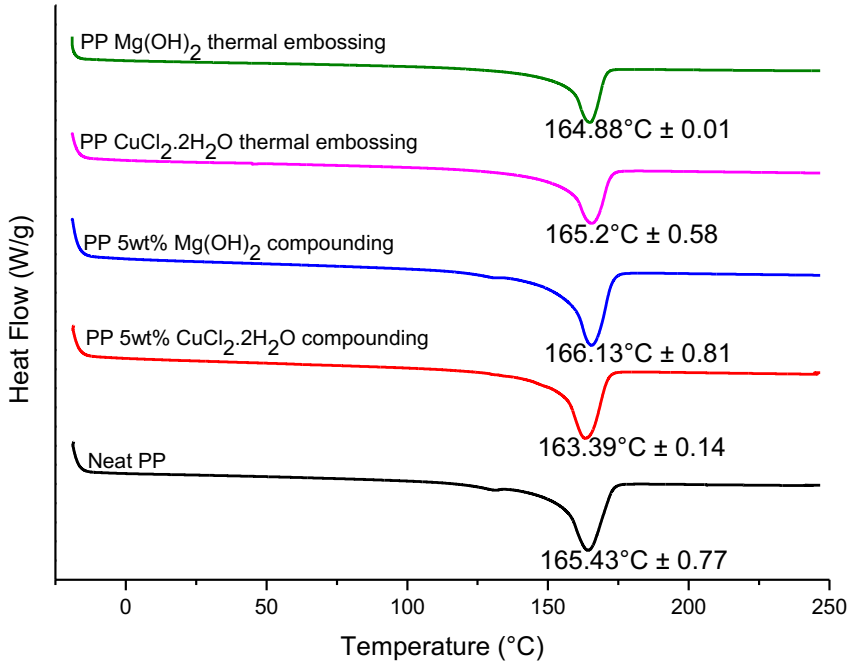

Figure 24. The (T_m) values were obtained from the DSC data for various PP samples.

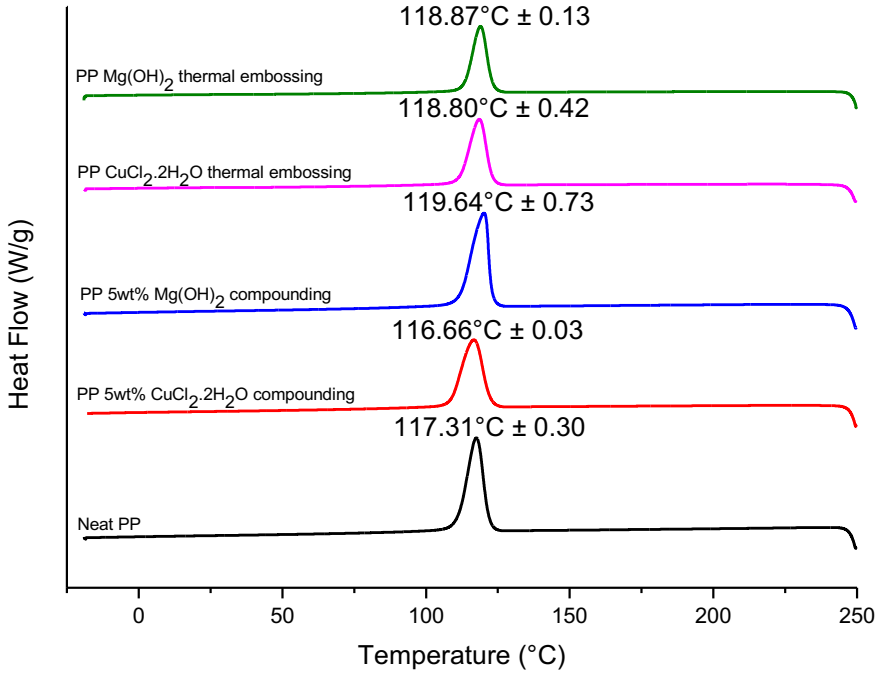

Figure 25. The (T_c) values were obtained from the DSC data for various PP samples.

Melting temperature (T_m) of the PP samples

The melt-compounded and injection-molded PP samples with 5 wt.% $CuCl_2 \cdot 2H_2O$ had a slightly lower T_m (163.39 °C ± 0.14), and those with 5 wt.% $Mg(OH)_2$ had a slightly higher T_m (166.13 °C ± 0.81) compared to the PP control T_m (165.43 °C ± 0.78). The PP samples that had been thermally embossed with $CuCl_2 \cdot 2H_2O$, and $Mg(OH)_2$ particles had almost the same T_m compared to the PP control (165.20 ± 0.58, 164.88 ± 0.01, and 165.43 ± 0.78 °C), respectively, as shown in (**Figure 24**).

Crystallization temperature (T_c) of the PP samples

The melt-compounded and injection-molded PP with 5 wt.% $CuCl_2 \cdot 2H_2O$ had a slightly lower T_c (116.66 °C ± 0.04), and that with 5 wt.% $Mg(OH)_2$ had a higher T_c (119.64 °C ± 0.73) compared to the PP control T_c (117.31 °C ± 0.30). The PP samples that had been thermally embossed with $CuCl_2 \cdot 2H_2O$ and $Mg(OH)_2$ particles had higher T_c values compared to the PP control (118.80 ± 0.42, 118.87 ± 0.13, and 117.31 ± 0.30 °C), respectively, as shown in (**Figure**

25). Often nano crystals have a nucleating effect on the crystallisation which leads to crystallisation occurring at an elevated temperature. However, there was no major effect with these two crystals.

Crystallinity (%) of the PP samples

The melt-compounded and injection-molded PP samples with $CuCl_2.2H_2O$, and $Mg(OH)_2$ had higher crystallinity (%) compared to the PP control sample (43.00 ± 1.65, 43.63 ± 0.83, and 39.99 ± 0.61 %), respectively. The PP samples that had been thermally embossed with $CuCl_2 \cdot 2H_2O$, and $Mg(OH)_2$ particles had higher crystallinity (%) compared to the PP control sample (43.25 ± 3.68, 44.71 ± 5.53, and 39.99 ± 0.61 %), respectively, as shown in (**Table 6**).

Table 6. The crystallinity of PP samples obtained from DSC measurements.

Samples	ΔH_m [J/g]	T_m [°C]	T_c [°C]	Crystallinity [%]
Neat PP	83.59 ± 1.27	165.43 ± 0.78	117.31 ± 0.30	39.99 ± 0.61
PP 5 wt.% $CuCl_2 \cdot 2H_2O$ (compounded)	85.38 ± 3.28	163.39 ± 0.14	116.66 ± 0.04	43.00 ± 1.65
PP 5 wt.% $Mg(OH)_2$ (compounded)	86.62 ± 1.64	166.13 ± 0.81	119.64 ± 0.73	43.63 ± 0.83
PP $CuCl_2 \cdot 2H_2O$ (thermally embossed)	89.49 ± 7.62	165.20 ± 0.58	118.80 ± 0.42	43.25 ± 3.68
PP $Mg(OH)_2$ (thermally embossed)	92.52 ± 11.43	164.88 ± 0.01	118.87 ± 0.13	44.71 ± 5.53

Thermogravimetric Analysis (TGA)

The TGA data for PP samples are presented in (**Figure 26**), and the temperatures at the 5 % weight loss are reported in (**Table 7**).

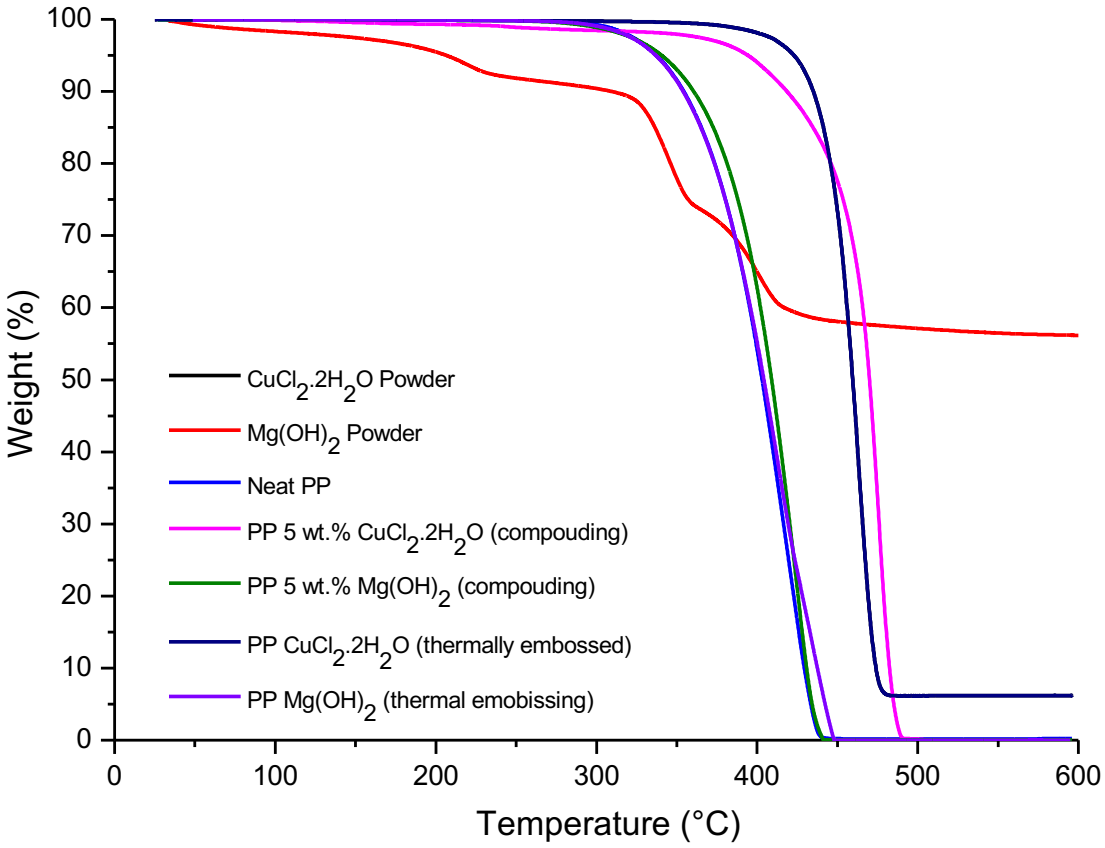

Figure 26. The TGA data for various PP samples.

Table 7. The temperature at which various PP samples underwent 5 % weight loss was determined via TGA measurements.

Sample	The temperature at which 5 % weight loss occurred (°C)
$CuCl_2.2H_2O$ Powder	101.20 ± 1.76
$Mg(OH)_2$ Powder	206.44 ± 0.13
Neat PP	349.56 ± 2.97
PP 5 wt.% $CuCl_2.2H_2O$ (compounded)	394.21 ± 0.07
PP 5 wt.% $Mg(OH)_2$ (compounded)	353.64 ± 1.62
PP 5 wt.% $CuCl_2.2H_2O$ (thermally embossed)	422.90 ± 3.60
PP 5 wt.% $Mg(OH)_2$ (thermally embossed)	336.88 ± 3.97

3.6.3 Anti-microbial Characterization

Anti-microbial Activity of Metallic Copper, Neat PP, and PP Compounded with (1 and 5 wt.% $CuCl_2 \cdot 2H_2O$ and $Mg(OH)_2$) Additives

The anti-microbial data was obtained for (i) metallic copper, (ii) PP control sample, and PP samples that were compounded with the following; (i) 1 wt.% $CuCl_2 \cdot 2H_2O$, (ii) 5 wt.% $CuCl_2 \cdot 2H_2O$, (iii) 1 wt.% $Mg(OH)_2$, and (iv) 5 wt.% $Mg(OH)_2$ are presented in (**Figure 27**).

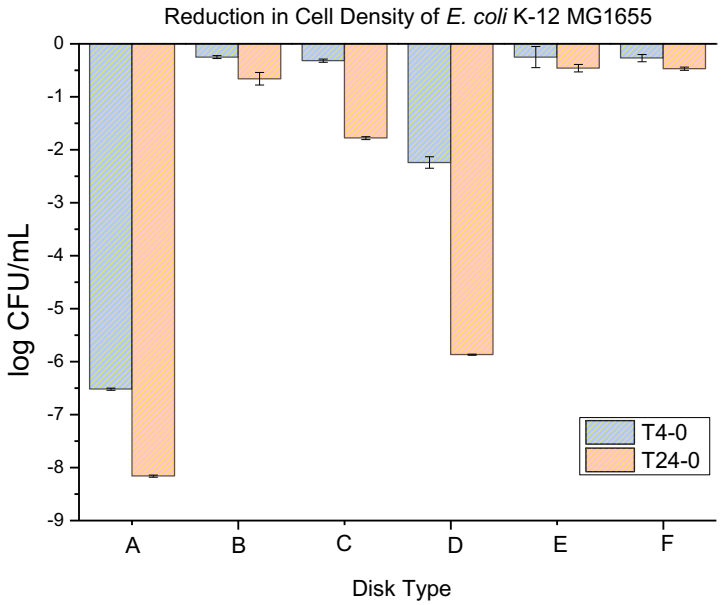

Figure 27. The anti-microbial data obtained for melt-compounded samples in the form of disks (25 mm in diameter): metallic copper (A), PP control (B), PP containing 1 wt.% $CuCl_2 \cdot 2H_2O$ (C), PP containing 5 wt.% $CuCl_2 \cdot 2H_2O$ (D), PP containing 1 wt.% $Mg(OH)_2$ (E), and PP containing 5 wt.% $Mg(OH)_2$ (F). Blue bar is after 4h, orange bar is after 24h.

The metallic copper disks showed a (6.52 ± 0.02 log) reduction of the *E. coli* K-12 MG1655 population at 4 h, and an (8.16 ± 0.02 log) reduction at 24 h. As expected, the neat PP disks did not show any significant reduction of their *E. coli* K-12 MG1655 populations, neither at 4 h nor at 24 h (< 1 log reduction). The PP disks that had been compounded with 1 and 5 wt.% of $CuCl_2 \cdot 2H_2O$ showed a (0.32 ± 0.03, and 2.24 ± 0.11 log) reduction respectively of *E. coli* K-12 MG1655 populations at 4 h, and a (1.78 ± 0.03, and 5.87 ± 0.01 log) reduction respectively and 24

h. Meanwhile, the PP that had been compounded with 1 and 5 wt.% of $Mg(OH)_2$ did not show any significant reduction of *E. coli* K-12 MG1655 neither at 4 h nor at 24 h (< 1 log reduction). As for both additives, no bare crystals were detected on the plaque surfaces; the activity of the copper salt can only occur through the migration of copper ions toward the surface of compounded PP. Indeed, $CuCl_2 \cdot 2H_2O$, which is highly soluble in water (680 g/L at 15 ºC) can leach Cu^{2+} ions which can destroy the bacterial membrane in the presence of moisture.[242] Both negative and positive ions have destructive effects on various bacterial species and fungi.[243] Unlike the copper salt, $Mg(OH)_2$ has a very low water solubility (~64 ppb at 25 ºC) and thus barely leaches any ions, and is thus inactive in compounded and injection molded disks. Such additives ($Mg(OH)_2$) only achieve anti-microbial properties when they are present on the surface, and thus a new method is needed to incorporate $Mg(OH)_2$ onto PP.

The Anti-microbial Activity of Metallic Copper, Neat PP, and PP sheet that had been Thermally Embossed with (10 mg/mL) $CuCl_2.2H_2O$ and $Mg(OH)_2$ Suspensions

The anti-microbial properties of (i) metallic copper, (ii) PP control sample, and PP samples that had been thermally embossed on to cast sheet with the following (i) $CuCl_2 \cdot 2H_2O$, and (ii) $Mg(OH)_2$ suspensions are presented in (**Figure 28**).

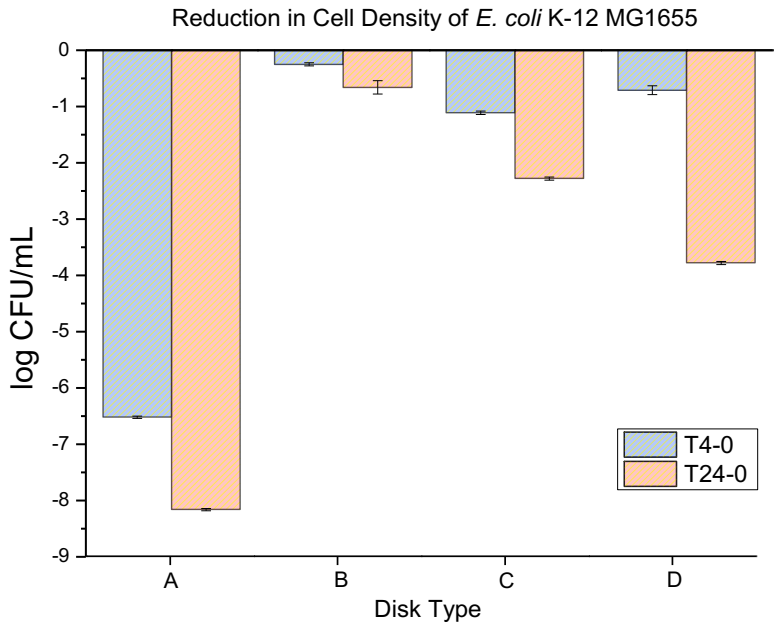

Figure 28. The anti-microbial data obtained for thermally embossed samples in the form of disks (20 mm in diameter): metallic copper (A), PP control (B), PP sheet thermally embossed with $CuCl_2 \cdot 2H_2O$ suspension (C), and PP sheet thermally embossed with $Mg(OH)_2$ suspension (D).

Again, the metallic copper disks, as "positive" control, showed a (> 6 log) reduction of the *E. coli* K-12 MG1655 population at 4 h, and an (> 8 log) reduction at 24 h. In contrast, the "neat" PP did not show any significant anti-microbial activity neither at 4 h nor at 24 h (< 1 log) reduction in both time intervals. The PP disks (from sheets that had been thermally embossed with $CuCl_2 \cdot 2H_2O$ suspension) showed a (1.11 ± 0.03 log) reduction of the *E. coli* K-12 MG1655 population at 4 h, and a (2.28 ± 0.03 log) reduction at 24 h. Meanwhile, the PP disks that had been thermally embossed with $Mg(OH)_2$ suspension showed a (0.71 ± 0.08 log) reduction of the *E. coli* K-12 MG1655 population at 4 h, and a (3.78 ± 0.03 log) reduction at 24 h.

3.6.4 Melt Flow Index (MFI) and Densities

The MFI of various PP samples (temperature 230 °C and 2.16 kg weight) and the densities are presented in (**Table 8**).

Table 8. The MFI and density values of various PP samples.

Samples	*MFI [g/10 min]*	*Density* [g/CC]
Neat PP	1.753 ± 0.036	0.927 ± 0.004
PP 5 wt.% $CuCl_2 \cdot 2H_2O$ (compounded)	3.843 ± 0.192	0.931 ± 0.004
PP 5 wt.% $Mg(OH)_2$ (compounded)	2.590 ± 0.135	0.934 ± 0.012
PP $CuCl_2 \cdot 2H_2O$ (thermally embossed)	-	0.928 ± 0.091
PP $Mg(OH)_2$ (thermally embossed)	-	0.930 ± 0.086

3.6.5 Mechanical Properties

Tensile

The tensile properties of various PP samples are presented in (**Figure 29**). The thermally embossed data in (D) and (E) were prepared as discussed in (**Section 3.2.6**) using neat PP specimens prepared earlier in (**Section 3.2.2**) via injection molding.

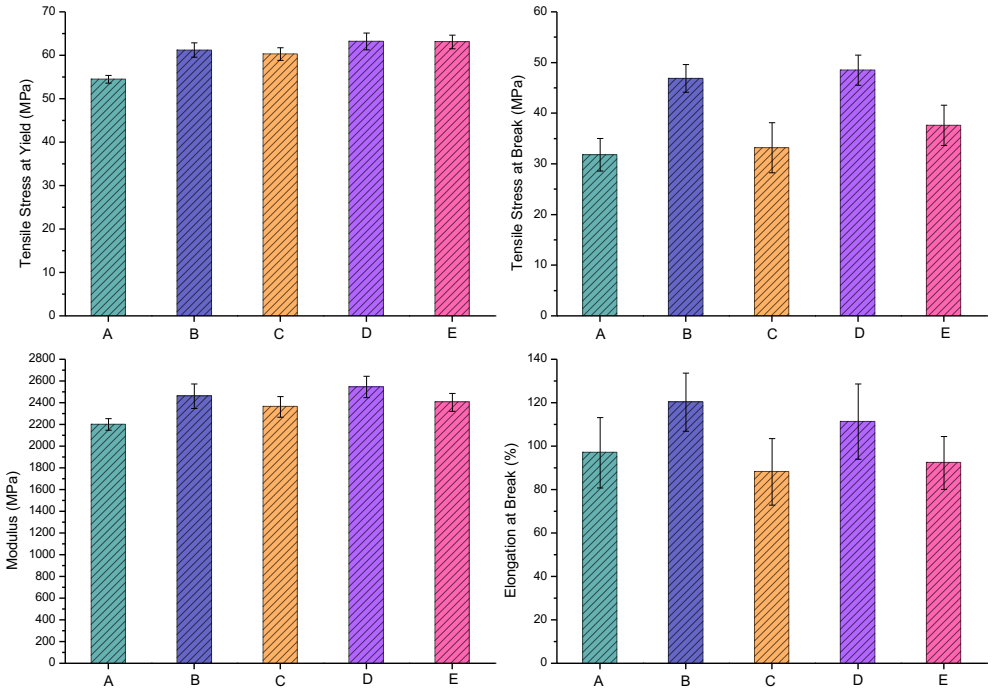

Figure 29. The tensile properties of PP samples are represented on the (y-axis). Each graph represents the following samples on the (x axis); neat PP (A), PP blended with 5 wt.% $CuCl_2 \cdot 2H_2O$ particles and injection moulded (B), PP blended with 5 wt.% $Mg(OH)_2$ particles and injection moulded (C), PP sheet thermally embossed with $CuCl_2.2H_2O$ suspension (D), and PP sheet thermally embossed with $Mg(OH)_2$ suspension (E).

Impact Resistance

The impact resistance properties of various PP samples are presented in (**Figure 30**). The thermally embossed data in (D) and (E) were prepared as discussed in (**Section 3.2.6**) using neat PP specimens prepared earlier in (**Section 3.2.2**) via injection molding. The results of the unnotched and notched Izod impact properties of various PP samples are summarized in (**Table 9**).

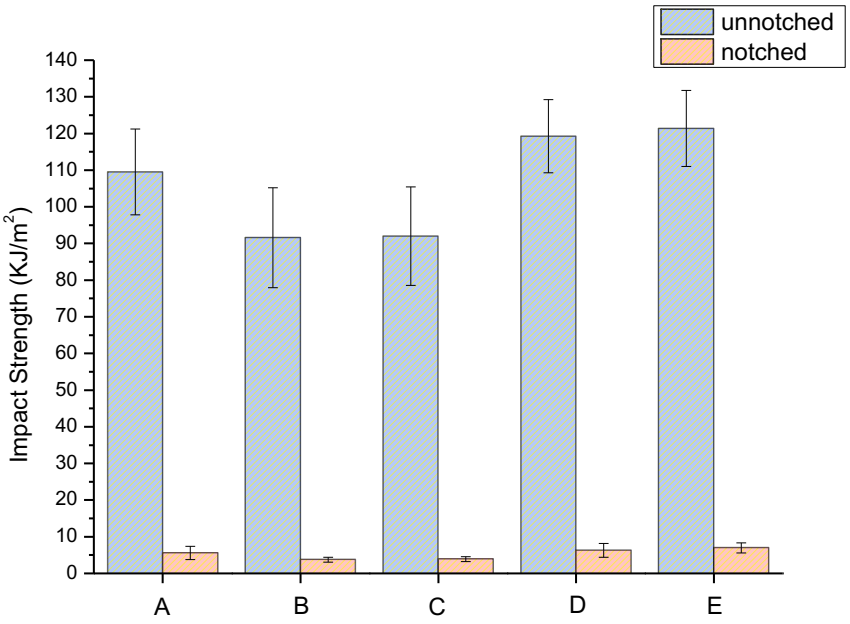

Figure 30. The unnotched and notched Izod impact properties of PP samples. Each graph represents the following samples on the (x axis); neat PP (A), PP blended with 5 wt.% $CuCl_2 \cdot 2H_2O$ particles (B), PP blended with 5 wt.% $Mg(OH)_2$ particles (C), PP thermally embossed with $CuCl_2.2H_2O$ suspension (D) and PP thermally embossed with $Mg(OH)_2$ suspension (E).

Table 9. The unnotched and notched Izod impact properties of various PP samples.

Samples	*Unnotched Izod [KJ/m^2]*	*Notched Izod [KJ/m^2]*
Neat PP	109.51 ± 11.73	5.57 ± 1.78
PP 5 wt.% $CuCl_2 \cdot 2H_2O$ (compounded)	91.57 ± 13.65	3.75 ± 0.66
PP 5 wt.% $Mg(OH)_2$ (compounded)	92.02 ± 13.45	3.89 ± 0.67
PP $CuCl_2 \cdot 2H_2O$ (thermally embossed)	119.24 ± 9.96	6.27 ± 1.89
PP $Mg(OH)_2$ (thermally embossed)	121.36 ± 10.36	6.96 ± 1.36

3.6.6 Barrier Properties

The barrier properties of various PP films are presented in (**Figure 31**). The thermally embossed data in (D) and (E) were prepared as discussed in (**Section 3.2.6**) using neat PP sheets prepared earlier in (**Section 3.2.3**) via cast sheet extrusion.

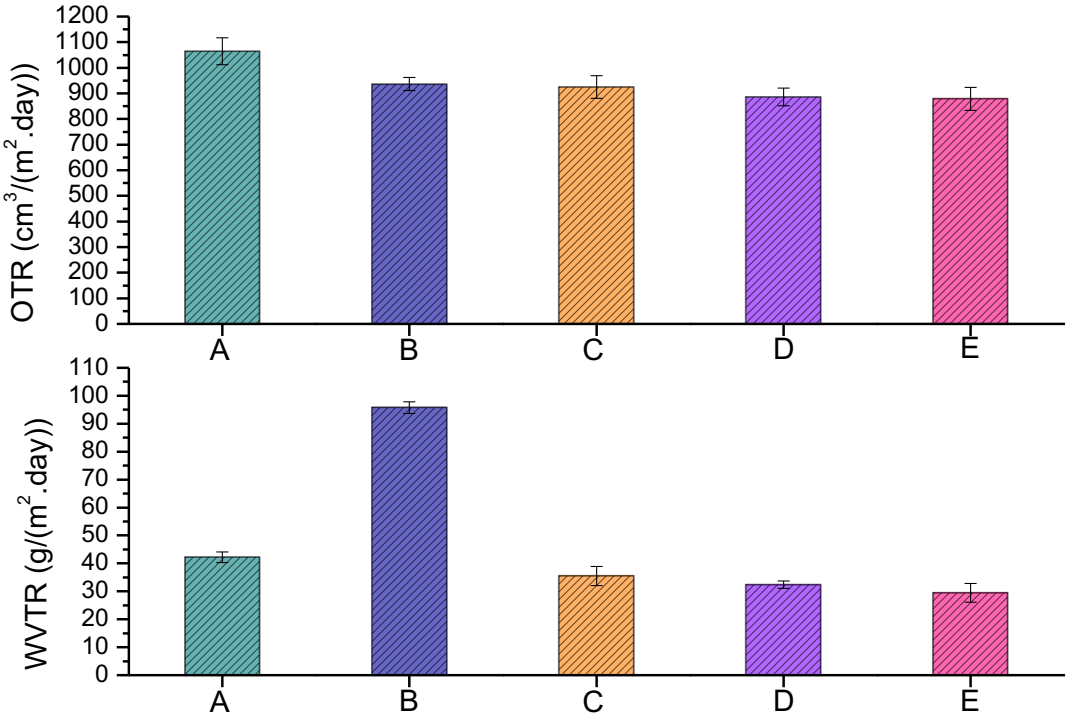

Figure 31. The WVTR and OTR of each graph represent the following samples on the (x axis); neat PP (A), PP blended with 5 wt.% $CuCl_2 \cdot 2H_2O$ particles (B), PP blended with 5 wt.% $Mg(OH)_2$ particles (C), PP thermally embossed with $CuCl_2 \cdot 2H_2O$ suspension (D), and PP thermally embossed with $Mg(OH)_2$ suspension (E).

3.6.7 Leachability of Agents

The UV spectra of DI water (considered as leachant's carrier), anti-microbial suspensions (1 ppm) in DI water, and DI water exposed to PP samples are presented in (**Figure 32**). Transmission of UV light through DI water (control) did not show any peak at any of the scanned ranges between (800 nm and 200 nm). DI water exposed to a neat PP sample started to increase around (320 nm to 200 nm). DI water exposed to PP blended with 5 wt.% $Mg(OH)_2$ samples started to decrease between (320 nm and 260 nm) and started to increase around (260 nm and 200 nm).

DI water exposed to PP thermally embossed with $Mg(OH)_2$ samples started to decrease between (320 nm and 260 nm) and started to increase to form a peak around (240 nm). $Mg(OH)_2$ suspension (1 ppm) started to increase gradually between (800 nm) and started to form a peak around (260 nm). DI water exposed to (i) PP blended with 5 wt.% $CuCl_2 \cdot 2H_2O$, (ii) PP thermally embossed with $CuCl_2 \cdot 2H_2O$ suspension, and (iii) $CuCl_2 \cdot 2H_2O$ suspension showed almost the same curve where the curve started to decrease between (330 nm and 315 nm) and started to increase to form a peak around (220 nm). There was no significant difference in absorption in the visible light region (400 nm to 800 nm) within the samples.

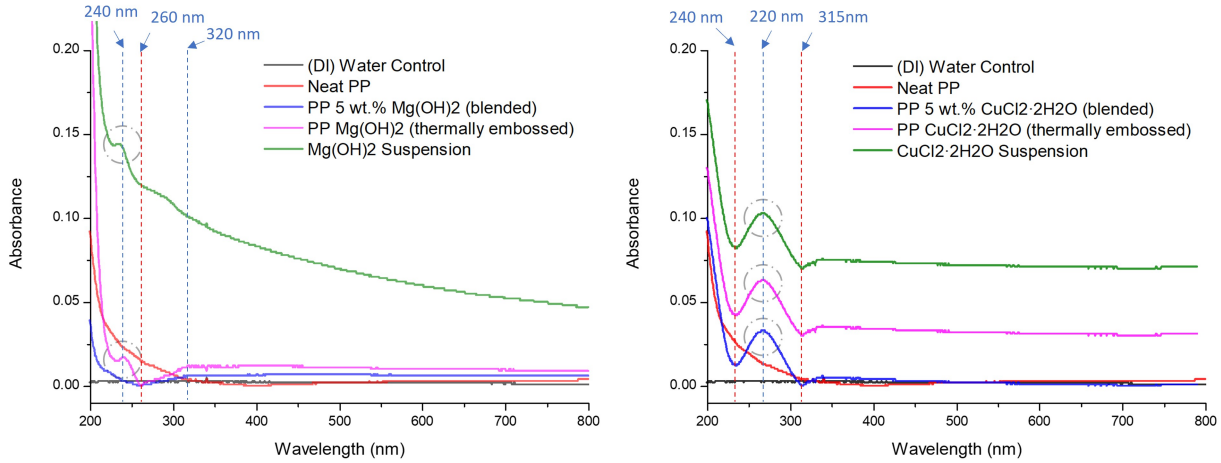

Figure 32. UV spectra of DI water (leachant's carrier) exposed to various PP samples, and the anti-microbial suspensions between (200 and 800 nm).

3.7 Discussion

We have undertaken this study to develop methods to fabricate anti-microbial plastic surfaces with non-leachable biocides (in de-ionised H_2O) with low or zero toxicity. In this study, we selected *E. coli* K-12 as a test microorganism because of the ease of handling this microbe in the laboratory.[244] Meanwhile, $CuCl_2.2H_2O$ was selected because it is cheap and effective against *E.coli*. More importantly, $CuCl_2 \cdot 2H_2O$ is classified as a leachable biocide (in H_2O) and thus it will offer a control for non-leachable $Mg(OH)_2$ biocide. $CuCl_2 \cdot 2H_2O$ was an effective anti-microbial

agent against both Gram-positive and Gram-negative bacteria such as *Staphylococcus Aureus* (*S. Aureus*) and *E.coli*, respectively,[245] and it was an effective anti-viral and anti-fungal agent against Influenza A and Candida Albicans, respectively.[245, 246] In addition, $CuCl_2{\cdot}2H_2O$ had significantly reduced the biofilm formation.[247] $Mg(OH)_2$ was selected as it is classified as a non-leachable biocide (in diH_2O), is non-toxic to human cells, and is FDA-approved.[248] $Mg(OH)_2$ was an effective anti-microbial agent when tested in vitro and in vivo against both Gram-positive and Gram-negative bacteria such as *S. Aureus* and *E.coli*, respectively.[249] The biosafety of anti-microbial $Mg(OH)_2$ was extensively investigated recently, and it was found to be a great biosafety to a normal biological system.[250] PP is a widely used plastic and accounts for around (15 %) of all plastics produced and used. PP is used as a film, and thus it is a good candidate for the thermal embossing approach used in this study. In addition, PP is also used for injection molding processes, and thus it offers suitable substrate for both extrusion and injection molding biocide incorporation. Our injection molding approach for biocide incorporation was straightforward where the biocide and PP were melt-mixed at the desired temperature and in the desired ratios. However, as expected, at such concentrations such as 5 wt.%, particles were not detected by neither SEM nor EDX on the surfaces of these injected molded PP samples as shown in (**Figure 21** and **Figure 22**). The non-leachable anti-microbial agent $Mg(OH)_2$ did not provide any anti-microbial activities to the PP. This was presumably due to the $Mg(OH)_2$ particles being masked in the polymer matrix, which prevented this biocide from interacting with the bacteria. In contrast, the anti-microbial biocides that work by leaching ionic charges (like $CuCl_2{\cdot}2H_2O$) are active in killing bacteria after they undergo melt compounding into plastics such as PP. The leachable biocidal crystals such as $CuCl_2{\cdot}2H_2O$ were also embedded inside the polymer matrix as seen from the SEM and EDX characterization (**Figure 23E** and **Figure 23F**), but its leachants (ionic charges) can leave the

matrix and reach the surface or even beyond. However, the disadvantage of $CuCl_2 \cdot 2H_2O$ is that the leaching of metal ions can be harmful to humans, but it was used in this study as a leachable control for our non-leachable biocides. On the other hand, injection molding is not a suitable approach for the non-leachable biocides-based anti-microbial surfaces at the concentration tested here (up to 5 wt.% with respect to PP) as they did not show any anti-microbial properties. If the concentration of biocides is increased to 20-40% higher ratios, it may be possible that one would observe some anti-microbial activity keeping in consideration not to weaken mechanical properties, but this aspect is beyond the scope of this work. Generally, high loading of filler particles decreases the strength and embrittles the material.

To test the effectiveness of non-leachable $Mg(OH)_2$ as an anti-microbial additive for PP via the thermal embossing approach, $Mg(OH)_2$ particles were embossed onto PP film. First, PP film was prepared with a thickness of 300 μm. However, the incorporation of $Mg(OH)_2$ and $CuCl_2 \cdot 2H_2O$ particles onto the PP sheet or film surface was not easy. Several approaches, concentrations, and liquids were tried to deposit the anti-microbial crystals via spray coating, dry coating, dip coating, and metallic rod coating onto the PP surface directly. Due to the intrinsic wetting issues, uniform coatings were not obtained using any of these methods. Although the samples showed good anti-microbial properties, it had lower reproducibility. The suspension showed good wetting behavior on aluminum foil before and after drying. This approach was much better than applying the suspension over the PP sheet directly due to the intrinsic wetting issue, which could not be effectively addressed by applying plasma treatment over the PP sheet.

To ensure that the particles were embossed firmly onto PP, a temperature of (143 °C and 2 bar of pressure for 10 s) was found to provide the best crystal fixation onto the PP materials. Less than (143 °C and 2 bar of pressure for 10 s) offered only modest particle fixation over the PP sheet,

and more than (143 °C and 2 bar of pressure for 10 s) caused the PP substrate to undergo noticeable warpage or to exhibit thermal defects. The optimized parameters led to a good transfer and deposition of the anti-microbial biocidal particles from the aluminum foil to the PP sheet. The transferred and thermally fixed coating (thermal embossing) could not be removed from the PP sheet's surface after rubbing, washing under a water tap, or applying the Scotch tape test (at least was not visually observable during the inspection). The two sides of the PP sheet were coated in this study, but it is technically possible to coat on only one side if needed.

The melt-compounded and injection-molded PP with 5 wt.% $CuCl_2 \cdot 2H_2O$ had a T_m (163.39 °C ± 0.14), and that with 5 wt.% $Mg(OH)_2$ had a T_m of (166.13 °C ± 0.81) compared to the PP control T_m (165.43 °C ± 0.78). The PP disks that had been thermally embossed with $CuCl_2 \cdot 2H_2O$ particles showed T_m (165.20 °C ± 0.58), and that which had been thermally embossed with $Mg(OH)_2$ particles showed T_m (164.88 °C ± 0.01) compared to the PP control T_m (165.43 °C ± 0.78), as shown in (**Figure 24**). The melt-compounded and injection-molded PP with 5 wt.% $CuCl_2 \cdot 2H_2O$ showed T_c of (116.66 °C ± 0.04), and that with 5 wt.% $Mg(OH)_2$ had a T_c of (119.64 °C ± 0.73). The PP disks that had been thermally embossed with $CuCl_2 \cdot 2H_2O$ particles showed T_c (118.80 °C ± 0.42), while that which had been thermally embossed with $Mg(OH)_2$ particles had a T_c (118.87 °C ± 0.13) compared to the PP control T_c (117.31 °C ± 0.30), as shown in (**Figure 25**). The melt-compounded and injection-molded PP with 5 wt.% $CuCl_2 \cdot 2H_2O$ had (7 %) higher crystallinity (%) (43.00 % ± 1.65), and that with 5 wt.% $Mg(OH)_2$ had (8.34 %) higher crystallinity (%) (43.63 % ± 0.83) compared to the PP control (39.99 % ± 0.61). The PP that had been thermally embossed with $CuCl_2 \cdot 2H_2O$ particles had (7.54 %) higher crystallinity (%) (43.25 % ± 3.68), and that which had been thermally embossed with $Mg(OH)_2$ particles had (10.56 %) higher crystallinity (%) (44.71 % ± 5.53) compared to the PP control T_c (39.99 °C ± 0.61), as shown in

(**Table 6**). In summary, both inorganic crystals did not show any nucleating effect for speeding crystallisation of the PP while there was a small increase in crystallinity of the PP.

The TGA data for PP samples presented in (**Figure 26**, and **Table 7**) showed the following; $CuCl_2 \cdot 2H_2O$ and $Mg(OH)_2$ particles (form of powder) showed a 5 % weight loss had occurred at (101.20 °C ± 1.76 °C, and 206.44 °C ± 0.13 °C, respectively). Similar TGA curves were observed in the literature for those particles.[251, 252] The 5 % weight loss for melt-compounded and injection molded PP with 5 wt.% $CuCl_2 \cdot 2H_2O$ and 5 wt.% $Mg(OH)_2$ had occurred at (394.21 °C ± 0.07 °C, and 353.64 °C ± 1.62 °C, respectively) which was (13, and 1 %, respectively) higher than neat PP (349.56 °C ± 2.97 °C). The 5 % weight loss for PP thermally embossed with $CuCl_2 \cdot 2H_2O$ and $Mg(OH)_2$ particles had occurred at (422.90 °C ± 3.60 °C, and 336.88 °C ± 3.97 °C, respectively) which was (21 % higher, and 4 % lower, respectively) compared to the neat PP (349.56 °C ± 2.97 °C). Overall, the $CuCl_2 \cdot 2H_2O$ had enhanced the thermal stability of PP samples. In contrast, $Mg(OH)_2$ did not show any significant change for PP samples.

The anti-microbial data of PP samples against (8.16 ± 0.08 log) *E. coli* K-12 MG1655 were presented in (**Figure 27** and **Figure 28**). The metallic copper disks (positive control) showed a (6.52 ± 0.02, and 8.16 ± 0.02 log reduction in 4 h and 24 h, respectively). The neat PP disks (negative control) showed a (0.25 ± 0.03, and 0.66 ± 0.12 log reduction in 4 h and 24 h, respectively). The melt-compounded and injection-molded PP disks with 1 wt.% $CuCl_2 \cdot 2H_2O$ showed (0.32 ± 0.03, and 1.78 ± 0.03 log reduction in 4 h and 24 h, respectively) which was (14.89, and 92.41 % reduction from the negative control, respectively). The melt-compounded and injection molded PP disks with 5 wt.% $CuCl_2 \cdot 2H_2O$ showed (2.24 ± 0.11, and 5.87 ± 0.01 log reduction in 4 h and 24 h, respectively) which was (98.98, and 99.99 % reduction from the negative control, respectively). The melt-compounded and injection-molded PP disks with 1 wt.%

$Mg(OH)_2$ showed (0.25 ± 0.20, and 0.46 ± 0.07 log reduction in 4 h and 24 h, respectively) which was (a 14.89 % reduction, and 58.49 % growth from the negative control, respectively). The melt-compounded and injection-molded PP disks with 5 wt.% $Mg(OH)_2$ showed (0.27 ± 0.07, and 0.47 ± 0.03 log reduction in 4 h and 24 h, respectively) which was (a 4.50 % reduction, and 54.88 % growth from the negative control, respectively) (**Figure 27**). The PP disks cut from thermally embossed sheets with $CuCl_2 \cdot 2H_2O$ particles showed (1.11 ± 0.03, and 2.28 ± 0.03 log reduction in 4 h and 24 h, respectively) which was (85.87, and 97.60 % reduction from the negative control, respectively). The PP disks thermally embossed with $Mg(OH)_2$ particles showed (0.71 ± 0.08, and 3.78 ± 0.03 log reduction in 4 h and 24 h, respectively) which was (65.33, and 99.92 % reduction from the negative control, respectively) (**Figure 28**). The $Mg(OH)_2$ biocide which was "ineffective" when compounded in the PP polymer (**Figure 27**) became "highly potent" when it was thermally embossed onto PP (**Figure 28**). The latter method causes the crystals to become "fixed" on the surface so that they do not flake off (**Figure 23J**). These observations confirm the assumption that $Mg(OH)_2$ is a non-leachable anti-microbial agent (in diH_2O), thus requiring direct contact with the bacteria to be effective.

The MFI (g/10 min) for melt-compounded and injection molded PP with 5 wt.% $CuCl_2 \cdot 2H_2O$ and 5 wt.% $Mg(OH)_2$ was (3.843 ± 0.192, and 2.590 ± 0.135, respectively) which was (119, and 48 %, respectively) higher compared to the neat PP (1.753 ± 0.036). Overall, the $CuCl_2 \cdot 2H_2O$ and $Mg(OH)_2$ particles had increased the MFI compared to the neat PP (**Table 8**). The density (g/CC) for melt-compounded and injection-molded PP with 5 wt.% $CuCl_2 \cdot 2H_2O$ and 5 wt.% $Mg(OH)_2$ was (0.931 ± 0.004, and 0.934 ± 0.012, respectively) which was (0.432, and 0.755 %, respectively) lower compared to the neat PP (0.927 ± 0.004). The density (g/CC) for PP thermally embossed with $CuCl_2 \cdot 2H_2O$ and $Mg(OH)_2$ particles was (0.928 ± 0.091, and 0.930 ±

0.086, respectively) which was (0.108, and 0.324 %, respectively) higher compared to the neat PP (0.927 ± 0.004). Overall, the $CuCl_2 \cdot 2H_2O$ and $Mg(OH)_2$ particles used via melt-compounding and thermal embossing did not show any significant change for PP samples (**Table 8**).

The tensile stress at yield (MPa) (**Figure 29**) for melt-compounded and injection molded PP with 5 wt.% $CuCl_2 \cdot 2H_2O$ and 5 wt.% $Mg(OH)_2$ was (61.24 ± 1.65, and 60.30 ± 1.47, respectively) which was (12, and 11 %, respectively) higher compared to the neat PP (54.54 ± 0.90). The tensile stress at yield (MPa) for thermally embossed PP with $CuCl_2 \cdot 2H_2O$ and $Mg(OH)_2$ particles was (63.24 ± 1.97, and 63.22 ± 1.60, respectively) which was (16, and 16 %, respectively) higher compared to the neat PP (54.54 ± 0.90). The tensile stress at break (MPa) for melt-compounded and injection molded PP with 5 wt.% $CuCl_2 \cdot 2H_2O$ and 5 wt.% $Mg(OH)_2$ was (46.89 ± 2.72, and 33.21 ± 4.93, respectively) which was (47, and 4 %, respectively) higher compared to the neat PP (31.82 ± 3.21). The tensile stress at break (MPa) for PP thermally embossed with $CuCl_2 \cdot 2H_2O$ and $Mg(OH)_2$ particles was (48.52 ± 2.98, and 37.64 ± 3.99, respectively) which was (16, and 4 %, respectively) higher compared to the neat PP (54.54 ± 0.90). The tensile modulus (MPa) for melt-compounded and injection molded PP with 5 wt.% $CuCl_2 \cdot 2H_2O$ and 5 wt.% $Mg(OH)_2$ was (2460.91 ± 112.91, and 2363.39 ± 95.01, respectively) which was (12, and 7 %, respectively) higher compared to the neat PP (2201.42 ± 3.21). The tensile modulus (MPa) for PP thermally embossed with $CuCl_2 \cdot 2H_2O$ and $Mg(OH)_2$ particles was (2546.13 ± 98.12, and 2405.65 ± 82.366, respectively) which was (16, and 9 %, respectively) higher compared to the neat PP (2201.42 ± 3.21). The elongation at break (%) for melt-compounded and injection molded PP with 5 wt.% $CuCl_2 \cdot 2H_2O$ and 5 wt.% $Mg(OH)_2$ was (120.36 ± 13.36, and 88.25 ± 15.36, respectively) which was (24 % higher, and 9 % lower, respectively) compared to the neat PP (97.06 ± 16.25). The elongation at break (%) for PP thermally embossed with $CuCl_2 \cdot 2H_2O$ and $Mg(OH)_2$ particles

was (111.36 ± 17.36, and 92.34 ± 12.12, respectively) which was (13 % higher, and 5 % lower, respectively) compared to the neat PP (97.06 ± 16.25). Overall, the $CuCl_2 \cdot 2H_2O$ and $Mg(OH)_2$ particles enhanced the tensile properties of PP samples when applied through melt-compounding and thermal embossing, at the levels of addition. The elongation at break (%) for $Mg(OH)_2$ had decreased compared to the neat PP.

The unnotched Izod impact strength (KJ/m^2) (**Figure 30** and **Table 9**) for melt-compounded and injection-molded PP with 5 wt.% $CuCl_2 \cdot 2H_2O$ and 5 wt.% $Mg(OH)_2$ was (91.57 ± 13.65, and 92.02 ± 13.45, respectively) which was (16, and 16 %, respectively) lower compared to the neat PP (109.51 ± 11.73). The unnotched Izod impact strength (KJ/m^2) for PP thermally embossed with $CuCl_2 \cdot 2H_2O$ and $Mg(OH)_2$ particles were (119.24 ± 9.96, and 121.36 ± 10.36, respectively) which was (9, and 11 %, respectively) higher compared to the neat PP (109.51 ± 11.73). All unnotched Izod impact specimens were not broken after testing. In contrast, the notched Izod impact strength (KJ/m^2) for melt-compounded and injection molded PP with 5 wt.% $CuCl_2 \cdot 2H_2O$ and 5 wt.% $Mg(OH)_2$ was (3.75 ± 0.66, and 3.89 ± 0.67, respectively) which was (33, and 30 %, respectively) lower compared to the neat PP (5.57 ± 1.78). The notched Izod impact strength (KJ/m^2) for PP thermally embossed with $CuCl_2 \cdot 2H_2O$ and $Mg(OH)_2$ particles was (6.27 ± 1.89, and 6.96 ± 1.36, respectively) which was (13, and 25 %, respectively) higher compared to the neat PP (5.57 ± 1.78). Overall, the $CuCl_2 \cdot 2H_2O$ and $Mg(OH)_2$ particles enhanced the tensile properties of PP samples when applied through melt-compounding and thermal embossing. The unnotched and notched Izod impact strength (KJ/m^2) for melt-compounded and injection-molded PP with 5 wt.% $CuCl_2 \cdot 2H_2O$ and 5 wt.% $Mg(OH)_2$ had decreased compared to the neat PP.

The WVTR ($g/(m^2 \bullet day)$) for melt-compounded and cast film extruded PP with 5 wt.% $CuCl_2 \cdot 2H_2O$ and 5 wt.% $Mg(OH)_2$ was (95.78 ± 2.10, and 35.45 ± 3.40, respectively) which was

(127 % higher, and 16 % lower, respectively) compared to the neat PP (42.23 ± 1.90). The WVTR (g/(m^2•day)) for PP thermally embossed with $CuCl_2 \cdot 2H_2O$ and $Mg(OH)_2$ particles was (32.36 ± 1.30, and 29.45 ± 3.40, respectively) which was (23, and 30 %, respectively) lower compared to the neat PP (42.23 ± 1.90). The OTR (cm^3/(m^2•day)) for melt-compounded and cast film extruded PP with 5 wt.% $CuCl_2 \cdot 2H_2O$ and 5 wt.% $Mg(OH)_2$ was (936.35 ± 25.63, and 924.75 ± 43.99, respectively) which was (12, and 13 %, respectively) lower compared to the neat PP (1064.97 ± 52.36). The OTR (cm^3/(m^2•day)) for PP thermally embossed with $CuCl_2 \cdot 2H_2O$ and $Mg(OH)_2$ particles were (886.45 ± 34.85, and 878.63 ± 45.52, respectively) which was (17, and 17 %, respectively) lower compared to the neat PP (1064.97 ± 52.36). Overall, the $CuCl_2 \cdot 2H_2O$ and $Mg(OH)_2$ particles used via melt-compounding and thermal embossing had enhanced the barrier properties of both WVTR and OTR for PP samples (**Figure 31**) except for PP 5 wt.% $CuCl_2 \cdot 2H_2O$ sample which increased WVTR.

The leachability study using the UV light transmission technique (**Figure 32**) showed that neat PP and PP compounded with 5 wt.% $Mg(OH)_2$ did not form any peak in the range of (800 nm to 200 nm), and both samples showed almost the same curve without any significant differences. The $Mg(OH)_2$ suspension and PP thermally embossed with $Mg(OH)_2$ particles formed the same peak around (240 nm). This is evidence of why PP blended with 5 wt.% $Mg(OH)_2$ did not show significant anti-microbial activity (**Figure 27**) because the particles did not leach out ions from the PP matrix when they were in contact with water. The UV spectra of $Mg(OH)_2$ were like what had been seen in literature.[253] In contrast, the PP thermally embossed with $Mg(OH)_2$ particles showed a peak around (240 nm), and provided significant anti-microbial activity (**Figure 28**). The peak coming from the PP thermally embossed with $Mg(OH)_2$ sample (240 nm) could be due to either the low solubility or the migration of the particles into the DI water at a very low level because the

samples were rotated at (20 rpm) for 24 h.[254] All samples prepared by $CuCl_2 \cdot 2H_2O$ particles such as (i) PP blended with 5 wt.% $CuCl_2 \cdot 2H_2O$, (ii) PP thermally embossed with $CuCl_2 \cdot 2H_2O$ particles, and (iii) $CuCl_2 \cdot 2H_2O$ suspension showed almost the same curve and formed a peak around (220 nm). This is evidence that $CuCl_2 \cdot 2H_2O$ is a leachable anti-microbial agent when used in polymer melt compounding such as PP and will provide the anti-microbial activity as seen in (**Figure 27**). The UV spectra of $CuCl_2 \cdot 2H_2O$ were like what had been seen in the literature.[255]

It is worth mentioning that the thermal embossing method incorporated the non-leachable anti-microbial agent (i.e., $Mg(OH)_2$) into the plastics in a very robust manner, so that the crystals cannot be wiped away, washed off, or peeled away from the PP substrate via a Scotch tape test (at least to the visible inspection). This robustness is mainly because one side of the biocidal crystals is thermally fixed over the plastic surface and the other side of the particles is exposed to the microbes. However, further studies will need to be undertaken in the future to test the toxicity of these thermally embossed PP anti-microbial surfaces. The thermal embossing approach would qualify as an industrially scalable roll-to-roll process, as it is readily applicable to sheets and films.

3.8 Conclusion

We have demonstrated the incorporation of anti-microbial agents into PP via injection molding and thermal embossing. The SEM analysis confirmed that the thermal embossing approach was able to affix anti-microbial particles onto PP surfaces, while the injection-molded PP surfaces were free of any nanoparticles. Chapter 2 had shown that direct application of nano crystal suspensions to PP does not lead to uniform coatings due to wetting issues. However, a new workable method was found by first applying the suspension to Al foil, drying it, and transferring the nano crystals it onto the PP sheet by heat embossing. The uniform nano crystal coating on the Al foil transfers surprisigly well to the PP sheet. In fact, this method was also tested successfully

with PC, PE and amorphous PET sheets. $CuCl_2 \cdot 2H_2O$ conferred anti-microbial properties to injection-molded PP as well as to thermally embossed PP, owing to the leaching of anti-microbial copper ions from the nanoparticles. In contrast, $Mg(OH)_2$ provided anti-microbial properties only when the thermal embossing technique was employed since it is a "non-leachable" additive. The advantage of $Mg(OH)_2$ is that it is safe for human health, and widely used in the medicine and food industries.

CHAPTER 4: INVESTIGATING ANTI-BACTERIAL AND ANTI-COVID-19 VIRUS PROPERTIES AND MODE OF ACTION OF $Mg(OH)_2$ AND COPPER-INFUSED $Mg(OH)_2$ NANOPARTICLES ON COATED POLYPROPYLENE SURFACES

4.1 Objective

The aim of this chapter is to introduce newly developed anti-microbial agents that had not been used earlier for polymer application (developed by Aqua Recourses, Patent No: US20220225610A1). In addition, this chapter focuses on the investigation of anti-bacterial and anti-viral properties, mode of action of $Mg(OH)_2$ and copper-infused $Mg(OH)_2$ nanoplatelets (NPs) in melt-compounded and thermally embossed polypropylene (PP) surfaces. The anti-viral activity of the NPs was studied in aqueous liquid suspensions against SARS-CoV-2, and the mode of action was investigated on neat NPs and PP samples that were thermally embossed with NPs. Plastics with anti-microbial surfaces from where biocides are non-leachable are highly desirable. This work provides a general fabrication strategy for developing anti-microbial plastic surfaces. The sub-objectives are described as follows:

- The melt blending as well as thermal surface embossing approaches were employed to incorporate $Mg(OH)_2$ and Cu-infused $Mg(OH)_2$ particles into PP and their anti-bacterial properties of these materials were investigated against *E. coli* K-12 MG1655 over periods of 0, 4, and 24 h.
- Similarly, the anti-viral activity of neat $Mg(OH)_2$ and Cu-infused $Mg(OH)_2$ NPs was studied in an aqueous solution against SARS-CoV-2 for 4 h to evaluate the anti-viral properties.
- The biocidal mechanisms of these anti-microbial agents were studied against *E. coli* K-12 MG1655 by measuring the total cellular ROS in the bacteria.

- The PP samples were further characterized by differential scanning calorimetry (DSC), thermogravimetric analysis (TGA), scanning electron microscopy (SEM), and energy dispersive X-ray spectroscopy (EDX).

4.2 Experimental

4.2.1 Materials

Polypropylene homopolymer (PP 500 P grade) was supplied by SABIC (Riyadh, Saudi Arabia) as a powder (used for melt-compounding) and pellets (used for sheet extrusion) having the following characteristics: melting point = 166 °C, density = 905 kg/m^3, and melt flow index (MFI) measured at 230 °C and 2.16 kg = 3 g/min. $Mg(OH)_2$ (purity: 99.99 %) and Cu-infused $Mg(OH)_2$ (purity: 99.99 %) were supplied by Aqua Resources Corp. (Florida, USA) as a dry powder of $Mg(OH)_2$ (used for melt-compounding) and a slurry of (i) $Mg(OH)_2$ and (ii) Cu-infused $Mg(OH)_2$ (suspended in water used for thermal surface embossing). Isopropyl alcohol was obtained from Macron Fine Chemicals (purity: 99.99 %). Dulbecco's Modified Eagle Mediam (DMEM), Avicel, phosphate-buffered saline (PBS), and L-glutamine were obtained from commercial suppliers. The total cellular reactive oxygen species (ROS) concentration in the bacteria was detected using the Image-iT^{TM} LIVE Green Reactive Oxygen Species Detection Kit (ThermoFisher Scientific, catalog number I36007), which included 5-(and-6-)-carboxy-2',7'-dichlorodihydrofluorescein diacetate (carboxy-H_2DCFDA) for ROS detection, the cell-permeant nucleic acid stain Hoechst 33342 to identify individual bacteria, and *tert*-butyl hydroperoxide (TBHP) which is a common inducer of ROS production and serves as positive control.

4.2.2 Melt-compounding and injection molding of PP with the anti-microbial NPs

The anti-microbial NPs were mixed manually with the PP powder and extrusion compounded using a DSM Xplore 15cc Micro extruder that was designed with co-rotating conical

twin screws (processing temperature: 250 °C, speed: 10 rpm, time: 2 min). The mixing ratio was PP with 5 wt.% of $Mg(OH)_2$ and PP with 5 wt.% of Cu-infused $Mg(OH)_2$. Extrusion compounding led to PP composites containing the biocidal additives at the desired level. The neat PP (without biocide) and PP composites were injected into disk-shaped samples (dimensions: 2.5 mm in diameter and 1.55 mm in thickness) using a 3.5 mL. Injection molder (**Figure 33**). The temperature of the cylinder was set at 250 °C and the mold temperature was fixed at 60 °C.

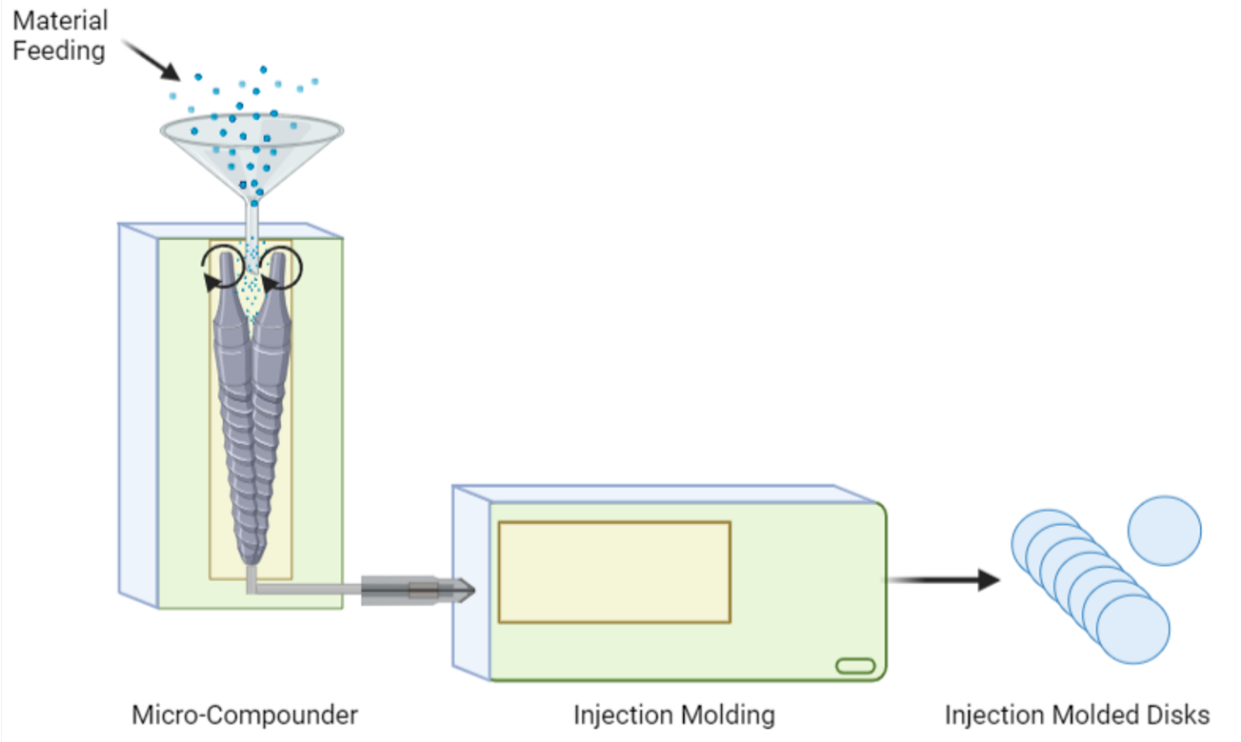

Figure 33. Micro-compounder and injection molding unit.

4.2.3 Sheet extrusion

The PP pellets were used to make the flat PP sheet (**Figure 34**) using Randcastle extruders model RCP-0625 (5/8 inch 24:1 L/D), and 8-inch flex lip die. The barrel zone temperature was 240 °C, and the hopper temperature was 45 °C. The adapter temperature was 235 °C, and the die temperature was 245 °C. The extruded PP sheet (dimensions: 20 x 80 x 0.03 cm^3) was cut into circular disks with a diameter of 2 cm and a thickness of 300 µm using an Esko Kongsberg X-24

digital cutting table. The disk size was sufficient for (i) thermal surface embossing, (ii) anti-microbial mechanism testing by confocal microscopy, and (iii) other characterization methods such SEM, EDX, DSC, and TGA.

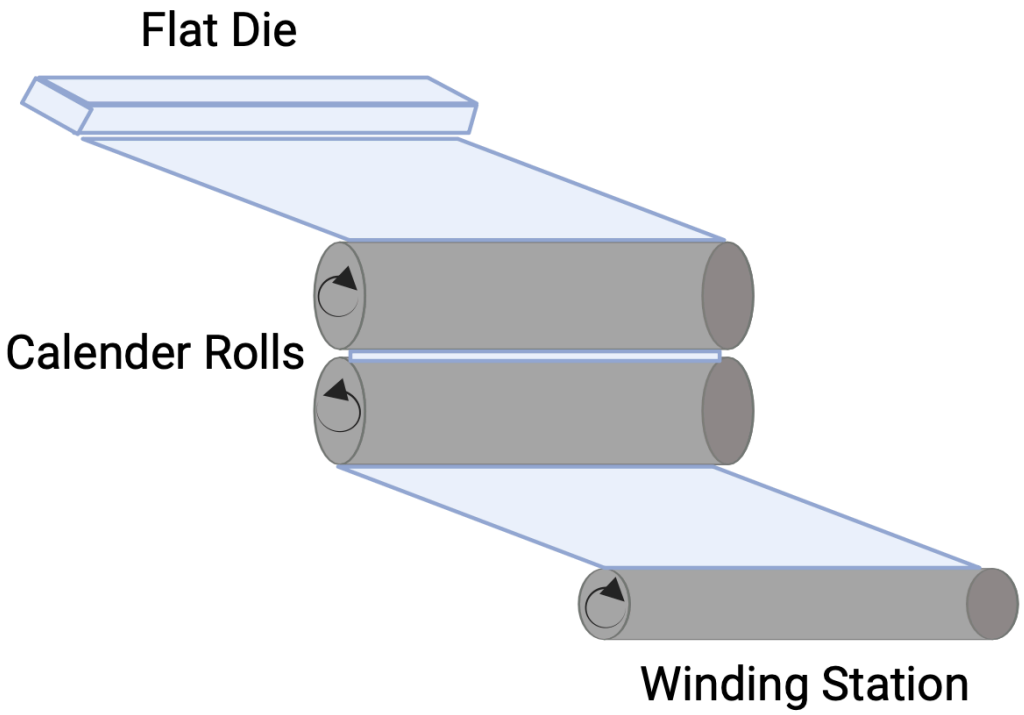

Figure 34. Cast film extrusion.

4.2.4 Coating of NPs on PP surface

Coating solution preparation:

The $Mg(OH)_2$ NPs were obtained commercially as a slurry (7 wt.% $Mg(OH)_2$ and 93 wt.% water). The $Mg(OH)_2$ slurry (14.3 mL) was diluted with isopropyl alcohol (85.7 mL) to prepare a $Mg(OH)_2$ suspension at a concentration of (10 mg/mL, **Figure 35)**. The suspension was vortexed at its maximum speed for 30 s, and subsequently sonicated in an ultrasonic bath at 23 °C for 10 min to ensure that the $Mg(OH)_2$ NPs were uniformly dispersed. After sonication, the suspension was vortexed once more at the maximum speed for 30 s.

The Cu-infused $Mg(OH)_2$ NPs were obtained commercially as a slurry (7.47 wt.% Cu-infused $Mg(OH)_2$ and 92.53 wt.% water). The Cu-infused $Mg(OH)_2$ slurry (1.34 mL) was diluted with isopropyl alcohol (8.66 mL) to prepare a Cu-infused $Mg(OH)_2$ suspension at a concentration of (10 mg/mL, **Figure 35**). The suspension was vortexed at a maximum speed for 30 s, and subsequently sonicated in an ultrasonic bath (Branson 2510 Ultrasonic Sonicator, Commack, NY, USA) at 23 °C for 10 min to ensure that the Cu-infused $Mg(OH)_2$ NPs were uniformly dispersed. After sonication, the suspension was vortexed once more at the maximum speed for 30 s.

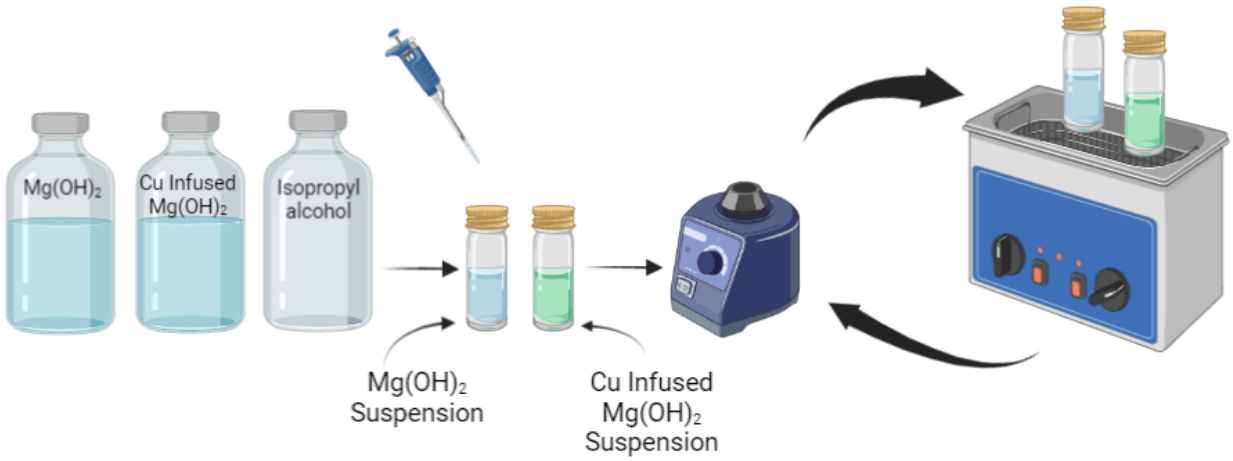

Figure 35. Preparation of the anti-microbial suspension.

Deposition of the NPs onto aluminum foil

A metallic rod applicator technique (K303, RK Print Coat Instruments Ltd., UK) was used to deposit the anti-microbial biocidal suspension over the aluminum foil (All-Foils, Inc. OH, USA, Dimensions: 0.00762 cm x 30.48 cm x 30.48 cm^3). The thickness of the wet deposited coating varied between 4-120 microns depending on the diameter of the wire (**Figure 36**). The anti-microbial suspension was spread as a wet film deposition over an aluminum foil (via 5 mL syringe) using the metallic rod number 5, corresponding to a thickness of 50 microns, and left to dry at 23 °C for 10 min.

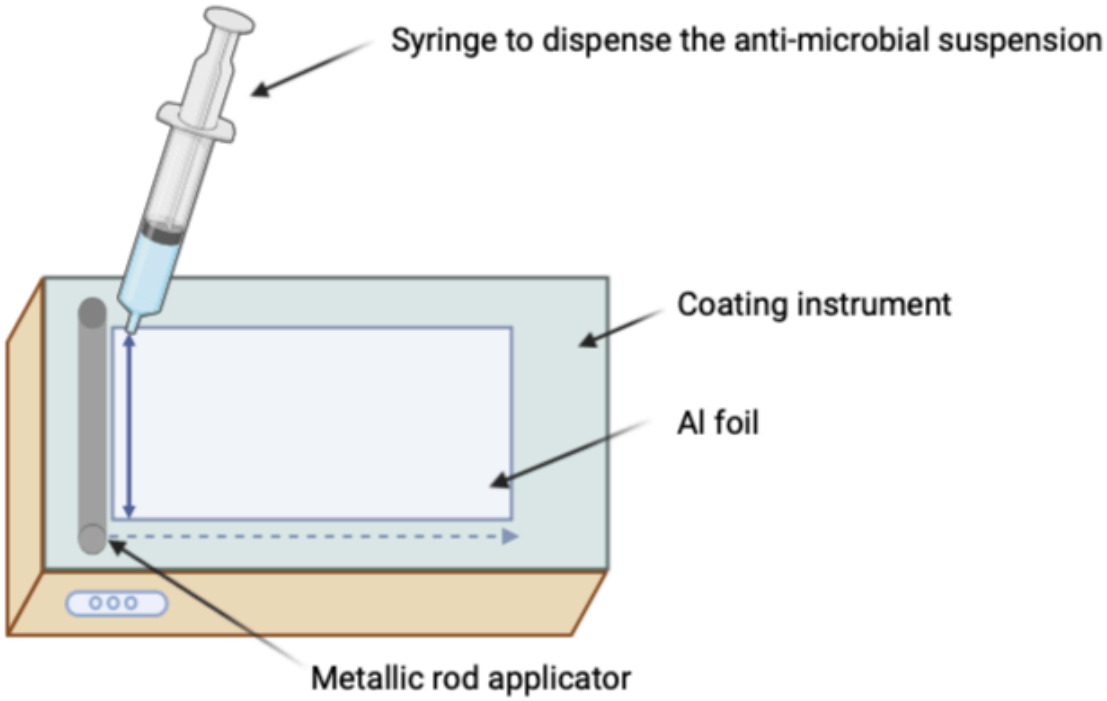

Figure 36. Deposition of the anti-microbial suspension onto a substrate using a metallic rod applicator.

Thermal embossing of NPs on PP surfaces

Disks were cut (dimensions: 2 cm in diameter, 0.5 mm in thickness) from PP extruded sheets (neat PP without biocides) using a Kongsberg X24 Edge Cutting Table, and from metallic copper sheets (Szone brand, China) using a Brother HS-70 A (wire EDMs) cutter device. Coated aluminum foil with anti-microbial crystals was used to transfer the temporarily deposited particles to the surface of the PP disks prior to the thermal embossing process where the particles were permanently fixed over the PP disk surfaces. The coated side of the aluminum foil was placed in contact with the PP (**Figure 37**) and pressed above the softening temperature of the PP using a compression molding press (PHI QL438-C, City of Industry, CA, USA). A temperature of 143 °C and 2 bars of pressure for 10 s were used for the PP disks.

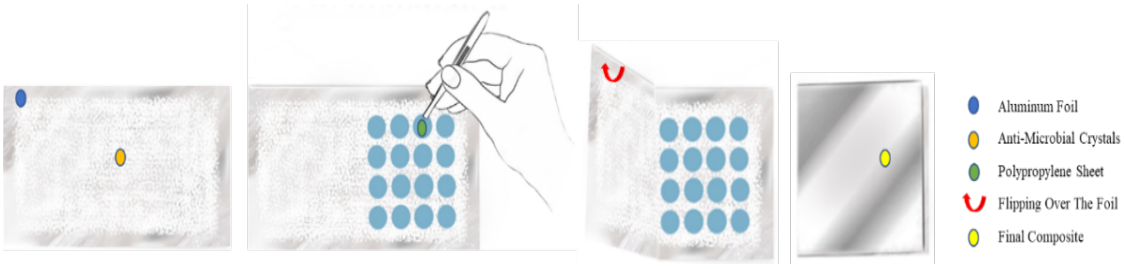

Figure 37. Transfer of anti-microbial particles to the surface of PP disks using coated aluminum foil prior to compression molding.

4.3 Characterization

4.3.1 Scanning electron microscopy (SEM) and energy dispersive X-ray (EDX) preparation methods

The anti-microbial particles (powders of $Mg(OH)_2$ and Cu-infused $Mg(OH)_2$), the compounded and injection molded PP disks (5% $Mg(OH)_2$ and 5% Cu-infused $Mg(OH)_2$ by weight), and the thermally embossed disks (suspension of $Mg(OH)_2$, and Cu-infused $Mg(OH)_2$ at 10 mg/mL) were characterized by SEM using a JEOL 7500F field emission emitter (JEOL Ltd., Tokyo, Japan), and by EDX analysis using an Oxford Instruments Aztec system (Oxford Instruments, High Wycomb, Bucks, England). Samples for EDX analysis were prepared by mounting samples on aluminum stubs affixed with epoxy glue. All mounted samples were coated with iridium (at a thickness of ~ 2.7 nm) utilizing a Quorum Technologies/Electron Microscopy Sciences Q150T turbo pumped sputter coater (Quorum Technologies, Laughton, East Sussex, England BN8 6BN) and purged with argon gas.

4.3.2 Differential scanning calorimetry (DSC)

The melting point and the crystallization temperature of the PP samples were determined by DSC using a TA Instrument Model Q100 system. The nitrogen flow was set at 70 mL min^{-1} for all measurements. The samples were thermally analyzed in the temperature range of -20 to 250 °C at a rate of 10 °C min^{-1} and held for 1 min to eliminate previous crystallization, mechanical,

thermal, processing, and shear history. The samples were additionally cooled to -20 °C at a rate of 10 °C min^{-1} and then re-heated to 250 °C at 10 °C min^{-1} and the thermal responses were recorded. All samples were analyzed in triplicate.

The degrees of crystallinity of the PP samples were calculated from the heat of fusion values determined from the **second heating** runs and evaluated according to the same equation mentioned in chapter 3. Equation (3):

$$X_c(\%) = \left[\frac{\Delta H_c}{\Delta H_0.W}\right] x100 \qquad \text{(Eq. 3)}$$

where X_c is the crystallinity of the PP samples, ΔH_c is the heat of fusion, ΔH_0 is the enthalpy of fusion for 100 % crystalline PP [209 J/g][241], and W is the fraction (weight) of PP in the composite.

4.3.3 Thermogravimetric analysis (TGA)

Thermal characterization of the PP samples was conducted with a TA Instruments (Model Q 50) system via thermogravimetric analysis (TGA) techniques. A quantity of (7 ± 2 mg) of each sample was placed in an aluminum pan.

The temperature was then ramped gradually from 25 to 600 °C at a heating rate of 10 °C min^{-1} under a nitrogen atmosphere with a flow rate of 40 mL min^{-1}. All samples were analyzed in triplicate.

4.3.4 Anti-microbial testing method

E. coli K-12 MG1655 was used for all experiments to evaluate the anti-microbial activities of the disks. The stock culture was stored at -80 °C in a ThermoFisher TSX400 system and applied as streaks onto Tryptic Soy Agar (TSA) plates (BBL/Difco, Sparks, MD, USA). After incubation at 37 °C for 24 h, a single colony was selected and transferred to 5 mL of Tryptic Soy Broth (TSB) (BBL/Difco, Sparks, MD, USA) and incubated at 37 °C for 18 h. After incubation, 1 mL of culture

was centrifuged at 13,000 x *g* for 5 min using a Fisher Scientific accuSpin micro 17 R centrifuge and the supernatant was discarded. Cells were suspended in 1 mL of phosphate-buffered saline (PBS, Crystalgen, Innovation for Science, Commack, NY, USA) by vortexing. The cell suspension was then transferred to a 15 mL tube and 11.5 mL of PBS was added. Aliquots of this suspension were then exposed to the different types of disks. Each single disk was placed separately in a pod which were contact lens cases manufactured by Bosch + Lomb. For each pod containing a single disk, 1 mL of bacterial suspension was added to submerge the disk into the culture broth and the pods were closed. The pods were then attached to a mini rotator (Benchmark Scientific, Roto Mini Plus R 2024, Sayreville, NJ, USA) and rotated at 20 rpm (**Figure 18**) around the machine's horizontal axis to continuously agitate the broth and cause liquid renewal on the surface of the disks. At 0, 4, and 24 h intervals, a 100 mL sample of the bacterial suspension was removed for the appropriate number of 1:10 dilutions, plated in TSA, and then incubated at 37 °C overnight. The colony forming units (CFU) were enumerated to determine the bacterial cell density at each time point (Scan300, InterScience). Neat PP disks were used as a "negative" control sample, while metallic copper disks were used as a "positive" control sample. In addition, the anti-microbial activity of different PP composite disks was tested individually.

4.3.5 Anti-viral testing method

$Mg(OH)_2$ NPs were prepared as described by Madden *et al*.[256] Cu-infused $Mg(OH)_2$ NPs were prepared according to (Maddan 2022).[257] The solid contents of the suspensions was determined by a Satrorius Moisture Analyzer (MA35-SV2). The solid content of the $Mg(OH)_2$ NPs suspension was adjusted by the addition of deionized water. $Mg(OH)_2$ was prepared at 2,780 ppm (vol. 3.6 mL), Cu-infused $Mg(OH)_2$ NPs were prepared at 2,780 ppm (vol. 3.6 mL) as concentrations suitable for dilution in subsequent steps.

The USA-WA1/2020 strain of SARS-CoV-2 was received from BEI Resources[258] and cultured on Vero E6 cells to establish master and working stocks. Virus stocks did not show any mycoplasma and titers were developed by standard plaque assay on Vero E6 cells as described below. The identity of the virus was confirmed by sequencing using the iSEQ 100 next generation sequencing platform (Illumina, SanDiego, USA).

All anti-viral experiments were conducted within the biosafety level 3 (BSL-3) in the Laboratory of Infectious Diseases, University of Southern Alabama. On the day of the experiment, SARS-CoV-2 virus was diluted in Dulbecco's phosphate-buffered saline (DPBS) to achieve 1 x 10^5 plaque forming units (PFU)/0.1 mL and kept on ice. Prior to use, the $Mg(OH)_2$ NPs suspension and Cu-infused $Mg(OH)_2$ NPs suspension were vortexed for 5 s prior to combining 0.9 mL of this suspension with 0.1 mL of virus in a 1.7 mL microcentrifuge tube to achieve final concentration of NPs 2,500 ppm. Cytotoxicity controls consisted of 0.9 mL of the test articles combined with 0.1 mL of DPBS alone. The virus control consisted of 0.1 mL of diluted virus in 0.9 mL of DPBS. Each treatment was performed in duplicate. Immediately following preparation, all samples were incubated at room temperature in a biological safety cabinet (BSC) with rotation to keep the NPs well dispersed. After 4 h, each sample tube was collected and stored at -80 ^oC until needed for titration. Plaque Assay: Vero E6 cells were seeded in a 12-well plate until the cell confluency reached greater than 95 %. Samples were removed from a freezer that was operated at -80 ^oC and allowed to thaw on ice before preparing 10-fold serial dilutions of each sample in virus diluent (DPBS containing 2 % FBS). Duplicate wells of Vero E6 cells were then inoculated with 0.1 mL of each diluted sample and incubated at 37 °C with rocking every 15 min. After 1 h, cells were overlayed with DMEM containing 1.2% Avicel, 2% PBS, and 1x L-glutamine and gently swirled. After 2 days of incubation at 37 °C with 5% CO_2, cells were fixed by adding 0.5 mL of 10 %

buffered formalin to each well and then incubating them for 1 h at room temperature. Formalin was decanted in a labeled hazardous waste container and enough 0.4 % crystal violet solution (~0.5 mL) was added to cover each well. After more than 1 minute of incubation at room temperature, plates were rinsed in a bucket filled with running tap water and tapped on absorbent material until the stain was visibly removed. Plates were inverted and allowed to air dry thoroughly before plaques were counted and used to calculate PFU/mL.

4.3.6 Confocal microscopy to study the anti-microbial mechanism

E. coli K-12 MG1655 (American Type Culture Collection, Manassas, VA) was used for all experiments to evaluate and compare the anti-microbial mechanism of (i) biocidal particles, and (ii) PP disks that were thermally embossed with the biocidal particles. *E. coli* was initially introduced onto the TSA surface (solid medium) and left to incubate at 37 °C overnight. Afterward, single colonies were selected and transferred into TSB (liquid medium) where they were agitated (MaxQ400, ThermoFisher) at 220 rpm overnight under aerobic conditions. The optical density of the bacterial solution was determined at OD 600 nm [OD_{600}] = 0.92 to 105 colony-forming units/mL (CFU/mL).

Confocal fluorescence images were acquired using an Olympus FluoView 1000 Confocal Laser Scanning Microscope (Olympus Corporation, Tokyo, Japan) that was configured on an automated IX81 inverted microscope with a 60x Plan Apo N oil objective lens (NA 1.42). Image acquisition and analysis were performed using the Olympus FV10-ASW software (version 4.02.03.06). ROS-positive bacteria were detected by exciting the carboxy-H_2DCFDA using a 488 nm Argon laser line and recording the green fluorescence emission through a 505 nm long pass emission filter. Hoechst fluorescence was sequentially excited using a 405 nm diode laser and recorded through a blue 430-470 nm band pass filter. Transmitted light brightfield images of the

bacteria were simultaneously recorded using the 488 nm laser line (data not shown). Metal, metal oxide, and metal hydroxide NPs are capable of generating ROS in cells with which they interact. The chemistry of metallic NPs has been reviewed in detail by Čapek and Roušar.[259]

A 250 mL aliquot of each bacterial sample was simultaneously labeled with 100 mM carboxy-H_2DCFDA (2.5 ml of 10mM carboxy-H_2DCFDA) and 20 mM Hoechst (5 mL of 1 mM Hoechst). Each sample was incubated for 30 min at 37 °C. The bacterial samples were then centrifuged to pellet the bacteria, and the supernatant was removed. The bacterial samples were then resuspended in 40 mL of deionized water and imaged by confocal microscopy. Positive ROS detection was indicated by green fluorescence within the treated bacteria. For a positive ROS control, a 250 mL aliquot of a control bacterial sample was incubated with 400 mM TBHP (4 mL of 25 mM TBHP) for 90 min at 37 °C. The TBHP-treated samples were then simultaneously labeled with 100 mM carboxy-H_2DCFDA and 20 mM Hoechst for 30 min at 37 °C. The bacterial samples were then centrifuged to pellet the bacteria, and the supernatant was removed. The bacterial samples were then resuspended in 40 mL of deionized water and imaged by confocal microscopy (**Figure 38**). For each sample, an average of ten confocal fluorescence images were collected and analyzed in Image J software. Positive ROS-labeled cells (displayed in green color) were identified using the "multi-point" feature in Image J software. The total number of ROS-labeled cells was then counted for each image, and the average number of ROS positive cells for each set of samples was calculated and reported.

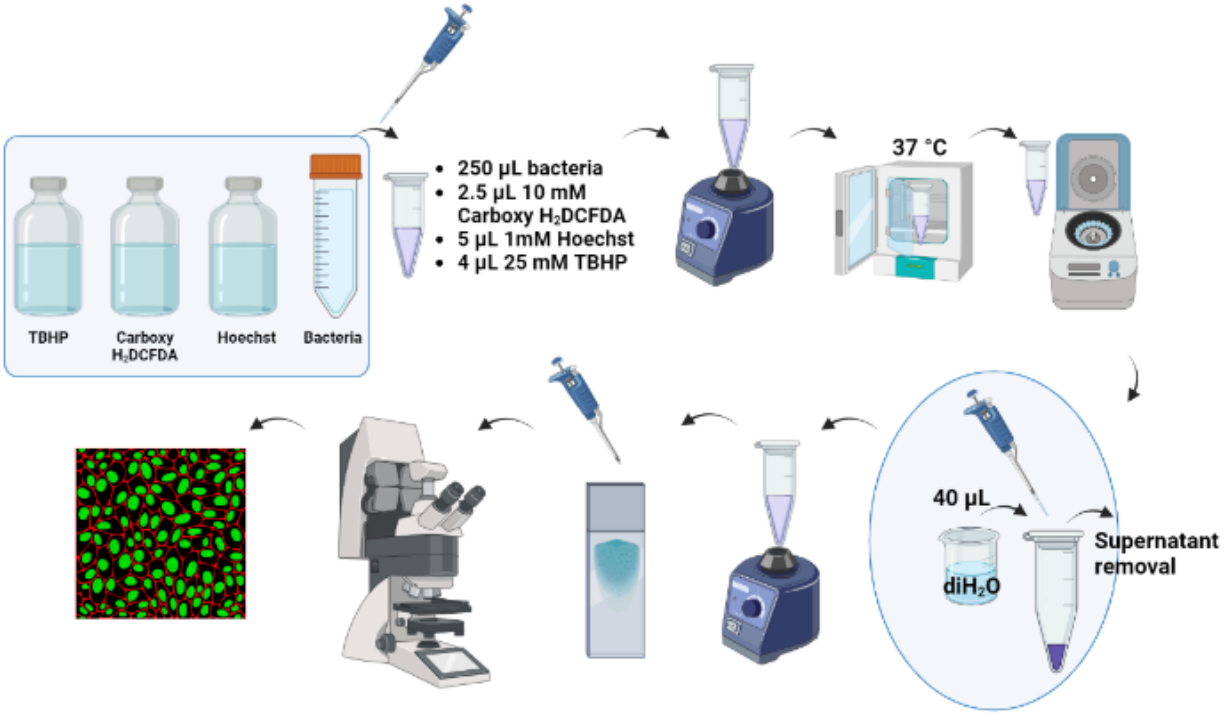

Figure 38. Carboxy-H_2DCFDA staining process.

4.3.7 Experimental design and statistical analysis

A 2x2 factorial experiment was used to investigate the effect of the non-leachable anti-microbial agents ($Mg(OH)_2$, and Cu-infused $Mg(OH)_2$) based on the method of incorporation (compounding and thermal embossing) against *E. coli* K-12 MG1655.

All experiments were independently replicated using at least three biological replicates. Differences between the means of *E. coli* K-12 MG1655 cell density as affected by the direct exposure to the: (1) metallic copper disk (positive control), (2) neat PP disk (negative control), and (3) PP disks incorporating anti-microbial agents were compared at 0, 4, and 24 h using Tukey's honest significant difference test and Student's *t*-tests at a 96% confidence level ($p \leq 0.05$). Interactions between the type of anti-microbial agent, methods of incorporating the anti-microbial agents with PP (compounding, thermal embossing), and anti-microbial activity were analyzed via

four-way analysis of variance (ANOVA) using Origin 2022b software (ver. 9.9.5.167: OriginLab Corporation, Massachusetts, USA).

4.4 Results

4.4.1 Characterization of Biocidal Crystals

The SEM images of the two selected inorganic biocides are presented in (**Figure 39** and **Figure 40**). The morphologies of the crystals in the compounded and injection molded disks and the thermally embossed disks are discussed and correlated with the disposition of the crystals in the PP.

SEM and EDX characterization of neat $Mg(OH)_2$ NPs

The $Mg(OH)_2$ crystals are visually white in color. SEM analysis of the $Mg(OH)_2$ particles (**Figure 39)** shows the particles to be platelet-like in shape, and approximately 160-260 nm wide, with a thickness of 30-50 nm. The EDX specturum has confirmed the NPs type which is Mg.

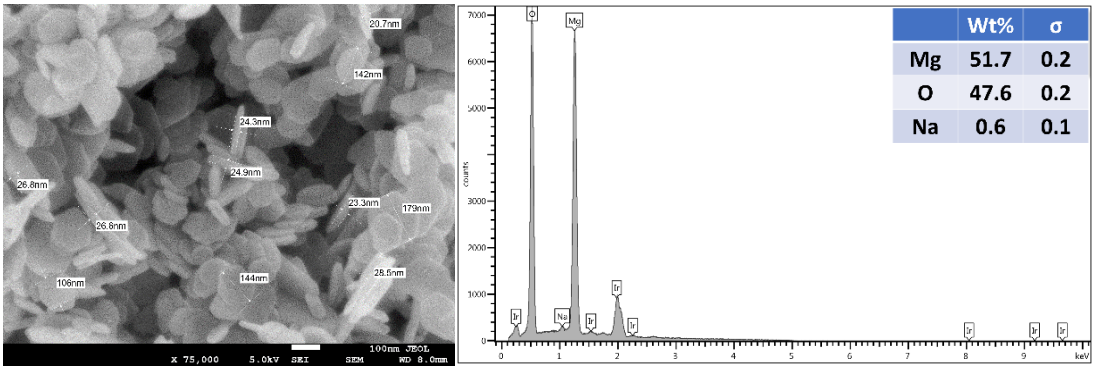

Figure 39. SEM image and EDX spectrum of the $Mg(OH)_2$ crystals.

SEM and EDX characterization of neat Cu-infused $Mg(OH)_2$ NPs

The Cu-infused $Mg(OH)_2$ crystals are visually green in color. SEM analysis of the Cu-infused $Mg(OH)_2$ particles (**Figure 40)** shows some of the particles to be in a platelet form and others to have a spherical morphology, with each in close association. The platelet shaped particles represent the $Mg(OH)_2$ and have a width in the range of 160-260 nm and a thickness of 30-50 nm,

while the spherical shaped particles represent the Cu-infused $Mg(OH)_2$ and have diameters in the range of 100-280 nm. Both particles are mixed together and adhere to each other through their outer surfaces via electrostatic interactions.

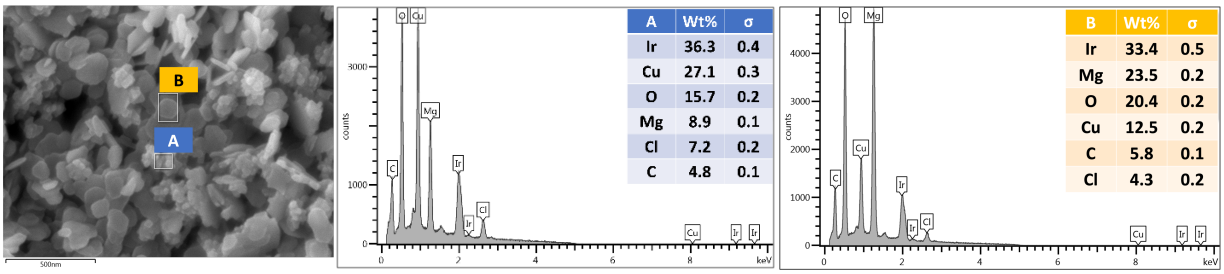

Figure 40. SEM image and EDX spectrum of the Cu-infused $Mg(OH)_2$ crystals.

Both crystals are attached together from the outer surface due to the ion exchange phenomena. The spectrum A was placed on the spherical crystals (**Figure 40, middle, inset**), and it revealed a higher weight percentage for Cu and a lower weight percentage for Mg. In contrast, when the spectrum B was placed on the platelet crystals (**Figure 40, right, inset**), it revealed a higher weight percentage for Mg and a lower weight percentage for Cu.

SEM and EDX characterization of melt-compounded NPs

Side view (surface) of PP compounded with 5 wt.% $Mg(OH)_2$

The SEM image (**Figure 41, left, inset**) and EDX spectrum (**Figure 41, right, inset**).

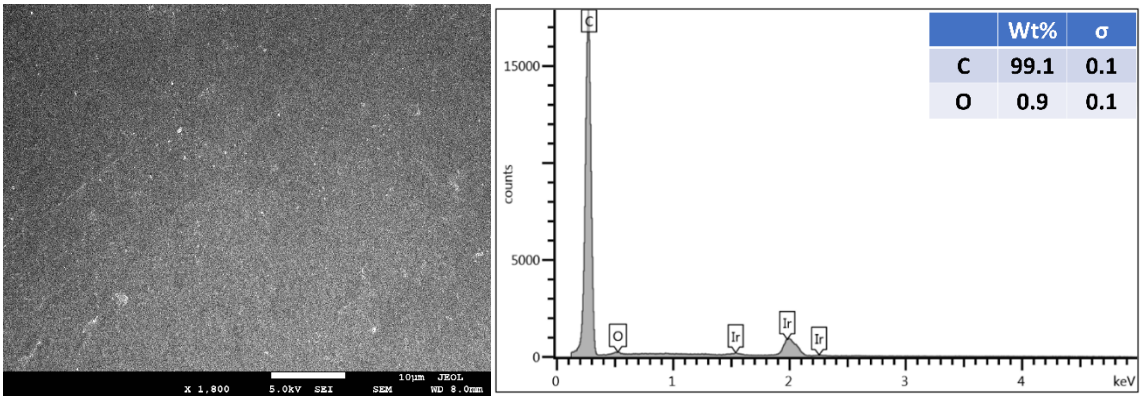

Figure 41. Side view (surface) of PP compounded with 5 wt.% $Mg(OH)_2$.

Cross-sectional view of PP that had been compounded with 5 wt.% $Mg(OH)_2$

The SEM image is presented in (**Figure 42, left, inset**) and EDX spectrum is in (**Figure 42, right, inset**).

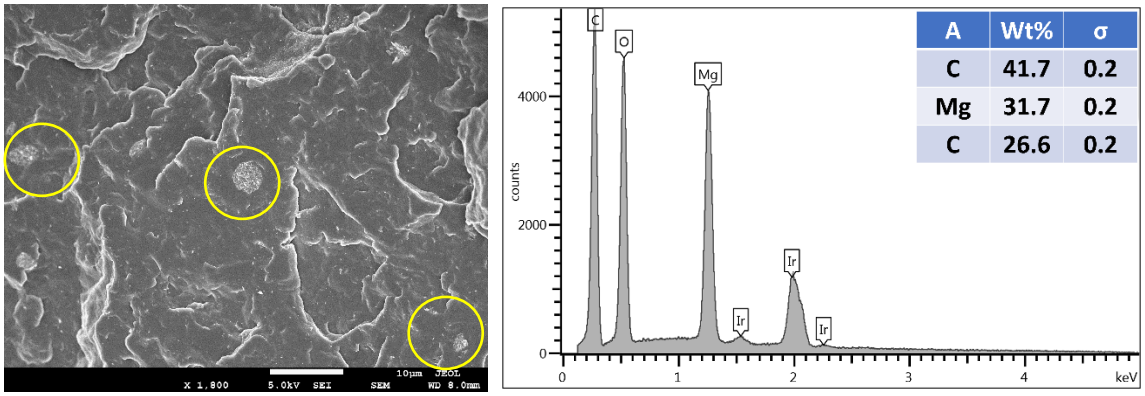

A	Wt%	σ
C	41.7	0.2
Mg	31.7	0.2
C	26.6	0.2

Figure 42. Cross-sectional view of PP that had been compounded with 5 wt.% $Mg(OH)_2$.

Side view (surface) of PP compounded with 5 wt.% Cu-infused $Mg(OH)_2$

The SEM image (**Figure 43, left, inset**) and EDX spectrum (**Figure 43, right, inset**).

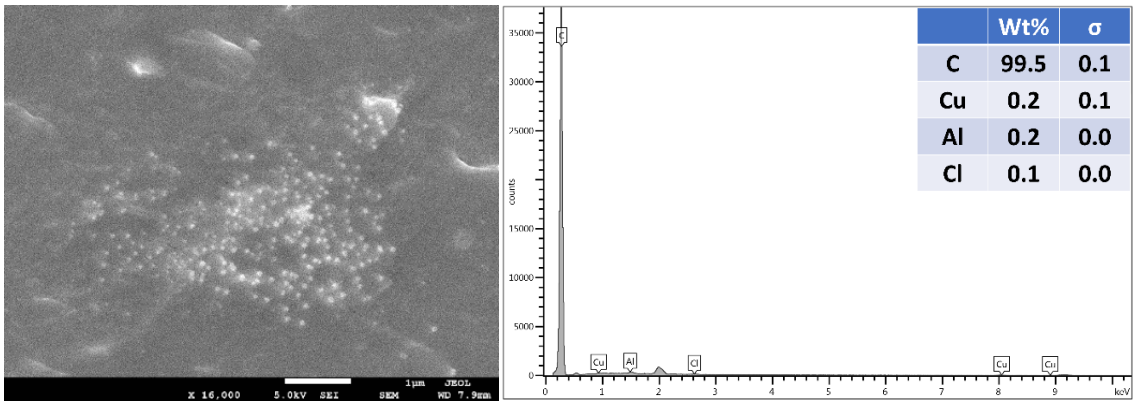

	Wt%	σ
C	99.5	0.1
Cu	0.2	0.1
Al	0.2	0.0
Cl	0.1	0.0

Figure 43. Side view (surfase) of PP compounded with 5 wt.% Cu-infused $Mg(OH)_2$.

Cross-sectional view of PP that had been compounded with 5 wt.% Cu-infused $Mg(OH)_2$

The SEM image is presented in (**Figure 44, left, inset**) and EDX spectrum is in (**Figure 44, right, inset**).

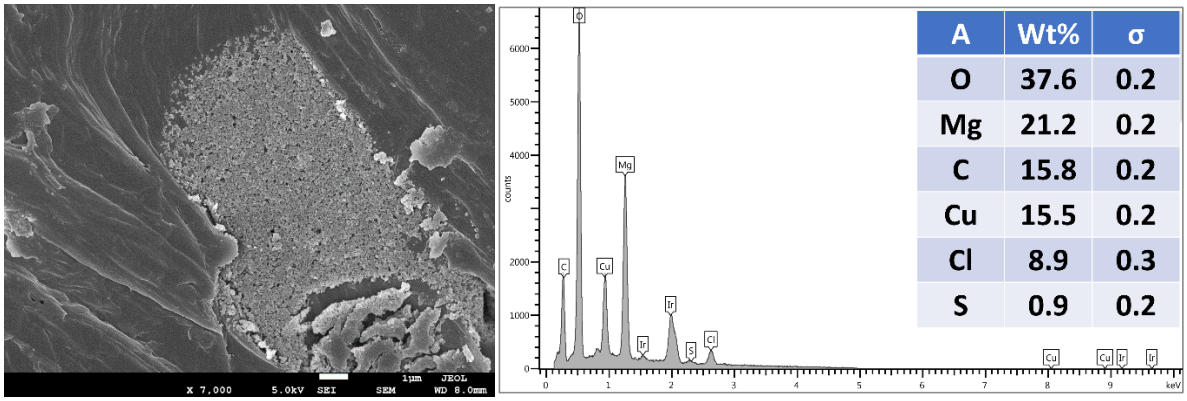

Figure 44. Cross-sectional view of PP compounded with 5 wt.% Cu-infused $Mg(OH)_2$.

SEM and EDX characterization of PP disks with thermally embossed NPs

The SEM image provided in (**Figure 45**) shows the surface characteristics of an untreated PP disk (A), the smooth packed surface of a PP disk that was thermally embossed with $Mg(OH)_2$ nanoplatelets (B), and the rougher surface of a PP disk that was thermally embossed with Cu-infused $Mg(OH)_2$ composed of nanoplatelets and spherical nanoparticles (C).

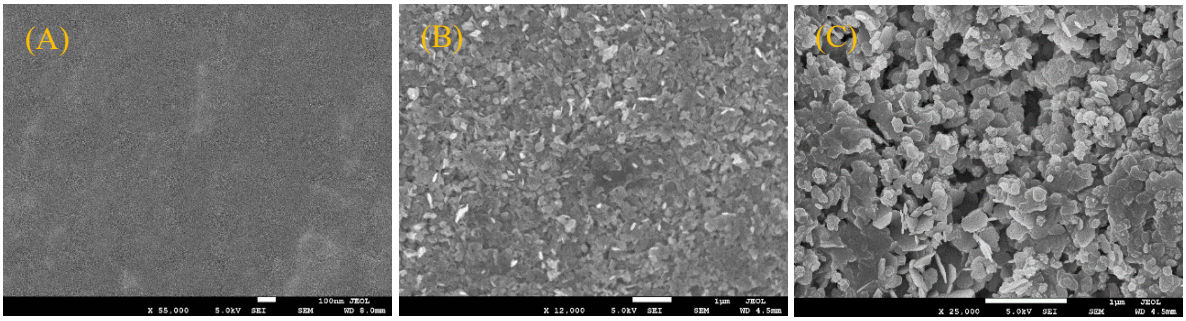

Figure 45. SEM images of (A) neat PP, (B) PP that was thermally embossed with $Mg(OH)_2$, and (C) PP that was thermally embossed with Cu-infused $Mg(OH)_2$.

4.4.2 Differential scanning calorimetry (DSC)

The DSC data showed a minor difference between the PP samples. In particular, (**Figure 46**) shows the melting temperature (T_m), and (**Figure 47**) shows the crystallization temperature (T_c) for the various PP samples.

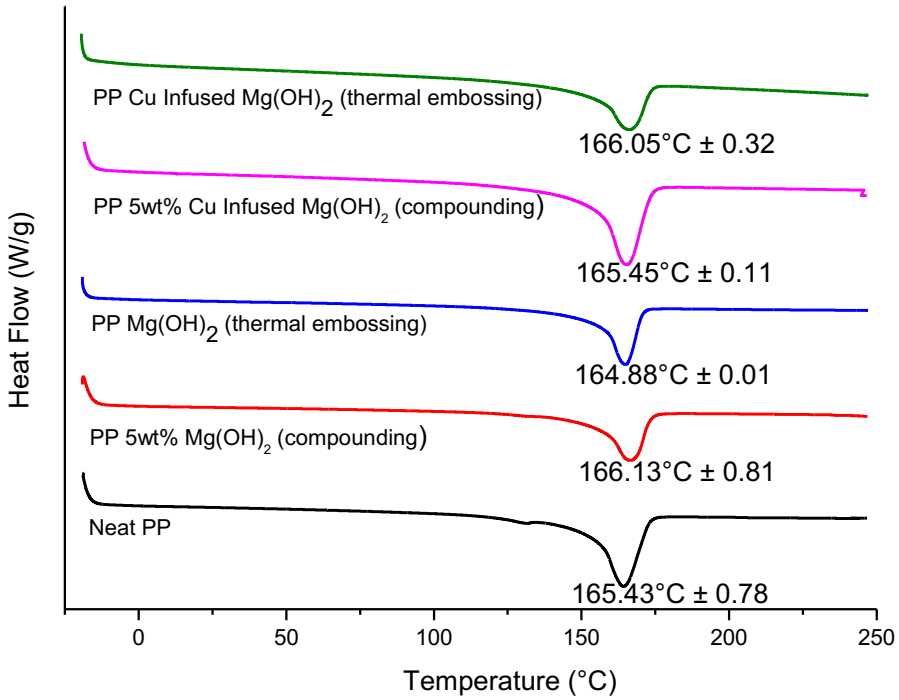

Figure 46. The T_m values were obtained from the DSC data for various samples.

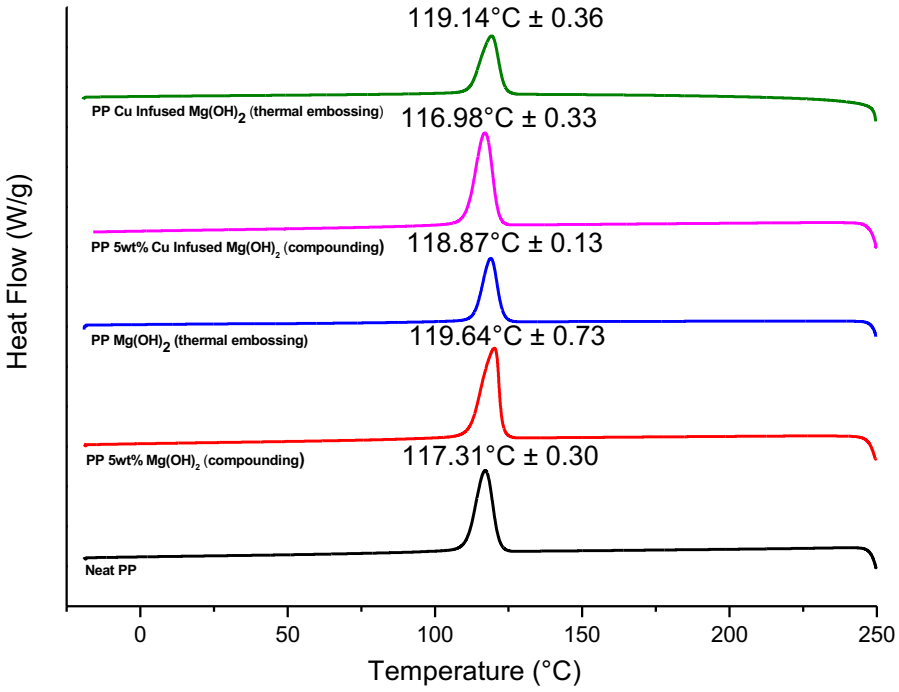

Figure 47. The T_c values were obtained from the DSC data for various samples.

Melting temperature (T_m) of the PP samples

The melt-compounded and injection molded PP samples with 5 wt.% $Mg(OH)_2$ had a slightly higher T_m (166.13 ± 0.81 °C), and those with 5 wt.% Cu-infused $Mg(OH)_2$ had a similar T_m (165.45 ± 0.11 °C) compared to the PP control T_m (165.43 ± 0.78 °C). The PP samples that had been thermally embossed with $Mg(OH)_2$ and Cu-infused $Mg(OH)_2$ had almost the same T_m compared to the PP control (164.88 ± 0.01, 166.05 ± 0.32, and 165.43 ± 0.78 °C, respectively), as shown in (**Figure 46**). Overall, both biocidal additives do not influence the thermal stability of the PP samples.

Crystallization temperature (T_c) of the PP samples

The melt-compounded and injection molded PP with 5 wt.% $Mg(OH)_2$ had a slightly higher T_c (119.64 ± 0.73 °C), and that with 5 wt.% Cu-infused $Mg(OH)_2$ had a lower T_c (116.98 ± 0.33 °C) compared to the PP control T_c (117.31 ± 0.30 °C). The PP samples that had been thermally embossed with $Mg(OH)_2$ and Cu-infused $Mg(OH)_2$ had higher T_c values compared to the PP control (118.87 ± 0.13, 119.14 ± 0.36, and 117.31 ± 0.30 °C, respectively), as shown in (**Figure 47**). Overall, neither of the biocides influences the thermal stability of the PP samples.

Crystallinity (%) of the PP samples

The melt-compounded and injection molded PP samples with $Mg(OH)_2$, and Cu-infused $Mg(OH)_2$ had higher crystallinity (%) compared to the PP control sample (43.63 ± 0.83%, 44.60 ± 1.01%, and 39.99 ± 0.61%, respectively). The PP samples that had been thermally embossed with $Mg(OH)_2$ had higher crystallinity, and Cu-infused $Mg(OH)_2$ had lower crystallinity (%) compared to the PP control sample (44.71 ± 5.53%, 39.00 ± 2.64%, and 39.99 ± 0.61%, respectively), as shown in (**Table 10**). Overall, both biocidal additives slightly influenced the crystallinity (%) of PP samples.

Table 10. The crystallinity of PP samples obtained from DSC measurements.

Samples	ΔH_m (J/g)	T_m (°C)	T_c (°C)	Crystallinity (%)
Neat PP	83.59 ± 1.27	165.43 ± 0.78	117.31 ± 0.30	39.99 ± 0.61
PP 5 wt.% $Mg(OH)_2$ (compounded)	86.62 ± 1.64	166.13 ± 0.81	119.64 ± 0.73	43.63 ± 0.83
PP $Mg(OH)_2$ (thermally embossed)	92.52 ± 11.43	164.88 ± 0.01	118.87 ± 0.13	44.71 ± 5.53
PP 5 wt.% Cu-infused $Mg(OH)_2$ (compounded)	88.56 ± 2.00	165.45 ± 0.11	116.98 ± 0.33	44.60 ± 1.01
PP Cu-infused $Mg(OH)_2$ (thermally embossed)	80.69 ± 5.47	166.05 ± 0.32	119.14 ± 0.36	39.00 ± 2.64

4.4.3 TGA characterization

The TGA analysis of anti-microbial agents, neat PP, and PP composites was conducted to determine their thermal stability (**Figure 48** and **Table 11**). The measurements were collected with a SETSYS Evo-lution (Setaram Instrumentation) system. Samples (~10 mg) were heated in the temperature range of 20–600 °C with a heating rate of 10 °C/min in crucibles made of α-Al_2O_3 under argon atmosphere with a flow rate of 100 cm^3/min.

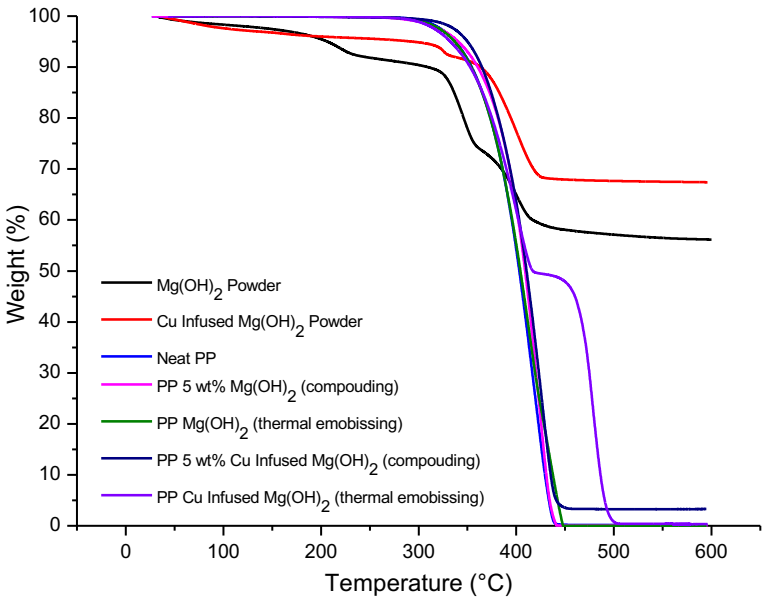

Figure 48. TGA characterization data was obtained for (a) powder samples of anti-microbial agents, (b) neat PP, (c) melt compounding PP, and (d) thermally embossed PP.

Table 11. The temperature at which various PP samples underwent 5% weight loss as determined via TGA measurements.

Sample	The temperature at which 5% weight loss occurred (°C)
$Mg(OH)_2$ Powder	206.52 ± 0.06
Cu-infused $Mg(OH)_2$ Powder	290.39 ± 0.78
Neat PP	337.54 ± 0.03
PP 5 wt.% $Mg(OH)_2$ (compounding)	340.46 ± 0.07
PP 5 wt.% $Mg(OH)_2$ (thermal embossing)	336.26 ± 0.06
PP 5 wt.% Cu-infused $Mg(OH)_2$ (compounding)	350.10 ± 1.39
PP 5 wt.% Cu-infused $Mg(OH)_2$ (thermal embossing)	332.44 ± 0.01

4.4.4 Anti-microbial Studies

Melt-compounding and injection molding of PP with the anti-microbial additives

PP disks (dimensions: 2.5 mm in diameter and 1.55 mm in thickness) constructed as described in **Section 4.2.2** were placed in pods containing approximately a log 8 *E. coli* in a volume of 1 mL PBS. The pods were rotated at 20 rpm at room temperature. 100 µL of the cultures were taken at 4 and 24 h and plated on TSA. Plates were incubated at 37 °C overnight and counted. Reduction in cell population within the pods was then calculated.

Anti-microbial properties of NPs in PP melt-compounded articles

The anti-microbai properties of the different studied NPs in PP melt-compounded articles are presented in (**Figure 49**).

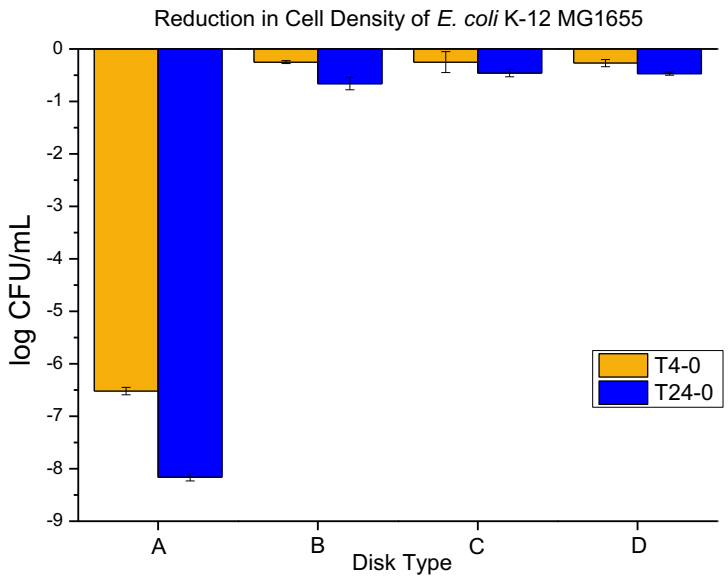

Figure 49. The anti-microbial data obtained for (A) metallic copper (positive control), (B) neat PP (negative control), (C) Injection moulded PP containing 5 wt.% $Mg(OH)_2$, and (D) Injection moulded PP containing 5 wt.% Cu-infused $Mg(OH)_2$.

No reduction in *E. coli* population was observed as a result of exposure to neither (i) $Mg(OH)_2$ nor (ii) Cu-infused $Mg(OH)_2$ (**Figure 49**). This finding demonstrates that there was no leaching of either agent from the interior of the compounded PP disks.

Thermally surface embossed NPs on the PP surface and their anti-microbial properties

After demonstrating that $Mg(OH)_2$ and Cu-infused $Mg(OH)_2$ NPs do not migrate from the interior of the PP matrix to affect externally located bacterial cells, NPs were placed on the surfaces of PP disks and their anti-bacterial performance was evaluated. Disks embossed with $Mg(OH)_2$ NPs or Cu-infused $Mg(OH)_2$ NPs were placed in small pods to which a log 8 *E. coli* suspension in water was added. The pods were rotated at 20 rpm at room temperature and samples were taken, diluted, and plated at 4 and 24 h after commencement of the experiment. Colonies were counted after the plates had been incubated for 18 to 24 h and cell counts were plotted as shown below in (**Figure 50**).

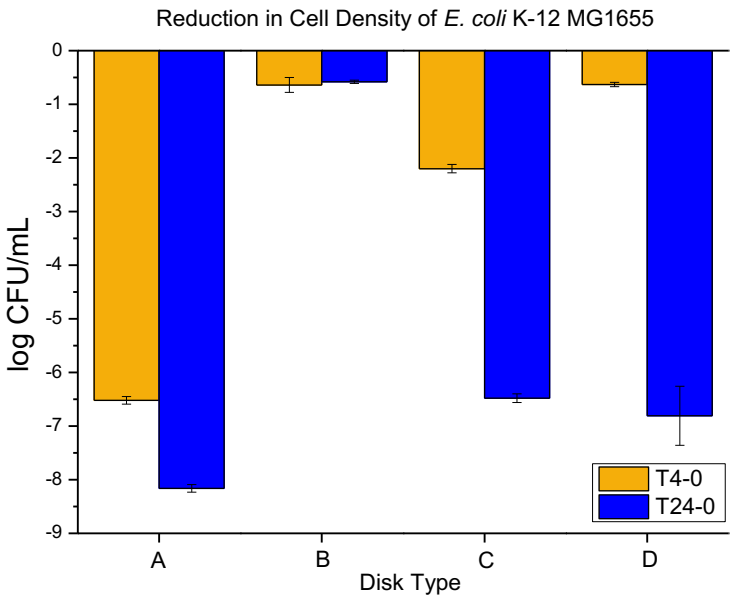

Figure 50. The anti-microbial data obtained for (A) metallic copper (positive control), (B) neat PP (negative control), (C) PP that had been thermally embossed with $Mg(OH)_2$, and (D) PP that had been thermally embossed with Cu-infused $Mg(OH)_2$.

When the NPs were on the surfaces of the PP disks, significant reductions in the bacterial population were observed, culminating in a complete log 8 kills in 24 h (**Figure 50**). This finding indicates that these nanoplatelet materials are highly effective anti-microbial surface treatments.

4.4.5 Anti-viral characterization of NPs

All experiments were conducted in BSL-3 containment. Cytotoxicity of the test specimens in the absence of the virus was assessed by plating 0.1 mL of 'test article only' samples and 10-fold dilutions on Vero E6 cells. As shown in (**Figure 51**), no evidence of cytotoxicity indicated by loss of staining with crystal violet was observed from DPBS as well as the $Mg(OH)_2$ NPs and Cu-infused $Mg(OH)_2$ NPs test specimens when they had been diluted from 10^{-1} to 10^{-3}. However, the staining of cells in the very first well (undiluted) of these test specimens was lightened, indicating that cell lysis had occurred, and suggesting that 2500 ppm of $Mg(OH)_2$ NPs and Cu-infused

$Mg(OH)_2$ NPs suspensions can cause cell damage (Note that cytotoxicity from $Mg(OH)_2$ NPs is marginal).

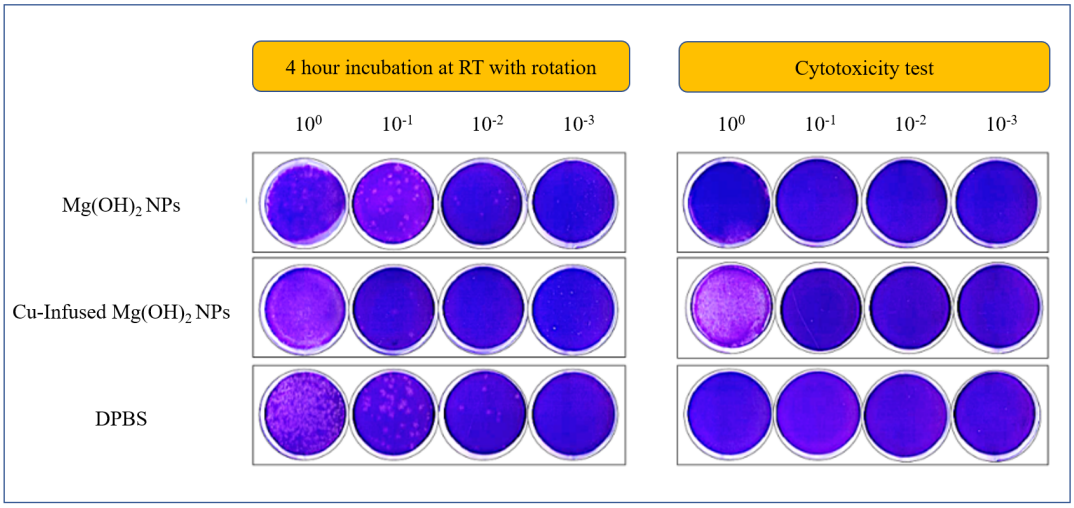

Figure 51. Plaque assays on Vero E6 cells: Infectivity of SARS-CoV-2 viruses incubated with NPs or DPBS. After the plaques had been assayed, cells were fixed with 10% buffered formalin for 1 h, followed by crystal violet staining. After completing plaque counting, plates were scanned. Images are representative of each condition.

Infectivity of SARS-CoV-2 viruses following incubation with test articles or DPBS (control) for 4 h at room temperatures with rotation was measured by plaques assay on Vero E6 cells, as shown in (**Figure 51**). The numerical results from the plaque assays are presented in (**Figure 52**). Infectivity of SARS-CoV-2 virus mixed with the control (DPBS) was maintained at 8.5 x 10^4 PFU/mL during the 4 h test period (**Figure 52**, **left**). In contrast viral titers in samples incubated with Cu-infused $Mg(OH)_2$ NPs were reduced to 4 x 10^2 PFU/mL during the same span of time. Titers were reduced to 6 x 10^4 PFU/mL when SARS-CoV-2 virus was incubated for 4 h in the presence of $Mg(OH)_2$ NPs. This represents a 95.3 and 29.4% reduction, respectively, in SARS-CoV-2 virus infectivity under the tested conditions (**Figure 52**, **right**).

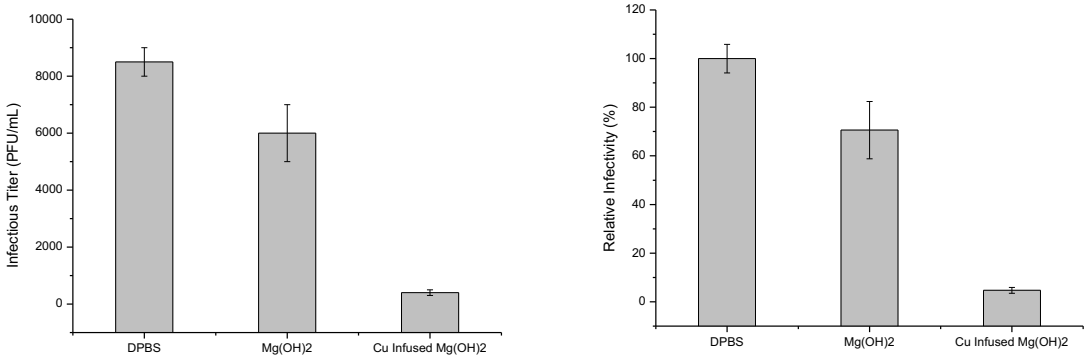

Figure 52. Inactivation of SARS-CoV-2 viral infectivity by incubation with the test specimens. The results shown on the left are plotted a viral titer (PFU/mL) and those shown on the right are plotted as percentage format (%). Relative values to DPBS control were plotted as an average of duplicates with standard error.

4.5 Mechanisms for killing of microbes

Many NPs cause the production of ROS in bacteria with which they interact. This ROS damages cellular structures, and this is one of the mechanisms by which nanoparticles are lethal to bacterial cells.[259] To demonstrate the production of ROS by bacteria in response to $Mg(OH)_2$ and Cu-infused $Mg(OH)_2$ NPs, the cell permeant dye 5-(and-6)-carboxy-2′,7′-dichlorodihydrofluorescein diacetate (carboxy- H_2DCFDA) was introduced to the cells. Within the cell, carboxy- H_2DCFDA is converted intracellularly to the intermediate carboxy-DCFH, which, in the presence of ROS can be oxidized to a green fluorescent molecule, namely carboxy-DCF (Molecular Probes, Thermo Fisher). The addition of DAPI, a blue fluorescent permeant DNA-binding dye, allows all bacterial cells to be located, and images captured at different wavelengths can then be overlapped to identify cells that produce ROS. In particular, the overlap of the blue fluorescent DAPI image and the green fluorescent carboxy-DCF image allows the identification of the ROS-producing bacteria.

In (**Figure 53**) the fluorescent signals of ROS positive *E. coli* cells in the presence of $Mg(OH)_2$ NPs suspended in liquid are shown in (**Figure 53 d**). When cells are incubated with PP

disks with $Mg(OH)_2$ embossed on the disk surface, fluorescent ROS positive *E. coli* are also seen (**Figure 53 e**). The average number of fluorescent signals is similar in each case as summarized and shown in (**Table 12**, and **Figure 54**).

4.5.1 $Mg(OH)_2$ biocide – Mode of action

The results in (**Figure 53** and **Figure 54**) show that $Mg(OH)_2$ NPs induce ROS production in *E. coli*. The ROS production in the bacterial populations exposed to suspensions of $Mg(OH)_2$ NPs is similar to that produced in *E. coli* populations that had been exposed to $Mg(OH)_2$ NPs which were embossed onto the surfaces of PP disks. Magnesium hydroxide is insoluble ($K_{sp}= 5.61 \times 10^{-12}$) and consequently no ionization will occur in these assays, and thus ROS production occurs as a result of direct interaction between bacteria and the nanoplatelets.

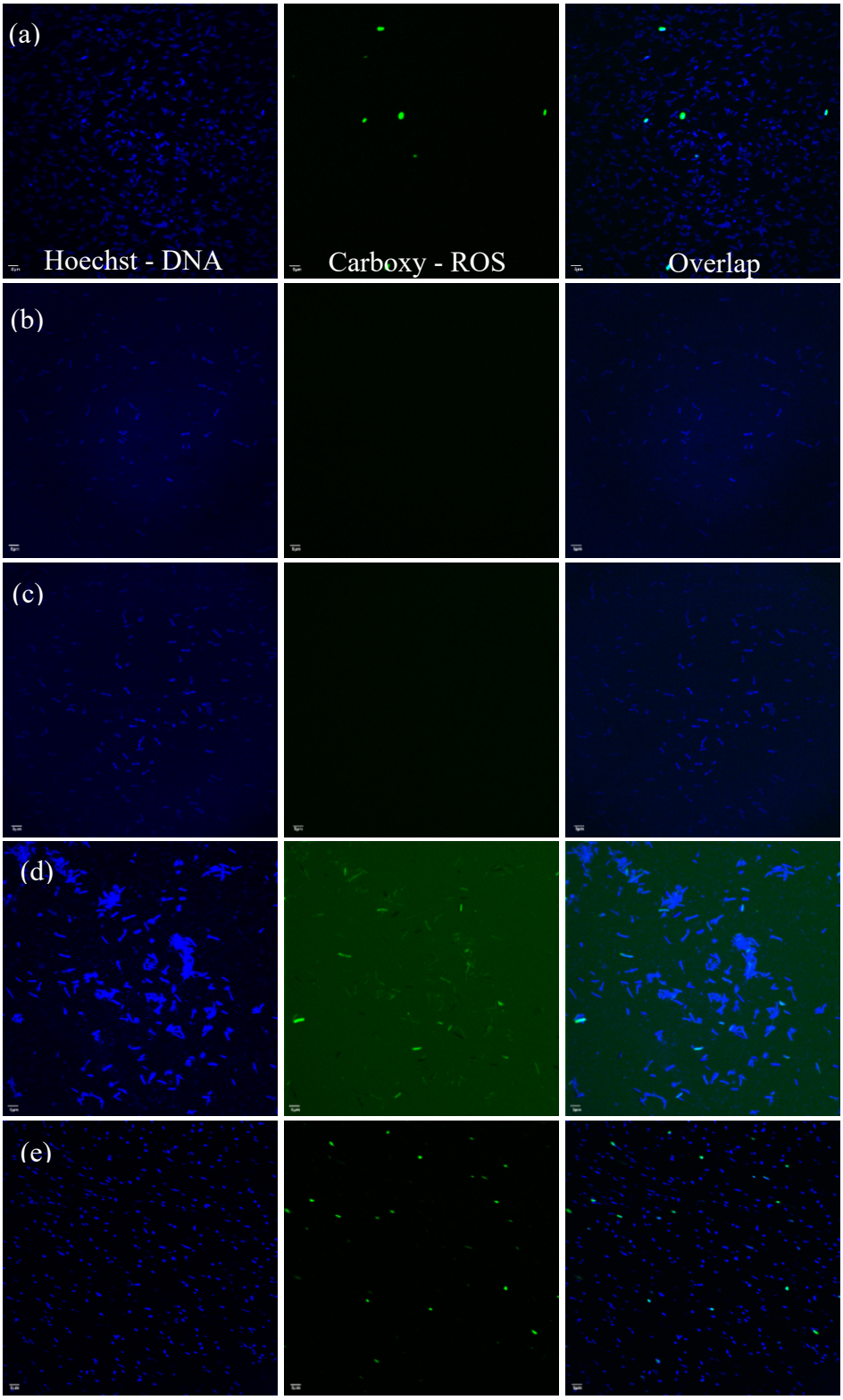

Figure 53. The fluorescent images for samples are presented in (Table 12). Bacterial suspension + TBHP (a), bacterial suspension alone (b), bacterial suspension + control disk (c), bacterial suspension + $Mg(OH)_2$ particles (d), bacterial suspension + plastic disk coated with $Mg(OH)_2$ (e).

Table 12. Average number of ROS positive bacteria when exposed to $Mg(OH)_2$ biocide.

	Sample	Avg number of ROS positive bacteria
(a)	Bacterial Suspension + TBHP	5
(b)	Bacterial Suspension Alone	0
(c)	Bacterial Suspension + Control Disk	0
(d)	Bacterial Suspension + $Mg(OH)_2$ particles	54
(e)	Bacterial Suspension + Plastic Disk Coated with $Mg(OH)_2$	47

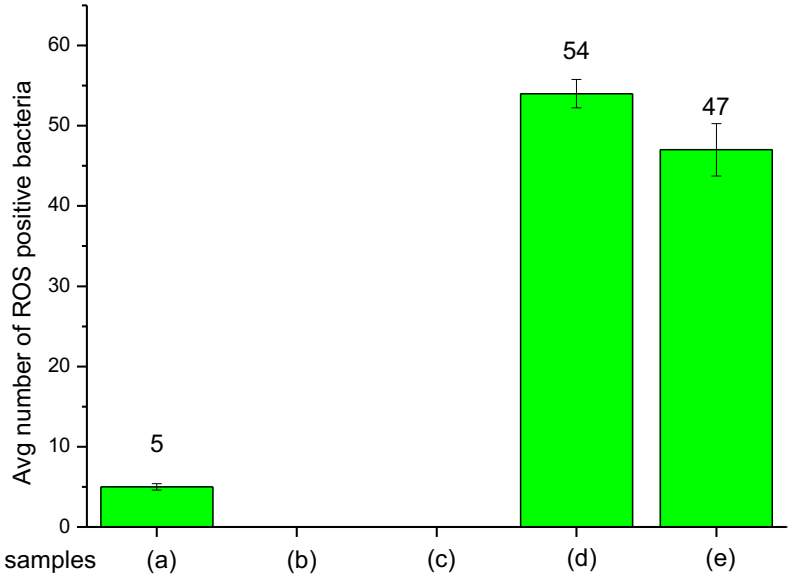

Figure 54. Average number of ROS positive bacteria when exposed to $Mg(OH)_2$ biocide. Bacterial suspension + TBHP (a), bacterial suspension alone (b), bacterial suspension + control disk (c), bacterial suspension + $Mg(OH)_2$ particles (d), bacterial suspension + plastic disk coated with $Mg(OH)_2$ (e).

4.5.2 Cu-infused $Mg(OH)_2$ biocide – Mode of action

In (**Figure 55** and **Figure 56**) fluorescent, ROS positive *E. coli* cells that had emerged in response to exposure to a suspension of Cu-infused $Mg(OH)_2$ NPs (**Figure 55 d**) and to PP disks with $Mg(OH)_2$ affixed to the disk surfaces (**Figure 55 e**) are shown. There does appear to be a higher number of ROS positive cells in the cultures that were exposed to the suspension compared to those that had been exposed to the disk-embossed Cu-infused $Mg(OH)_2$ NPs. However, these results are broadly similar to those observed for the $Mg(OH)_2$ NPs in (**Table 13** and **Figure 56**).

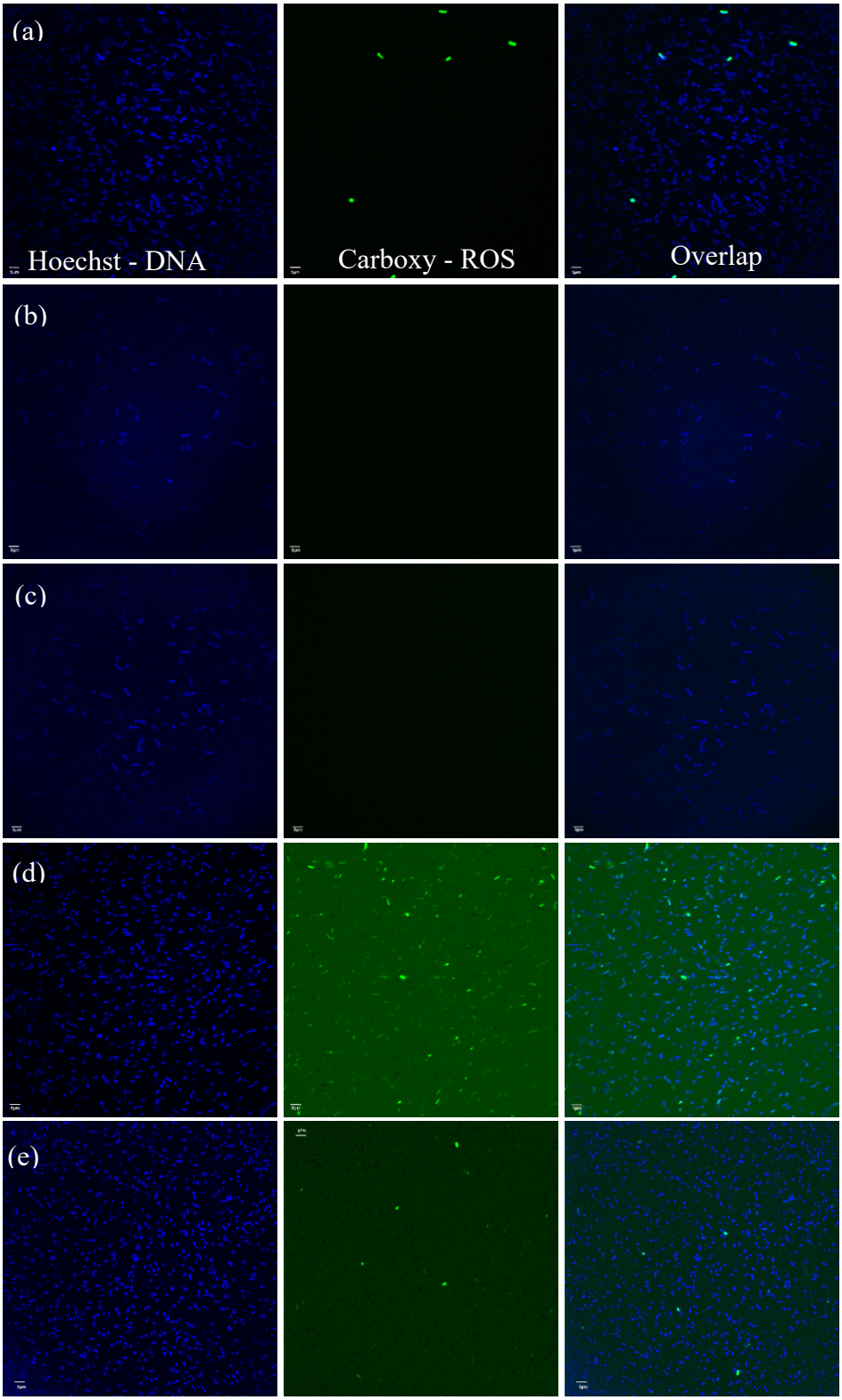

Figure 55. The fluorescent images of samples are presented in (Table 13). Bacterial suspension + TBHP (a), bacterial suspension alone (b), bacterial suspension + control disk (c), bacterial suspension + Cu-infused $Mg(OH)_2$ particles (d), and bacterial suspension + plastic disk coated with Cu-infused $Mg(OH)_2$ (e).

Table 13. Average number of ROS positive bacteria when exposed to Cu-infused $Mg(OH)_2$ biocide.

	Sample	Avg number of ROS positive bacteria
(a)	Bacterial Suspension + TBHP	5
(b)	Bacterial Suspension Alone	0
(c)	Bacterial Suspension + Control Disk	0
(d)	Bacterial Suspension + Cu-infused $Mg(OH)_2$ particles	89
(e)	Bacterial Suspension + Plastic Disk Coated with Cu-infused $Mg(OH)_2$	30

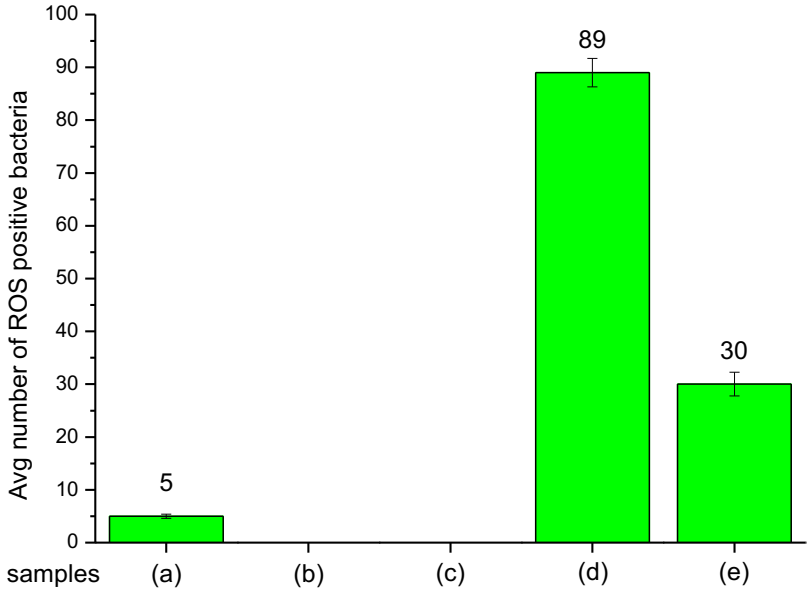

Figure 56. Average number of ROS positive bacteria detected following exposure to the Cu-infused $Mg(OH)_2$ biocides. Bacterial suspension + TBHP (a), bacterial suspension alone (b), bacterial suspension + PP control disk (c), bacterial suspension + Cu-infused $Mg(OH)_2$ particles (d), and bacterial suspension + plastic disk coated with Cu-infused $Mg(OH)_2$ (e).

ROS production in the *E. coli* populations that had been exposed to Cu-infused $Mg(OH)_2$ NPs in suspension is approximately three times higher than that produced in *E. coli* populations that were exposed to Cu-infused $Mg(OH)_2$ NPs which had been embossed onto the surfaces of PP disks (**Figure 55**). This is in contrast to the results observed for $Mg(OH)_2$ (**Figure 53**). $Mg(OH)_2$ is essentially insoluble while Cu-infused $Mg(OH)_2$ includes the highly soluble Cu^{2+} ion. The difference in ROS production due to exposure to the suspension versus the surface bound Cu-

infused $Mg(OH)_2$ may be due to the ionization and release of anti-microbial Cu^{2+} ions in the suspension while these ions remain associated with PP disks when Cu-infused $Mg(OH)_2$ NPs are embossed on the surface. Metal ions, including copper ions, can generate ROS in bacteria. The results in (**Figure 56**) imply that ionization may contribute to ROS production when Cu-infused $Mg(OH)_2$ NPs are present in suspension.

4.6 Discussion

The SEM images and EDX spectra of $Mg(OH)_2$ and Cu-infused $Mg(OH)_2$ crystals (shown in **Figure 39** and **Figure 40**, respectively) confirmed that the $Mg(OH)_2$ particles had a platelet-shaped morphology. Meanwhile, they also revealed that the Cu-infused $Mg(OH)_2$ crystals had two different shapes; nanoplatelets for $Mg(OH)_2$, and spherical for Cu-infused $Mg(OH)_2$. Both crystals are attached together from the outer surface due to the ion exchange phenomena. The platelet-shaped $Mg(OH)_2$ particles had a width in the range of 160-260 nm and a thickness of 30-50 nm thickness, while the spherical Cu-infused $Mg(OH)_2$ particles had a diameter in the range of 100-280 nm. The SEM images and EDX spectra of the surfaces of compounded and injection molded PP disks bearing 5 wt.% $Mg(OH)_2$ and 5 wt.% Cu-infused $Mg(OH)_2$ (**Figure 41** and **Figure 43**, respectively) do not show any evidence of biocidal crystals on the outer surfaces of the PP disks. In agreement with this observation, when the interior of the compounded disks are viewed by SEM and EDX (**Figure 42** and **Figure 44**, respectively) biocrystals are seen to be entirely within the structure and appear to be agglomerated. The SEM image of the surface embossed PP disks from the cast sheet (**Figure 45 (B)** and **Figure 45 (C)**, respectively) shows a complete coverage with the biocidal crystals. The PP surface that had been thermally embossed with $Mg(OH)_2$ is smooth and evenly packed. In contrast, the PP surface bearing the Cu-infused $Mg(OH)_2$, which is

composed of both platelet and spherically shaped crystals, is less evenly packed so that it exhibits a slightly rougher surface due to the mixture of crystal morphologies.

The melt-compounded and injection molded PP with 5 wt.% $Mg(OH)_2$ had a T_m of 166.13 ± 0.81 °C, and that with 5 wt.% Cu-infused $Mg(OH)_2$ had T_m of 165.45 ± 0.11 °C, while the PP control had a T_m of 165.43 ± 0.78 °C. The PP that had been thermally embossed with $Mg(OH)_2$ showed a T_m of 164.88 ± 0.01 °C, and that which had been thermally embossed with Cu-infused $Mg(OH)_2$ showed a T_m of 166.05 ± 0.32 °C compared to the PP control which had a T_m of 165.43 ± 0.78 °C, as shown in (**Figure 46**). The melt-compounded and injection molded PP with 5 wt.% $Mg(OH)_2$ showed a T_c of 119.64 ± 0.73 °C, and that with 5 wt.% Cu-infused $Mg(OH)_2$ had a T_c of 116.98 ± 0.33 °C. The PP that had been thermally embossed with $Mg(OH)_2$ showed a T_c of 118.87 ± 0.13 °C, while that which had been thermally embossed with Cu-infused $Mg(OH)_2$ had a T_c of 119.14 ± 0.36 °C compared to the PP control which had a T_c of 117.31 ± 0.30 °C, as shown in (**Figure 47**). The melt-compounded and injection molded PP with 5 wt.% $Mg(OH)_2$ had 8.34% higher crystallinity (%) (43.63 ± 0.83%), and that with 5 wt.% Cu-infused $Mg(OH)_2$ had 2.54% lower crystallinity (%) (39.00 ± 0.83%) compared to the PP control (39.99 ± 0.61%). The PP samples that had been thermally embossed with $Mg(OH)_2$ had 10.56% higher crystallinity (%) (44.71 ± 5.53%), and that which had been thermally embossed with Cu-infused $Mg(OH)_2$ had 2.54% lower crystallinity (%) (39.00 ± 2.64%) compared to the PP control (T_c = 39.99 °C ± 0.61), as shown in (**Table 10**). Overall, both biocidal additives slightly influenced the crystallinity (%) of the PP samples.

The TGA characterization data (**Table 11**) shows that $Mg(OH)_2$ powder has lost 5 wt.% of its original weight at 206.52 ± 0.06 °C, and the Cu-infused $Mg(OH)_2$ powder has lost 5 wt.% of its original weight at 290.39 ± 0.78 °C. The most significant weight reduction (5 to 40%) has

occurred around 330 and 450 °C (**Figure 48**) due to the high-temperature oxidization (HTO) of metal and metal hydroxide.[260] $Mg(OH)_2$ is a metal hydroxide and Cu-infused $Mg(OH)_2$ is a combination of both metal (Cu) and a metal hydroxide ($Mg(OH)_2$). The HTO would cause these particles to start releasing the H_2O around 330 °C, and it will reach a complete drying around 450 °C. According to the TGA data (**Figure 48**), if $Mg(OH)_2$ and Cu-infused $Mg(OH)_2$ NPs are heated up to 450 °C then they will become converted into MgO and Cu-infused MgO which are expected to have even stronger anti-microbial activity compared to the metal hydroxide. The PP samples that had been compounded with 5 wt.% $Mg(OH)_2$ and Cu-infused $Mg(OH)_2$ have lost 5 wt.% of their weights (at 340.46 ± 0.07 and 350.10 ± 1.39 °C, respectively) which were comparatively higher temperatures (by 0.6 and 3.4%, respectively) than that observed for neat PP (337.54 ± 0.03 °C). The PP samples that had been thermally embossed with 10 mg/mL $Mg(OH)_2$ and Cu-infused $Mg(OH)_2$ have lost 5 wt.% of their weights at (336.26 ± 0.06, and 332.44 ± 0.01 °C, respectively) which was comparatively lower (by 0.6 and 1.8%, respectively) than neat PP (337.54 ± 0.03 °C). The loss of 5 wt.% in weight was higher in the PP compounded material compared to that observed for the neat PP because the particles were within the PP matrix, and the particles in the PP composite would need a longer time to release the H_2O. Meanwhile, the loss of 5 wt.% in weight was observed at lower temperatures in PP thermally embossed samples compared to the neat PP because the particles were thermally embossed on the PP surface, and the particles would undergo HTO faster and release the H_2O contents. Overall, neither of the biocidal additives influences the thermal stability of the PP samples.

E. coli is a common test bacteria and is among the five bacterial species that are most responsible for illness and death worldwide.[261] The anti-microbial testing data shown in (**Figure 49**) indicates that the PP disks prepared by melt-compounding and injection molding bearing 5

wt.% $Mg(OH)_2$ and 5 wt.% Cu-infused $Mg(OH)_2$ (where the crystals are within the matrix of the polymer) do not exhibit anti-microbial activity. There is no migration of anti-microbial material to and beyond the surface of the polymer, and apparently no migration of Cu ions from the polymer to a degree where bacteria are inhibited (**Figure 49 C** and **Figure 49 D**). When $Mg(OH)_2$ NPs or Cu-infused $Mg(OH)_2$ NPs are thermally embossed to the surface of the PP polymer disks, bacteria in contact with these surfaces are eliminated (**Figure 50 C** and **Figure 50 D**). In these assays, approximately a log 2-3 reduction of *E. coli* killing occurs within 4 h and a complete killing within 24 h. A small difference in the initial rate of killing was observed, with the anti-microbial effect of the $Mg(OH)_2$ NPs acting slightly faster than the Cu-infused $Mg(OH)_2$ NPs after 4 h. However, both coatings achieved complete elimination of bacteria when they had been assayed at 24 h.

An anti-viral study was conducted to evaluate the abilities of the $Mg(OH)_2$ NPs suspension and Cu-infused $Mg(OH)_2$ NPs suspension to inactivate SARS-CoV-2 virus infectivity in solution. After 4 h of incubation at room temperature, the $Mg(OH)_2$ NPs suspension, at 0.25 % reduced SARS-CoV-2 virus titers in the solution by 2.5×10^3 PFU/mL or 29.4%, while the Cu-infused $Mg(OH)_2$ NPs suspension, at 0.25 % reduced titers by 8.1×10^3 PFU/mL or 95.3% (**Figure 52**). These assays involved a physico-chemical assault on the virus structure followed by an assay of the ability of the assaulted virus to successfully infect mammalian cells. While damage to bacterial cell walls may cause leakage of cell material from a pressurized cell and loss of viability, a virus enveloped by a cell membrane may maintain infectivity until severe disruption occurs such that the nucleic acid is degraded, or key surface proteins are inactivated. Alteration of concentrations may produce more rapid virus destruction.

A previous study has indicated that anti-bacterial drugs derived from $Mg(OH)_2$ NPs have the potential to be effective.[237, 262-265] However, the mechanism of action through which $Mg(OH)_2$

NPs exhibit their bactericidal activity has yet to be well studied.[237, 263, 266] When they used $Mg(OH)_2$ NPs manufactured by Aqua Resources Corp (similar to those used in this study), Dong et al. showed that physical contact was necessary to kill *E. coli* cells, but that bacterial destruction did not appear to involve the uptake of nanoplatelets by cells.[263] Dong et al. hypothesized that the direct presence of surface areas with a high concentration of hydroxyl (-OH) groups of $Mg(OH)_2$ NPs would be damaging to bacterial cell walls.[263, 266] Pan et al. conducted microbial experiments with $Mg(OH)_2$ NPs that were manufactured by three different methods and showed that perturbation of the bacterial membranes occurred when *E. coli* cells were exposed to $Mg(OH)_2$ NPs, but studies using energy-dispersive X-ray spectroscopy (EDS) found no evidence for internalization of $Mg(OH)_2$ NPs nor were there elevated Mg levels within cells.[237] Dong et al. showed that neither high pH nor high concentrations of magnesium ions ($MgSO_4$) showed lethality.[263] Nakamura et al. created mutant bacterial strains where genes for various magnesium transport systems had been deleted, and used them to demonstrate that magnesium uptake did not affect on the killing potency of $Mg(OH)_2$ NPs. Physical damage was assigned as a principal cause of bacterial cell death.[267] Pan et al. proposed that the $Mg(OH)_2$ NPs attach to the surface of the bacterial cells due to charge attraction before rupturing the cell walls and killing the bacteria.[237]

While physical damage to bacterial cell walls with concomitant leakage of cell contents is taking place, loss of integrity of membrane bound enzymatic systems, and dissipation of electron motive force are all potent assaults upon bacterial viability. The current work demonstrates that, in addition, $Mg(OH)_2$ NPs (like many other nanoparticles) cause the production of ROS in bacteria with which they interact. This is the first demonstration of ROS production being induced by $Mg(OH)_2$ and Cu-infused $Mg(OH)_2$ nanoplatelets. Both PP embossed $Mg(OH)_2$ and Cu-infused $Mg(OH)_2$ NPs induced ROS production in bacterial cells to a similar degree. This is consistent

with their similar potency in destroying *E. coli* in thermally embossed PP surfaces (**Figure 50**). The results in (**Figure 53** and **Figure 54**) show similar ROS production in *E. coli* exposed to $Mg(OH)_2$ NPs suspension and $Mg(OH)_2$ NPs bound to PP surfaces. $Mg(OH)_2$ NPs are insoluble and ionization will not contribute to ROS production. In contrast, a suspension of Cu-infused $Mg(OH)_2$ NPs produced three times more ROS than PP-bound Cu-infused $Mg(OH)_2$ NPs (**Figure 55**). Cu ions are highly soluble and can produce ROS in bacteria.[268, 269] The reduced ROS level for PP-bound Cu-infused $Mg(OH)_2$ NPs (**Figure 56**) implies that Cu ionization and migration into the media does not occur as readily when the NPs are embossed onto the PP surface. This may have positive implications in terms of rendering surfaces anti-bacterial without the problem associated with the leaching of agents from a treated surface. The contribution of membrane disruption and ROS production to the killing of bacteria may be different for different types of nanoparticles and the role of each mechanism in killing Gram-positive and Gram-negative pathogens remains to be determined.

4.7 Conclusion

Our findings suggest that $Mg(OH)_2$ and Cu-infused $Mg(OH)_2$ NPs have strong anti-bacterial and anti-viral activity. ROS is found to be the main mode of action, thus indicating that ROS production has a key role in their anti-microbial mechanism. Interestingly, surfaces embossed with $Mg(OH)_2$ and Cu-infused $Mg(OH)_2$ NPs and NPs suspensions eliminate bacteria with similar efficacy. Thermal surface embossing showed an 8 log reduction of *E. coli* in 24 h. Similarly, NPs exhibit anti-viral activity against (SARS-CoV-2) covid-19 virus. This efficacy is supported by SEM-EDX data where the neat NPs and surfaces embossed with NPs have similar chemical compositions. Thus, surface embossing holds the promise for broad applications in both commercial and household settings.

CHAPTER 5: CONCLUSION AND FUTURE RECOMMENDATIONS

5.1 Conclusion

Throughout this Ph.D dissertation, an in-depth understanding of the anti-microbial agents had been introduced in chapter 1 such as the classification of anti-microbial agents, (natural, organic, and inorganic). Moreover, the type of anti-microbial agents, advantages, disadvantages, and how it was used earlier have been described and discussed. The leachable anti-microbial agents were very popular for a long time especially in the traditional way of polymer processing such as melt-compounding because the ionic charge can leave the polymer matrix toward the surface or even beyond where it shows a good anti-microbial activity. However, this type of anti-microbial agent is considered to be toxic, therefore, a layer of limitation on the loading concentrations must be considered when it comes to healthcare and food packaging applications.

Unlike the leachable anti-microbial agents, the non-leachable anti-microbial agents are considered to be either non- or low-toxic to human cells. The non-leachable agents are very popular in healthcare and pharmaceutical applications, but they are not very popular in polymer applications. The reason would be that the non-leachable anti-microbial agents would require a direct contact with the microorganism to show an effect, and this could not be found through the melt-compounding processing technique because most of the particles would be embedded inside the polymer matrix. A very high loading, well beyond 5 wt.% would be needed, but this would increase expense (most of the nano crystals in the interior of the article would be non funcitonal) and high loadings impairs the mechanical properties.

The comparative study of melt-compounding PP with leachable and non-leachable anti-microbial agents showed how the nanoparticles were masked into the polymer matrix, and there were no particles detected on the external surface for both types of agents. Moreover, the leachable

anti-microbial agents showed good anti-microbial activity owing to the ionic charges, and the non-leachable anti-microbial agents showed no activity because there was no interaction between the nanoparticles and the microorganisms. Therefore, a new method was developed in this work to affix the anti-microbial particles (especially the non-leachable type) onto the external surface of the polymeric articles. This was a very important technique to enable this type of anti-microbial agent in polymer applications.

The thermal embossing technique applicable to sheet geometry was not an easy approach to conduct due to poor wetting of polymer surfaces by nano crystal dispersions, therefor, several designs of experiments were conducted to study the type of liquids (water, ethanol, and isopropyl), coating concentration (3000, 5000, and 10,000 ppm), coating thickness (applicator rod # 3, 5, 6), and type of coating (dip, spray, dry). The intrinsic wetting was found to be a major issue that caused a non-uniform coating with all the above parameters, and this challenge could not be significantly solved by using the plasma treatment over the polymeric sheets as described in chapter 2.

In chapter 3, the aluminum foil technique has been proven to provide the best coating uniformity among all other types of coating such as dry, dip, or spray. It was found that the dispersions in water, ethanol, and isopropyl spread well on Al foil and on drying a uniform coating of crystals was obtained. The Al need not be a foil, it also worked with crystals deposited on a thick Al plate. Somewhat surprisingly, the nano crystals could be transferred from the Al foil to heated and softened polymer sheets and fixed on them. Only results for PP sheet were shown here, but such transfer also worked with PC, PE, and PET sheets. A continuous processing method for sheets may be envisaged where dry crytsal powder is deposited on an Al roller and then transferred by heat and pressure on to the plastic sheet.

It was demonstrated that when $Mg(OH)_2$ NPs were used in melt-compounding, it did not show any significant anti-microbial activity, and when it was used through the thermal embossing technique, it showed a very significant anti-microbial activity. The overall properties such as thermal, mechanical, and barrier were not impacted by adding the anti-microbial agents either through melt-compounding or thermal embossing. To enable the non-leachable anti-microbial agents to be part of the polymer application, $Mg(OH)_2$ NPs had been selected because of their features such as particle shape, size, cost-effectiveness, low solubility, and low toxicity to human cells.

This was the same experience for Cu-infused $Mg(OH)_2$ NPs which was presented in chapter 4. The Cu-infused $Mg(OH)_2$ NPs are novel materials (developed by Aqua Recourses, Patent No: US20220225610A1), and were introduced for the first time as an anti-microbial agent through this dissertation research. The mechanism of $Mg(OH)_2$ and Cu-infused $Mg(OH)_2$ had been confirmed to be through ROS. This was confirmed through the neat NPs, and through the PP disks thermally embossed with anti-microbial NPs.

While the research shows that anti-microbial nanocrystals like $Mg(OH)_2$ that require physical contact with the microbe can be engineered into sheets, it would be even better if they can be incorporated on to the surfaces of 3D shapes. Injection moulding allows 3D shapes to be made from plastics, but as shown, non-leaching anti-microbial nanocrystals like $Mg(OH)_2$ are not effective as they function only with direct contact with the microbes. Preliminary work done with a 3D printing method called High Speed Sintering allowed the surfaces of 3D printed polyamide 12 article to be coated with nano crystals, and the articles then showed the same anti-microbial activity as the surface embossed PP sheets. Thus, the $Mg(OH)_2$ nano crystals can be used across other polymer fabrication platforms. These results on the 3D printed polyamide 12 with $Mg(OH)_2$

nano crystals were not included here due to the submission deadline but are available for incorporation if time permits.

In chapter 5, a general conclusion from the research dissertation had been outlined. In addition, the recommendations and optimal approaches for the secure management of NPs had been provided to properly handle the NPs. Finally, the future recommendation on how to apply the anti-microbial suspensions directly through the polymer processing is described.

5.2 Recommendations and optimal approaches for the secure management of NPs

Engineered nanomaterials, such as nanospheres, nanotubes, nanowires, and nanosheets, exhibit a distinct combination of physical, chemical, biological, mechanical, electrical, and thermal properties. This unique set of characteristics makes them promising candidates for various structural and functional applications. However, owing to their incredibly small size, expansive surface area, and high reactivity, they have the potential to readily enter living cells. As a result, the unique nanoscale characteristics of these particles may present potential hazards to both human health and the environment. Consequently, there is a widespread initiative in research and development institutions, universities, and industries globally to evaluate their toxicity and establish crucial exposure thresholds. At present, the available scientific and technical literature shows insufficient evidence regarding the negative impacts of nanomaterials on human health, leaving their risks largely unknown.

Recognizing the potential risks of NPs

The initial phase in evaluating risk and exposure is the recognition of potential hazards. This step entails the identification of chemicals or nanomaterials and the processes related to them that could give rise to toxic, physical (such as excessive noise, high pressures, vacuum conditions, strong electromagnetic fields, etc.), and physicochemical risks. When appraising the risks linked

to nanomaterials, it is crucial to pay close attention to the unique impacts of surface chemistry, shape, size, and structure on the toxicity in various organs. When evaluating the risk associated with nanomaterials, the following principal hazard categories should be taken into account.

Surface charge

The generation of free radicals and the resultant impact on overall surface reactivity and toxicity of ingested particles can be influenced by the surface chemistry of nanoparticles.[270]

Surface chemistry

The surface chemistry of nanoparticles can play a role in the generation of free radicals, which affects the overall surface reactivity and toxicity of ingested particles.

Particle shape

Studies have confirmed that being exposed to fibrous particles such as asbestos increases the likelihood of developing fibrosis and cancer. Likewise, the tubular configuration of carbon nanotubes is believed to trigger lung inflammation and lesions.

Particle size

Smaller particles, such as nanoparticles, have a higher likelihood of being deposited in the lungs, posing a risk of damage either directly at the deposition site, through translocation to other organs, or absorption into the bloodstream. Nanoparticles have the capability to breach membrane barriers, leading to significant harm. For instance, silver nanoparticles with a size smaller than 9 nm can penetrate the nuclear membrane of specific human cell nuclei, causing considerable DNA damage or mutations.

Solubility

Inhaled nanoparticles with low solubility can induce oxidative stress, potentially resulting in inflammation, fibrosis, or even cancer. Research has demonstrated the markedly elevated

toxicity of nanometals compared to nanoceramics, primarily ascribed to their increased dissolution rate in water.

5.3 Future Recommendations

In this Ph.D research dissertation, the thermal embossing technique has been proven and validated to be a cost-effective solution for polymer application. For future research, it is recommended to apply the anti-microbial suspension directly through the different types of polymer processing such as injection molding, extrusion blow molding, thermoforming, sheet or film extrusion, etc. This could be applied in the cavity of the molds or the calendering rollers through a robotic dispensing unit to keep up the production efficiency.

BIBLIOGRAPHY

1. *Microbiology by numbers.* Nature Reviews Microbiology, 2011. **9**(9): p. 628-628.

2. Sugden, R., R. Kelly, and S. Davies, *Combatting antimicrobial resistance globally.* Nature Microbiology, 2016. **1**(10): p. 16187.

3. Morales, E., et al., *Hospital costs of nosocomial multi-drug resistant Pseudomonas aeruginosa acquisition.* BMC Health Services Research, 2012. **12**(1): p. 122.

4. Nathwani, D., et al., *Clinical and economic consequences of hospital-acquired resistant and multidrug-resistant Pseudomonas aeruginosa infections: a systematic review and meta-analysis.* Antimicrobial Resistance and Infection Control, 2014. **3**(1): p. 32.

5. Levy, S.B. and B. Marshall, *Antibacterial resistance worldwide: causes, challenges and responses.* Nat Med, 2004. **10**(12 Suppl): p. S122-9.

6. Encyclopaedia, T.E.o., *antibiotic. Encyclopedia Britannica.* Britannica, 2023, May 21.

7. Shlaes, D.M., *Research and Development of Antibiotics: The Next Battleground.* ACS Infectious Diseases, 2015. **1**(6): p. 232-233.

8. Ghani, S., *Why is the Pharmaceutical Industry Not Developing New Antibiotics?* 2021.

9. Darouiche, R.O.J.N.E.J.o.M., *Treatment of infections associated with surgical implants.* 2004. **350**(14): p. 1422-1429.

10. Zhang, N., et al., *Evidence for lack of transmission by close contact and surface touch in a restaurant outbreak of COVID-19.* J Infect, 2021. **83**(2): p. 207-216.

11. Lemiech-Mirowska, E., et al., *Nosocomial infections as one of the most important problems of healthcare system.* Ann Agric Environ Med, 2021. **28**(3): p. 361-366.

12. Chua, M.H., et al., *Face Masks in the New COVID-19 Normal: Materials, Testing, and Perspectives.* Research (Wash D C), 2020. **2020**: p. 7286735.

13. Liu, M., et al., *Antimicrobial polymeric composites for high-touch surfaces in healthcare applications.* Curr Opin Biomed Eng, 2022. **22**: p. 100395.

14. Muñoz-Bonilla, A. and M.J.P.i.P.S. Fernández-García, *Polymeric materials with antimicrobial activity.* 2012. **37**(2): p. 281-339.

15. Olatunji, O., *Natural polymers: industry techniques and applications*. 2015: Springer.

16. Wypych, G., *PDMS Polydimethylsiloxane, Handbook of Polymers.* 2012.

17. Shakiba, M., et al., *Nylon—A material introduction and overview for biomedical applications.* 2021. **32**(9): p. 3368-3383.

18. Ghosh, P., *Polymer science and technology: plastics, rubbers, blends and composites*. 2011: McGraw-Hill Education.

19. Bhat, S.V. and S.V.J.B. Bhat, *Synthetic polymers.* 2002: p. 51-71.

20. Liechty, W.B., et al., *Polymers for drug delivery systems.* Annu Rev Chem Biomol Eng, 2010. **1**: p. 149-73.

21. Gagliardi, A., et al., *Biodegradable polymeric nanoparticles for drug delivery to solid tumors.* 2021. **12**: p. 601626.

22. Begines, B., et al., *Polymeric nanoparticles for drug delivery: Recent developments and future prospects.* 2020. **10**(7): p. 1403.

23. Wang, L., C. Hu, and L.J.I.j.o.n. Shao, *The antimicrobial activity of nanoparticles: present situation and prospects for the future.* 2017. **12**: p. 1227.

24. Lam, S.J., et al., *Antimicrobial polymeric nanoparticles.* 2018. **76**: p. 40-64.

25. Lam, S.J., et al., *Combating multidrug-resistant Gram-negative bacteria with structurally nanoengineered antimicrobial peptide polymers.* 2016. **1**(11): p. 1-11.

26. Aguilar, Z., *Nanomaterials for medical applications*. 2012: Newnes.

27. Nederberg, F., et al., *Biodegradable nanostructures with selective lysis of microbial membranes.* 2011. **3**(5): p. 409-414.

28. Silhavy, T.J., D. Kahne, and S. Walker, *The bacterial cell envelope.* Cold Spring Harb Perspect Biol, 2010. **2**(5): p. a000414.

29. Cetin-Karaca, H. and M.C.J.J.o.F.R. Newman, *Antimicrobial efficacy of natural phenolic compounds against gram positive foodborne pathogens.* 2015. **4**(6): p. 14.

30. Qiao, Y., et al., *Highly dynamic biodegradable micelles capable of lysing Gram-positive and Gram-negative bacterial membrane.* 2012. **33**(4): p. 1146-1153.

31. Fukushima, K., et al., *Broad-spectrum antimicrobial supramolecular assemblies with distinctive size and shape.* 2012. **6**(10): p. 9191-9199.

32. Fukushima, K., et al., *Supramolecular high-aspect ratio assemblies with strong antifungal activity.* 2013. **4**(1): p. 2861.

33. Waschinski, C.J. and J.C.J.B. Tiller, *Poly (oxazoline) s with telechelic antimicrobial functions.* 2005. **6**(1): p. 235-243.

34. Kiss, É., et al., *Membrane affinity and antibacterial properties of cationic polyelectrolytes with different hydrophobicity.* 2012. **12**(9): p. 1181-1189.

35. Antonietti, M. and S.J.A.m. Förster, *Vesicles and liposomes: a self-assembly principle beyond lipids.* 2003. **15**(16): p. 1323-1333.

36. Zhang, C., et al., *Antibacterial vesicles by direct dissolution of a block copolymer in water.* 2013. **4**(2): p. 255-259.

37. Zhu, H., et al., *Antibacterial high-genus polymer vesicle as an "armed" drug carrier.* 2013. **1**(40): p. 5496-5504.

38. Grayson, S.M. and J.M.J.C.r. Frechet, *Convergent dendrons and dendrimers: from synthesis to applications.* 2001. **101**(12): p. 3819-3868.

39. Gupta, U. and O. Perumal, *Dendrimers and its biomedical applications*, in *Natural and synthetic biomedical polymers*. 2014, Elsevier. p. 243-257.

40. Ganewatta, M.S. and C.J.P. Tang, *Controlling macromolecular structures towards effective antimicrobial polymers.* 2015. **63**: p. A1-A29.

41. Chen, C.Z., et al., *Quaternary ammonium functionalized poly (propylene imine) dendrimers as effective antimicrobials: Structure− activity studies.* 2000. **1**(3): p. 473-480.

42. Jain, A., et al., *Antimicrobial polymers. Adv Healthc Mater 3: 1969–1985*. 2014.

43. Chen, C.Z. and S.L.J.A.M. Cooper, *Recent advances in antimicrobial dendrimers.* 2000. **12**(11): p. 843-846.

44. Gillies, E.R. and J.M.J.D.d.t. Frechet, *Dendrimers and dendritic polymers in drug delivery.* 2005. **10**(1): p. 35-43.

45. Yang, K., et al., *Antimicrobial hydrogels: promising materials for medical application.* 2018. **13**: p. 2217.

46. Salomé Veiga, A. and J.P.J.P.S. Schneider, *Antimicrobial hydrogels for the treatment of infection.* 2013. **100**(6): p. 637-644.

47. Vranic, E.J.B.J.o.B.M.S., *Amorphous pharmaceutical solids.* 2004. **4**(3): p. 35.

48. Paul, D.R., *Polymer Blends Volume 1*. Vol. 1. 2012: Elsevier.

49. Lu, Z., et al., *The correlation between reduced glass transition temperature and glass forming ability of bulk metallic glasses.* 2000. **42**(7): p. 667-673.

50. Wypych, G.J.H.o.P., *SBC styrene-butadiene block copolymer.* 2012: p. 637-640.

51. Greene, J.P., *Automotive Plastics and Composites: Materials and Processing*. 2021: William Andrew.

52. Wagner Jr, J.R., *Multilayer flexible packaging*. 2016: William Andrew.

53. *Polypropylene Market Size, Trends and Global Forecast To 2032.* 2023.

54. Shan, C.L.P., J.B. Soares, and A.J.P. Penlidis, *HDPE/LLDPE reactor blends with bimodal microstructures—part I: mechanical properties.* 2002. **43**(26): p. 7345-7365.

55. Gilbert, M., *Brydson's plastics materials*. 2016: William Andrew.

56. *Polyethylene Market to Worth USD 140.21 Billion by 2029*, in *Fortune Business Insights*. 2023.

57. Sin, L.T. and B.S. Tueen, *Plastics and Sustainability: Practical Approaches*. 2022: Elsevier.

58. Zohuri, G., *Polymer science: a comprehensive reference.* 2012.

59. Al-Haydari, I.S. and H.S. Al-Haidari. *Mechanical properties of polyethylene terephthalate-modified pavement mixture*. in *IOP Conference Series: Materials Science and Engineering*. 2020. IOP Publishing.

60. Wang, L., C. Hu, and L.J.I.j.o.n. Shao, *The antimicrobial activity of nanoparticles: present situation and prospects for the future.* 2017: p. 1227-1249.

61. Filella, M.J.C., *Antimony and PET bottles: Checking facts.* 2020. **261**: p. 127732.

62. Weller, J.E., *Synthesis of a manufacturing process for making microcellular polycarbonate parts*. 1991, University of Washington.

63. Kausar, A., S. Zulfiqar, and M.I.J.P.R. Sarwar, *Recent developments in sulfur-containing polymers.* 2014. **54**(2): p. 185-267.

64. Park, S.-J. and M.-K. Seo, *Interface science and composites*. Vol. 18. 2011: Academic Press.

65. *Global Polycarbonate Market Size, Share, Growth Analysis By 2030.* Spherical Insights, 2023.

66. Li, L., et al., *Protein adsorption on oligo (ethylene glycol)-terminated alkanethiolate self-assembled monolayers: the molecular basis for nonfouling behavior.* 2005. **109**(7): p. 2934-2941.

67. Hamilton-Brown, P., et al., *End terminal, poly (ethylene oxide) graft layers: surface forces and protein adsorption.* 2009. **25**(16): p. 9149-9156.

68. Barbey, R., et al., *Polymer brushes via surface-initiated controlled radical polymerization: synthesis, characterization, properties, and applications.* 2009. **109**(11): p. 5437-5527.

69. Feng, W., J.L. Brash, and S.J.B. Zhu, *Non-biofouling materials prepared by atom transfer radical polymerization grafting of 2-methacryloloxyethyl phosphorylcholine: Separate effects of graft density and chain length on protein repulsion.* 2006. **27**(6): p. 847-855.

70. Zhang, Z., et al., *Blood compatibility of surfaces with superlow protein adsorption.* 2008. **29**(32): p. 4285-4291.

71. Kuang, J. and P.B.J.L. Messersmith, *Universal surface-initiated polymerization of antifouling zwitterionic brushes using a mussel-mimetic peptide initiator.* 2012. **28**(18): p. 7258-7266.

72. Harding, J.L. and M.M.J.T.i.b. Reynolds, *Combating medical device fouling.* 2014. **32**(3): p. 140-146.

73. Freschauf, L.R., et al., *Shrink-induced superhydrophobic and antibacterial surfaces in consumer plastics.* 2012.

74. Zhang, X., L. Wang, and E.J.R.A. Levänen, *Superhydrophobic surfaces for the reduction of bacterial adhesion.* 2013. **3**(30): p. 12003-12020.

75. Singha, P., J. Locklin, and H. Handa, *A review of the recent advances in antimicrobial coatings for urinary catheters.* Acta Biomaterialia, 2017. **50**: p. 20-40.

76. Zheng, S., et al., *Implication of Surface Properties, Bacterial Motility, and Hydrodynamic Conditions on Bacterial Surface Sensing and Their Initial Adhesion.* 2021. **9**.

77. Gao, G., et al., *Antibacterial surfaces based on polymer brushes: investigation on the influence of brush properties on antimicrobial peptide immobilization and antimicrobial activity.* 2011. **12**(10): p. 3715-3727.

78. Gao, G., et al., *The biocompatibility and biofilm resistance of implant coatings based on hydrophilic polymer brushes conjugated with antimicrobial peptides.* 2011. **32**(16): p. 3899-3909.

79. Bakhshi, H., et al., *Synthesis and characterization of antibacterial polyurethane coatings from quaternary ammonium salts functionalized soybean oil based polyols.* 2013. **33**(1): p. 153-164.

80. Majumdar, P., et al., *Development of environmentally friendly, antifouling coatings based on tethered quaternary ammonium salts in a crosslinked polydimethylsiloxane matrix.* 2008. **5**: p. 405-417.

81. Hui, F. and C.J.B. Debiemme-Chouvy, *Antimicrobial N-halamine polymers and coatings: a review of their synthesis, characterization, and applications.* 2013. **14**(3): p. 585-601.

82. Jang, J. and Y.J.C.c. Kim, *Fabrication of monodisperse silica–polymer core–shell nanoparticles with excellent antimicrobial efficacy.* 2008(34): p. 4016-4018.

83. Dong, A., et al., *Synthesis of N-halamine-functionalized silica–polymer core–shell nanoparticles and their enhanced antibacterial activity.* 2011. **22**(29): p. 295602.

84. Chen, Y. and Q.J.A.S.S. Han, *Designing N-halamine based antibacterial surface on polymers: Fabrication, characterization, and biocidal functions.* 2011. **257**(14): p. 6034-6039.

85. Petrie, E.M.J.H.o.A. and T.E. Sealants, *Methods of joining plastics other than with adhesives.* 2021.

86. Lowe, S., N.M. O'Brien-Simpson, and L.A.J.P.C. Connal, *Antibiofouling polymer interfaces: poly (ethylene glycol) and other promising candidates.* 2015. **6**(2): p. 198-212.

87. Yu, Q., et al., *Anti-fouling bioactive surfaces.* 2011. **7**(4): p. 1550-1557.

88. Kokubo, T., et al., *Development of bioactive materials based on surface chemistry.* 2009. **29**(7): p. 1267-1274.

89. Muszanska, A.K., et al., *Pluronic–lysozyme conjugates as anti-adhesive and antibacterial bifunctional polymers for surface coating.* 2011. **32**(26): p. 6333-6341.

90. Voo, Z.X., et al., *Antimicrobial/antifouling polycarbonate coatings: Role of block copolymer architecture.* 2015. **48**(4): p. 1055-1064.

91. Bastarrachea, L.J. and J.M.J.A.S.S. Goddard, *Self-healing antimicrobial polymer coating with efficacy in the presence of organic matter.* 2016. **378**: p. 479-488.

92. Irshad, K., et al., *Antimicrobial polymer coating.* 2020: p. 347-358.

93. Salwiczek, M., et al., *Emerging rules for effective antimicrobial coatings.* 2014. **32**(2): p. 82-90.

94. Tsuchiya, H., et al., *Innovative antimicrobial coating of titanium implants with iodine.* 2012. **17**(5): p. 595-604.

95. Han, W., et al., *Graphene family nanomaterials (GFNs)—promising materials for antimicrobial coating and film: A review.* 2019. **358**: p. 1022-1037.

96. Chidanand B, N.M., Eswara P, *Antimicrobial Coatings Market Trends.* 2022.

97. Tejero, R., et al., *Tailoring Macromolecular Structure of Cationic Polymers towards Efficient Contact Active Antimicrobial Surfaces.* 2018. **10**(3): p. 241.

98. Bratek-Skicki, A., et al., *Reversible Protein adsorption on mixed PEO/PAA Polymer brushes: Role of Ionic strength and PEO content.* 2018. **34**(9): p. 3037-3048.

99. Muszanska, A.K., et al., *Antiadhesive polymer brush coating functionalized with antimicrobial and RGD peptides to reduce biofilm formation and enhance tissue integration.* 2014. **15**(6): p. 2019-2026.

100. Ibrahim, A., et al., *Antimicrobial agents for textiles: types, mechanisms and analysis standards.* 2021. **13**(2): p. 261-293.

101. Bruenke, J., et al., *Quantitative comparison of the antimicrobial efficiency of leaching versus nonleaching polymer materials.* 2016. **16**(5): p. 647-654.

102. Brunke, S., et al., *Virulence factors in fungal pathogens of man.* 2016. **32**: p. 89-95.

103. Raloff, J.J.S.N.N., *Nanosilver Disinfects, But at What Price?* 2008. **30**.

104. Prabhu, S. and E.K.J.I.n.l. Poulose, *Silver nanoparticles: mechanism of antimicrobial action, synthesis, medical applications, and toxicity effects.* 2012. **2**: p. 1-10.

105. Alkarri, S., et al., *P22 Fabrication methodologies for antimicrobial polypropylene surfaces with leachable and non-leachable antimicrobial agents.* 2023. **5**(Supplement_2): p. dlad066. 026.

106. Kregiel, D.J.F.C., *Advances in biofilm control for food and beverage industry using organo-silane technology: A review.* 2014. **40**: p. 32-40.

107. Thamilselvi, V. and K.J.I.J.P. Radha, *A review on the diverse application of silver nanoparticle.* 2017. **7**(01): p. 21-27.

108. Zhang, X.-F., et al., *Silver nanoparticles: synthesis, characterization, properties, applications, and therapeutic approaches.* 2016. **17**(9): p. 1534.

109. Loza, K., et al., *The dissolution and biological effects of silver nanoparticles in biological media.* 2014. **2**(12): p. 1634-1643.

110. Liu, Y., et al., *Characteristics of the silver-doped TiO2 nanoparticles.* 2003. **220**(1-4): p. 7-11.

111. Zhang, J., et al., *Nano silver-induced toxicity and associated mechanisms.* 2022: p. 1851-1864.

112. Yin, I.X., et al., *The antibacterial mechanism of silver nanoparticles and its application in dentistry.* 2020: p. 2555-2562.

113. Paladini, F. and M.J.M. Pollini, *Antimicrobial silver nanoparticles for wound healing application: progress and future trends.* 2019. **12**(16): p. 2540.

114. Nirmala, T.S., et al., *Effect of Cu2+ ions on structural, morphological, optical and magnetic behaviors of ZnAl2O4 spinel.* 2020. **7**(4): p. 046104.

115. Hejazy, M., et al., *Toxicity of manufactured copper nanoparticles-A review.* 2018. **3**(1): p. 1-9.

116. Ma, X., et al., *Copper-containing nanoparticles: Mechanism of antimicrobial effect and application in dentistry-a narrative review.* 2022. **9**: p. 905892.

117. Grigore, M.E., et al., *Methods of synthesis, properties and biomedical applications of CuO nanoparticles.* 2016. **9**(4): p. 75.

118. Asemani, M., N.J.G.P. Anarjan, and Synthesis, *Green synthesis of copper oxide nanoparticles using Juglans regia leaf extract and assessment of their physico-chemical and biological properties.* 2019. **8**(1): p. 557-567.

119. Yang, Q., et al., *Dissolution kinetics and solubility of copper oxide nanoparticles as affected by soil properties and aging time.* 2022. **29**(27): p. 40674-40685.

120. Kayestha, R. and K.J.F.l. Hajela, *ESR studies on the effect of ionic radii on displacement of Mn2+ bound to a soluble β-galactoside binding hepatic lectin.* 1995. **368**(2): p. 285-288.

121. Naz, S., A. Gul, and M.J.I.n. Zia, *Toxicity of copper oxide nanoparticles: a review study.* 2020. **14**(1): p. 1-13.

122. Angelé-Martínez, C., et al., *Reactive oxygen species generation by copper(II) oxide nanoparticles determined by DNA damage assays and EPR spectroscopy.* Nanotoxicology, 2017. **11**(2): p. 278-288.

123. Bharathiraja, D.B., et al., *Calcium Oxide Nanoparticles as An Effective Filtration Aid for Purification of Vehicle Gas Exhaust*. 2018. p. 181-192.

124. Khine, E.E., et al., *Synthesis and characterization of calcium oxide nanoparticles for CO2 capture.* Journal of Nanoparticle Research, 2022. **24**(7): p. 139.

125. Sato, Y., et al., *Preparation and Application of Bioshell Calcium Oxide (BiSCaO) Nanoparticle-Dispersions with Bactericidal Activity.* Molecules, 2019. **24**(18).

126. Han, C., et al., *Proton-assisted calcium-ion storage in aromatic organic molecular crystal with coplanar stacked structure.* Nat Commun, 2021. **12**(1): p. 2400.

127. Liang, X., et al., *Antibacterial mechanism of biogenic calcium oxide and antibacterial activity of calcium oxide/polypropylene composites.* Colloids and Surfaces A: Physicochemical and Engineering Aspects, 2022. **650**: p. 129446.

128. *Calcium Oxide: Crops. Agricultural Marketing Service.* USDA, 2002.

129. Hornak, J., *Synthesis, Properties, and Selected Technical Applications of Magnesium Oxide Nanoparticles: A Review.* Int J Mol Sci, 2021. **22**(23).

130. Leitner, J., D. Sedmidubský, and O.J.M. Jankovský, *Size and shape-dependent solubility of CuO nanostructures.* 2019. **12**(20): p. 3355.

131. Makshakova, O.N., M.R. Gafurov, and M.A. Goldberg, *The Mutual Incorporation of Mg2+ and CO32− into Hydroxyapatite: A DFT Study.* 2022. **15**(24): p. 9046.

132. Lu, X., et al., *Right or Left: The Role of Nanoparticles in Pulmonary Diseases.* 2014. **15**(10): p. 17577-17600.

133. Fouda, A., et al., *Enhanced Antimicrobial, Cytotoxicity, Larvicidal, and Repellence Activities of Brown Algae, Cystoseira crinita-Mediated Green Synthesis of Magnesium Oxide Nanoparticles.* Front Bioeng Biotechnol, 2022. **10**: p. 849921.

134. Qiu, L., et al., *Preparation and Characterization of Mg(OH)2 Nanoparticles and Flame-Retardant Property of Its Nanocomposites with EVA.* Composite Structures, 2003. **62**: p. 391-395.

135. Zhu, Y., et al., *Mg(OH)2 nanoparticles enhance the antibacterial activities of macrophages by activating the reactive oxygen species.* 2021. **109**(11): p. 2369-2380.

136. Ropp, R.C. *Encyclopedia of the Alkaline Earth Compounds*. 2013.

137. Sakar, M., R.G. Balakrishna, and T.-O. Do, *Photocatalytic Systems by Design: Materials, Mechanisms and Applications*. 2021: Elsevier.

138. Gaetke, L.M., H.S. Chow-Johnson, and C.K. Chow, *Copper: toxicological relevance and mechanisms.* Arch Toxicol, 2014. **88**(11): p. 1929-38.

139. Ameh, T., et al., *Silver and Copper Nanoparticles Induce Oxidative Stress in Bacteria and Mammalian Cells.* 2022. **12**(14): p. 2402.

140. Okamoto, K., et al., *Magnesium Hydroxide Nanoparticles Inhibit the Biofilm Formation of Cariogenic Microorganisms.* 2023. **13**(5): p. 864.

141. PubChem, *Cupric chloride.* 2023.

142. Ma, Z., et al., *Cu-Doped ZnO Electronic Structure and Optical Properties Studied by First-Principles Calculations and Experiments.* 2019. **12**(1): p. 196.

143. Bayade, G., et al., *Biocidal properties of copper nanoparticles.* 2021(159): p. 2-17.

144. Longano, D., et al., *Synthesis and Antimicrobial Activity of Copper Nanomaterials*, in *Nano-Antimicrobials: Progress and Prospects*, N. Cioffi and M. Rai, Editors. 2012, Springer Berlin Heidelberg: Berlin, Heidelberg. p. 85-117.

145. Waghmode, M.S., et al., *Studies on the titanium dioxide nanoparticles: biosynthesis, applications and remediation.* SN Applied Sciences, 2019. **1**(4): p. 310.

146. Hyewon, Y., *Extraordinary Enhancement of UV Absorption in TiO2 Nanoparticles Enabled by Low-Oxidized Graphene Nanodots.* Journal of physical chemistry, 2018. **v. 122**(no. 22): p. pp. 12114-12121-2018 v.122 no.22.

147. Mbanga, O., E. Cukrowska, and M. Gulumian, *Dissolution of titanium dioxide nanoparticles in synthetic biological and environmental media to predict their biodurability and persistence.* Toxicol In Vitro, 2022. **84**: p. 105457.

148. Shi, H., et al., *Titanium dioxide nanoparticles: a review of current toxicological data.* Part Fibre Toxicol, 2013. **10**: p. 15.

149. Hou, J., et al., *Toxicity and mechanisms of action of titanium dioxide nanoparticles in living organisms.* J Environ Sci (China), 2019. **75**: p. 40-53.

150. Jiang, J., J. Pi, and J. Cai, *The Advancing of Zinc Oxide Nanoparticles for Biomedical Applications.* Bioinorg Chem Appl, 2018. **2018**: p. 1062562.

151. Talam, S., S.R. Karumuri, and N.J.I.S.R.N. Gunnam, *Synthesis, Characterization, and Spectroscopic Properties of ZnO Nanoparticles.* 2012. **2012**: p. 1-6.

152. Siddiqi, K.S., et al., *Properties of Zinc Oxide Nanoparticles and Their Activity Against Microbes.* Nanoscale Res Lett, 2018. **13**(1): p. 141.

153. OHASHI, H.J.J.O.M., PETROLOGY and E. GEOLOGY, *Effective ionic radii of Ni and Zn in orthopyroxenes.* 1989. **84**(9): p. 329-334.

154. Jin, M., et al., *Toxicity of different zinc oxide nanomaterials and dose-dependent onset and development of Parkinson's disease-like symptoms induced by zinc oxide nanorods.* Environment International, 2021. **146**: p. 106179.

155. Mendes, C.R., et al., *Antibacterial action and target mechanisms of zinc oxide nanoparticles against bacterial pathogens.* Scientific Reports, 2022. **12**(1): p. 2658.

156. Tiwari, V., et al., *Mechanism of Anti-bacterial Activity of Zinc Oxide Nanoparticle Against Carbapenem-Resistant Acinetobacter baumannii.* 2018. **9**.

157. Cotton, G., et al., *Efficacy and safety of alpha lipoic acid-capped silver nanoparticles for oral applications.* 2019. **9**(12): p. 6973-6985.

158. Idisi, D.O., J.A. Oke, and I.T. Bello, *Graphene oxide/Au nanoparticles: Synthesis, properties, and application: A mini-review.* 2021. **45**(14): p. 19772-19788.

159. Rhazouani, A., et al., *Synthesis and Toxicity of Graphene Oxide Nanoparticles: A Literature Review of In Vitro and In Vivo Studies.* Biomed Res Int, 2021. **2021**: p. 5518999.

160. Johnson, D.W., B.P. Dobson, and K.S. Coleman, *A manufacturing perspective on graphene dispersions.* Current Opinion in Colloid & Interface Science, 2015. **20**(5): p. 367-382.

161. Sánchez-López, L., et al., *Covalent immobilization of graphene oxide on biomedical grade CoCr alloy by an improved multilayer system assembly via Silane/GO bonding.* Materials Chemistry and Physics, 2022. **287**: p. 126296.

162. Yadav, S., et al., *An Update on Graphene Oxide: Applications and Toxicity.* ACS Omega, 2022. **7**(40): p. 35387-35445.

163. Dimiev, A.M. and J.M. Tour, *Mechanism of Graphene Oxide Formation.* ACS Nano, 2014. **8**(3): p. 3060-3068.

164. Sharma, H. and S. Mondal, *Functionalized Graphene Oxide for Chemotherapeutic Drug Delivery and Cancer Treatment: A Promising Material in Nanomedicine.* 2020. **21**(17): p. 6280.

165. Wani, I., et al., *Silver nanoparticles: Ultrasonic wave assisted synthesis, optical characterization and surface area studies.* Materials Letters, 2011. **65**: p. 520–522.

166. Kailasa, S., et al., *Antimicrobial activity of silver nanoparticles*. 2019. p. 461-484.

167. Cheon, J.Y., et al., *Shape-dependent antimicrobial activities of silver nanoparticles.* Int J Nanomedicine, 2019. **14**: p. 2773-2780.

168. Di Martino, P., *Antimicrobial agents and microbial ecology.* AIMS Microbiology, 2022. **8**(1): p. 1-4.

169. *Antiseptics.* 2023.

170. Ahmed, S., M. Ahmad, and S. Ikram, *Chitosan: A Natural Antimicrobial Agent-A Review.* journal of applicable chemistry, 2014.

171. Babutan, I., A.-D. Lucaci, and I.J.P. Botiz, *Antimicrobial polymeric structures assembled on surfaces.* 2021. **13**(10): p. 1552.

172. Song, J., et al., *Aqueous synthesis of silver nanoparticle embedded cationic polymer nanofibers and their antibacterial activity.* 2012. **4**(1): p. 460-465.

173. Dacarro, G., et al., *Monolayers of polyethilenimine on flat glass: a versatile platform for cations coordination and nanoparticles grafting in the preparation of antibacterial surfaces.* Dalton Transactions, 2012. **41**(8): p. 2456-2463.

174. Li, J.-h., et al., *Excellent hydrophilic and anti-bacterial fouling PVDF membrane based on ag nanoparticle self-assembled PCBMA polymer brush.* 2017. **35**(7): p. 809-822.

175. Turalija, M., et al., *Antimicrobial PLA films from environment friendly additives.* 2016. **102**: p. 94-99.

176. Iurciuc-Tincu, C.E., et al., *Drug Delivery System Based on pH-Sensitive Biocompatible Poly(2-vinyl pyridine)-b-poly(ethylene oxide) Nanomicelles Loaded with Curcumin and 5-Fluorouracil.* Polymers (Basel), 2020. **12**(7).

177. Ben-Sasson, M., et al., *Surface functionalization of thin-film composite membranes with copper nanoparticles for antimicrobial surface properties.* Environ Sci Technol, 2014. **48**(1): p. 384-93.

178. Demchenko, V., et al., *X-ray study of structural formation, thermomechanical and antimicrobial properties of copper-containing polymer nanocomposites obtained by the thermal reduction method.* European Polymer Journal, 2017. **96**: p. 326-336.

179. Joo, Y.T., et al., *Preparation of antibacterial PDMAEMA-functionalized multiwalled carbon nanotube via atom transfer radical polymerization.* 2013. **127**: p. 1508-1518.

180. Murugan, E. and G. Vimala, *Effective functionalization of multiwalled carbon nanotube with amphiphilic poly(propyleneimine) dendrimer carrying silver nanoparticles for better dispersability and antimicrobial activity.* Journal of Colloid and Interface Science, 2011. **357**(2): p. 354-365.

181. Mural, P.K.S., et al., *Polyolefin based antibacterial membranes derived from PE/PEO blends compatibilized with amine terminated graphene oxide and maleated PE.* Journal of Materials Chemistry A, 2014. **2**(41): p. 17635-17648.

182. Wang, L., C. Hu, and L.J.I.J.o.N. Shao, *The antimicrobial activity of nanoparticles: present situation and prospects for the future.* 2017. **12**: p. 1227 - 1249.

183. Ozdal, M. and S. Gurkok, *Recent advances in nanoparticles as antibacterial agent.* ADMET and DMPK, 2022. **10**(2): p. 115-129.

184. Wang, L., C. Hu, and L. Shao, *The antimicrobial activity of nanoparticles: present situation and prospects for the future.* Int J Nanomedicine, 2017. **12**: p. 1227-1249.

185. Jindal, H., et al., *Net charge, hydrophobicity and specific amino acids contribute to the activity of antimicrobial peptides.* Journal of Health and Translational Medicine, 2014. **17**: p. 1-7.

186. Singh, R., M.S. Smitha, and S.P. Singh, *The role of nanotechnology in combating multi-drug resistant bacteria.* J Nanosci Nanotechnol, 2014. **14**(7): p. 4745-56.

187. Kapoor, G., S. Saigal, and A.J.J.o.a. Elongavan, clinical pharmacology, *Action and resistance mechanisms of antibiotics: A guide for clinicians.* 2017. **33**(3): p. 300.

188. Yu, Z., et al., *Reactive oxygen species-related nanoparticle toxicity in the biomedical field.* 2020. **15**(1): p. 1-14.

189. Park, J.T. and J.L.J.S. Strominger, *Mode of action of penicillin: biochemical basis for the mechanism of action of penicillin and for its selective toxicity.* 1957. **125**(3238): p. 99-101.

190. Di Somma, A., et al., *Inhibition of bacterial biofilm formation*, in *Bacterial Biofilms*. 2020, IntechOpen.

191. Asfahl, K.L. and M.J.F.M.R. Schuster, *Social interactions in bacterial cell–cell signaling.* 2017. **41**(1): p. 92-107.

192. Aliashkevich, A., L. Alvarez, and F.J.F.i.m. Cava, *New insights into the mechanisms and biological roles of D-amino acids in complex eco-systems.* 2018. **9**: p. 683.

193. Beyth, N., et al., *Alternative antimicrobial approach: nano-antimicrobial materials.* 2015. **2015**.

194. Kohanski, M.A., D.J. Dwyer, and J.J.J.N.R.M. Collins, *How antibiotics kill bacteria: from targets to networks.* 2010. **8**(6): p. 423-435.

195. Guo, L., et al., *Polymer/nanosilver composite coatings for antibacterial applications.* Colloids and Surfaces A: Physicochemical and Engineering Aspects, 2013. **439**: p. 69-83.

196. Kamaruzzaman, N.F., et al., *Antimicrobial Polymers: The Potential Replacement of Existing Antibiotics?* Int J Mol Sci, 2019. **20**(11).

197. Tamayo, L., et al., *Copper-polymer nanocomposites: An excellent and cost-effective biocide for use on antibacterial surfaces.* Mater Sci Eng C Mater Biol Appl, 2016. **69**: p. 1391-409.

198. V V, A., et al., *Functionalization of fabrics with PANI/CuO nanoparticles by precipitation route for anti-bacterial applications.* Journal of Nanoparticle Research, 2015. **17**.

199. Chapman, J., et al., *Antifouling performances of macro- to micro- to nano-copper materials for the inhibition of biofouling in its early stages.* J. Mater. Chem. B, 2013. **1**.

200. Motoike, K., et al., *Antiviral activities of heated dolomite powder.* Biocontrol Sci, 2008. **13**(4): p. 131-8.

201. Leung, Y.H., et al., *Mechanisms of antibacterial activity of MgO: non-ROS mediated toxicity of MgO nanoparticles towards Escherichia coli.* Small, 2014. **10**(6): p. 1171-83.

202. He, Y., et al., *Study on the mechanism of antibacterial action of magnesium oxide nanoparticles against foodborne pathogens.* Journal of Nanobiotechnology, 2016. **14**(1): p. 54.

203. Tan, S.Y. and Y. Tatsumura, *Alexander Fleming (1881-1955): Discoverer of penicillin.* Singapore Med J, 2015. **56**(7): p. 366-7.

204. Dong, C., et al., *Investigation of Mg(OH)2 nanoparticles as an antibacterial agent. Journal of Nanoparticles Research, 12, 2101-2109.* Journal of Nanoparticle Research, 2010. **12**: p. 2101-2109.

205. Lee, C., et al., *Measurement of the elastic properties and intrinsic strength of monolayer graphene.* Science, 2008. **321**(5887): p. 385-8.

206. Sajjad, S., S.A. Khan Leghari, and A. Iqbal, *Study of Graphene Oxide Structural Features for Catalytic, Antibacterial, Gas Sensing, and Metals Decontamination Environmental Applications.* ACS Appl Mater Interfaces, 2017. **9**(50): p. 43393-43414.

207. Tarcan, R., et al., *A new, fast and facile synthesis method for reduced graphene oxide in N,N-dimethylformamide.* Synthetic Metals, 2020. **269**: p. 116576.

208. Kang, S., et al., *Single-Walled Carbon Nanotubes Exhibit Strong Antimicrobial Activity.* Langmuir, 2007. **23**(17): p. 8670-8673.

209. Han, W., et al., *Graphene family nanomaterials (GFNs)—promising materials for antimicrobial coating and film: A review.* Chemical Engineering Journal, 2019. **358**: p. 1022-1037.

210. Zou, P., W. Hartleb, and K. Lienkamp, *It takes walls and knights to defend a castle – synthesis of surface coatings from antimicrobial and antibiofouling polymers.* Journal of Materials Chemistry, 2012. **22**(37): p. 19579-19589.

211. Mangadlao, J.D., et al., *On the antibacterial mechanism of graphene oxide (GO) Langmuir–Blodgett films.* Chemical Communications, 2015. **51**(14): p. 2886-2889.

212. Zou, X., et al., *Mechanisms of the Antimicrobial Activities of Graphene Materials.* Journal of the American Chemical Society, 2016. **138**(7): p. 2064-2077.

213. Council, N.R., et al., *Size Limits of Very Small Microorganisms: Proceedings of a Workshop*. 1999: National Academies Press. 164.

214. Baron, E.J., in *Medical Microbiology*, S. Baron, Editor. 1996, University of Texas Medical Branch at Galveston. Copyright © 1996, The University of Texas Medical Branch at Galveston.: Galveston (TX).

215. Lorimer, J. and T. Hodgetts, *Good germs, bad germs: Citizen science and microbiology.* Biochemist, 2017. **39**: p. 35-37.

216. Webster, J. and R. Weber, *Introduction to Fungi*. 2007: Cambridge University Press.

217. McCoy, C., R. Samson, and D.J.C.P. Boucias, Boca Raton, FL, *Entomogenous fungi. In "Handbook of Natural Pesticides," Vol. V:"Microbial Insecticides, Part A: Entomogenous Protozoa and Fungi"(CM Ignoffo and NB Mandava, Eds.).* 1988. **2**: p. 157-172.

218. Zarandi, M.M., A. Bonakdar, and I. Stiharu. *Investigations on natural frequencies of individual spherical and ellipsoidal bakery yeast cells*. in *COMSOL conference*. 2010.

219. Louten, J., *Chapter 2 - Virus Structure and Classification*, in *Essential Human Virology*, J. Louten, Editor. 2016, Academic Press: Boston. p. 19-29.

220. Wiegand, C., et al., *Critical physiological factors influencing the outcome of antimicrobial testing according to ISO 22196 / JIS Z 2801.* PLOS ONE, 2018. **13**(3): p. e0194339.

221. Perez-Gavilan, A., et al., *Antibacterial activity testing methods for hydrophobic patterned surfaces.* Sci Rep, 2021. **11**(1): p. 6675.

222. Balouiri, M., M. Sadiki, and S.K. Ibnsouda, *Methods for in vitro evaluating antimicrobial activity: A review.* J Pharm Anal, 2016. **6**(2): p. 71-79.

223. Furer, L.A., et al., *A novel inactivated virus system (InViS) for a fast and inexpensive assessment of viral disintegration.* Scientific Reports, 2022. **12**(1): p. 11583.

224. Berkow, E.L., S.R. Lockhart, and L. Ostrosky-Zeichner, *Antifungal Susceptibility Testing: Current Approaches.* Clin Microbiol Rev, 2020. **33**(3).

225. Saeidnia, S., A. Manayi, and M. Abdollahi, *From in vitro Experiments to in vivo and Clinical Studies; Pros and Cons.* Curr Drug Discov Technol, 2015. **12**(4): p. 218-24.

226. Fini, M. and R. Giardino, *In vitro and in vivo tests for the biological evaluation of candidate orthopedic materials: Benefits and limits.* J Appl Biomater Biomech, 2003. **1**(3): p. 155-63.

227. Ghallab, A. and H.M. Bolt, *In vitro systems: current limitations and future perspectives.* Archives of Toxicology, 2014. **88**(12): p. 2085-2087.

228. Pfaller, M.A., et al., *Temporal and Geographic Variation in Antimicrobial Susceptibility and Resistance Patterns of Enterococci: Results From the SENTRY Antimicrobial Surveillance Program, 1997–2016.* Open Forum Infectious Diseases, 2019. **6**(Supplement_1): p. S54-S62.

229. Campos, M.D., et al., *The Activity of Antimicrobial Surfaces Varies by Testing Protocol Utilized.* PLOS ONE, 2016. **11**(8): p. e0160728.

230. Dahlia, F., et al., *Influence of environment variations on anti-glycaemic, anti-cholesterolemic, antioxidant and antimicrobial activities of natural wild fruits of Ziziphus lotus (L.).* South African Journal of Botany, 2020. **132**: p. 215-225.

231. Boks, N.P., et al., *Forces involved in bacterial adhesion to hydrophilic and hydrophobic surfaces.* Microbiology (Reading), 2008. **154**(Pt 10): p. 3122-3133.

232. Zhou, C., et al., *In Vivo Anti-Biofilm and Anti-Bacterial Non-Leachable Coating Thermally Polymerized on Cylindrical Catheter.* ACS Appl Mater Interfaces, 2017. **9**(41): p. 36269-36280.

233. Huh, A.J. and Y.J. Kwon, *"Nanoantibiotics": a new paradigm for treating infectious diseases using nanomaterials in the antibiotics resistant era.* J Control Release, 2011. **156**(2): p. 128-45.

234. Viitanen, H. and T.J.T.P.o.t.E.E.o.W.B.X.P.C. Ojanen, *Improved model to predict mold growth in building materials.* 2007: p. 2-7.

235. Savage, D.T., J.Z. Hilt, and T.D. Dziubla, *In Vitro Methods for Assessing Nanoparticle Toxicity*, in *Nanotoxicity: Methods and Protocols*, Q. Zhang, Editor. 2019, Springer New York: New York, NY. p. 1-29.

236. *Antimicrobial plastics market size. Growth Report [2023-2030].* 2023.

237. Pan, X., et al., *Investigation of antibacterial activity and related mechanism of a series of nano-Mg(OH)₂.* ACS Appl Mater Interfaces, 2013. **5**(3): p. 1137-42.

238. Ferdous, Z. and A. Nemmar, *Health Impact of Silver Nanoparticles: A Review of the Biodistribution and Toxicity Following Various Routes of Exposure.* Int J Mol Sci, 2020. **21**(7).

239. Cheeseman, S., et al., *Antimicrobial Metal Nanomaterials: From Passive to Stimuli-Activated Applications.* 2020. **7**(10): p. 1902913.

240. Geddes, L. *Antimicrobial Surface*. [cited 2023 April 22nd].

241. Brandrup, J., et al., *Polymer handbook*. Vol. 89. **1999**: Wiley New York.

242. Fowler, L., et al., *Antibacterial investigation of titanium-copper alloys using luminescent Staphylococcus epidermidis in a direct contact test. Mater Sci Eng C Mater Biol Appl*, **2019**. **97**: p. 707-714.

243. Vincent, C., et al., *Safety analysis over time: seven major changes to adverse event investigation. Implementation Science*, **2017**. **12**(1): p. 151.

244. Cooper, G.M., *The Cell: A Molecular Approach. 2nd edition*. **2000**: Sinauer Associates 2000.

245. Maity, S. and R.K.J.T. Shringirishi, *Sustainable antimicrobial finishes for Textiles from natural bio-extracts and conductive polymers: Sustainable antimicrobial finishes for Textiles.* 2021. **4**(1).

246. Gordon, N.A., *Divalent Copper Compounds as Inhibitory Agents of Influenza A*. 2014, Brigham Young University: United States -- Utah. p. 133.

247. Sheela Titus, T., N. Sivakumar, and G. Selvakumar, *Effect of CuCl2 on Growth and Biofilm Formation of Marine Pseudomonas sp. Pb-2a on Glass Surface.*

248. Halbus, A.F., T.S. Horozov, and V.N. Paunov, *Controlling the Antimicrobial Action of Surface Modified Magnesium Hydroxide Nanoparticles.* Biomimetics (Basel), 2019. **4**(2).

249. Alves, M.M., et al., *Enhanced antibacterial activity of Rosehip extract-functionalized Mg(OH)2 nanoparticles: An in vitro and in vivo study.* Colloids and Surfaces B: Biointerfaces, 2022. **217**: p. 112643.

250. Wang, Y., et al., *Investigation of the Biosafety of Antibacterial Mg(OH)2 Nanoparticles to a Normal Biological System.* 2023. **14**(4): p. 229.

251. Pittol, M., et al., *Evaluation of commercial Mg (OH) 2, Al (OH) 3 and TiO2 as antimicrobial additives in thermoplastic elastomers.* 2017. **46**(5): p. 223-230.

252. Salih, K.S., et al., *New tetradentate Schiff base Cu (II) complexes: synthesis, physicochemical, chromotropism, fluorescence, thermal, and selective catalytic oxidation.* 2021. **4**: p. 423-434.

253. Bhargava, R. and S.J.A.P.T. Khan, *Effect of reduced graphene oxide (rGO) on structural, optical, and dielectric properties of Mg (OH) 2/rGO nanocomposites.* 2017. **28**(11): p. 2812-2819.

254. Shkol'nikov, E.V., *Thermodynamic calculation of the solubility of solid hydroxides M(OH)2 in water and alkaline media.* Russian Journal of Applied Chemistry, 2004. **77**(8): p. 1255-1258.

255. Phuong, T.D.V., et al., *Electrochemical Behavior and Electronucleation of Copper Nanoparticles from CuCl2· H2O Using a Choline Chloride-Urea Eutectic Mixture.* 2021. **2021**: p. 1-14.

256. Maddan, O.L., *Nanoplatelet copper hydroxides and methods of preparing same*. 2008, Google Patents.

257. Maddan, O.L., *Hydroxides monolayer nanoplatelet and methods of preparing same*. 2022, Google Patents.

258. *BEI resources web portal > home.* BEI resources, 2023.

259. Čapek, J. and T. Roušar, *Detection of Oxidative Stress Induced by Nanomaterials in Cells—The Roles of Reactive Oxygen Species and Glutathione.* 2021. **26**(16): p. 4710.

260. Perez, N., *High-Temperature Oxidation*, in *Electrochemistry and Corrosion Science*, N. Perez, Editor. 2016, Springer International Publishing: Cham. p. 389-425.

261. *Global mortality associated with 33 bacterial pathogens in 2019: a systematic analysis for the Global Burden of Disease Study 2019.* Lancet, 2022. **400**(10369): p. 2221-2248.

262. Dong, C., et al., *Antibacterial study of Mg(OH)2 nanoplatelets.* Materials Research Bulletin, 2011. **46**(4): p. 576-582.

263. Dong, C., et al., *Investigation of Mg(OH)2 nanoparticles as an antibacterial agent.* Journal of Nanoparticle Research, 2010. **12**(6): p. 2101-2109.

264. Lih, E., et al., *Modified magnesium hydroxide nanoparticles inhibit the inflammatory response to biodegradable poly (lactide-co-glycolide) implants.* 2018. **12**(7): p. 6917-6925.

265. Meng, Y., et al., *Antimicrobial activity of nano-magnesium hydroxide against oral bacteria and application in root canal sealer.* 2020. **26**: p. e922920-1.

266. Dong, C., et al., *Study on antibacterial mechanism of Mg (OH) 2 nanoparticles.* 2014. **134**: p. 286-289.

267. Nakamura, Y., et al., *Magnesium Hydroxide Nanoparticles Kill Exponentially Growing and Persister Escherichia coli Cells by Causing Physical Damage.* 2021. **11**(6): p. 1584.

268. *7.7 million people die from bacterial infections every year – 2022 – ReAct.* ReAct, 2022.

269. *Global burden of bacterial antimicrobial resistance in 2019: a systematic analysis.* Lancet, 2022. **399**(10325): p. 629-655.

270. Villanueva, A., et al., *The influence of surface functionalization on the enhanced internalization of magnetic nanoparticles in cancer cells.* Nanotechnology, 2009. **20**(11): p. 115103.